TIME INTEGRATION ALGORITHMS FOR FINITE ELEMENT ANALYSIS OF CREEP PROBLEMS

by

N J MARAIS

A thesis submitted for the degree of
Doctor of Philosophy in Engineering

September 1989

Department of Civil Engineering
University of Cape Town
Republic of South Africa

ABSTRACT

The fundamental principles involved in the selection and implementation of time integration schemes for finite element analysis of nonlinear creep problems are investigated. The relationship between the nature of the integration algorithms and the mechanical principles of the time-dependent problem is explored. The emphasis is on uniaxial creep and simple constitutive laws are adopted.

The essential nature of the problem is presented in different formulations. The creep problem is contained in a system of nonlinear first order ordinary differential equations in the creep strains only. This suggests that the integration scheme should be applied to the creep strains whereas traditional methods approximate the stresses. An internal variable framework is used to demonstrate the links between a consistent mathematical programming formulation and the conventional Newton-Raphson procedures. The incremental creep problem is cast as a nonlinear programming problem and is written as a minimum principle in the incremental displacements and creep strains.

An implicit algorithm, based on successive minimisation, is developed for solution of the incremental problem. This results in a Newton-Raphson scheme, employing a consistent predictor and corrector step to iterate towards the correct solution. Numerical studies are performed to determine optimal integration parameters.

The stress and strain paths implied by different applications of the trapezoidal rule are presented. The mechanics of the problem is used to find the appropriate choice of integration path and a maximum net complementary work path is identified. These are implemented in the implicit algorithm and compared by means of simple examples. Linear and bilinear approximations of the actual stress history lead to suitable criteria for the choice of integration parameters. More accurate solutions can be achieved when these criteria are used in an improved procedure.

The solution procedures are closely linked to the mathematical programming approach. The mechanics of the creep problem provides insight into the time integration schemes used in finite element analysis. The extreme cases of linear creep and perfect plasticity provide the bounds for the choice of the integration path and an optimal form of the trapezoidal scheme for the general creep problem is proposed.

DECLARATION

I, Nicholas John Marais, declare that this thesis is essentially my own work and has not been submitted for a degree at any other university.

Signed by candidate

N J Marais

September 1989

ACKNOWLEDGEMENTS

I would like to express my gratitude to the following:

My supervisor, Professor J B Martin, for his patience and encouragement during my research and write-up.

Professor A Nappi from Politecnico di Milano for many helpful discussions and ideas during his visits in 1987 and 1988.

My past and present colleagues at the Centre for Research in Computational and Applied Mechanics (formerly the Applied Mechanics Research Unit) for the helpful discussions and encouragement.

The Foundation for Research and Development for their financial assistance during my postgraduate studies.

Mrs Shirley Breed for the typing of this manuscript.

Finally, to my family and friends for their continuous support and encouragement.

TABLE OF CONTENTS

NOMENCLATURE

This is a list of symbols used in the main text of this thesis.

Special Symbol

$\cdot$	the differential with respect to a time scale
$\sim$	a vector or matrix
$\| \ \|$	the absolute value of
T	(superscript) the transpose of a vector or matrix
-1	(superscript) the inverse of a matrix
d	differentiation with respect to
∂	the partial differentiation with respect to
Δ	the increment in

Lower Case Characters

a, b, c, d	constants used to define the bilinear stress path
$\underset{\sim}{e}$	the deviator strain vector
e_{ij}	the deviator strain tensor
e%	percentage error in predicted values
f	the function defining the creep strain rate
$\underset{\sim}{g}$	a general nonlinear function
k	a material parameter: fluidity constant in Norton's creep law
$\underset{\sim}{k}$	a material matrix defined in the text
m	a material parameter: power index in Norton's creep law
$\underset{\sim}{s}$	the deviator stress vector
s_{ij}	the deviator stress tensor

t time

t_{cr} a critical time parameter

$\hat{t}$ point of intersection in the bilinear stress path

t_* denotes trapezoidal approximation of the creep strains

$\underset{\sim}{u}$ the global displacement vector

u_i the local displacement vector

x_i the position vector

x_i numerical prediction of variable x in member i

$\bar{x}_i$ analytical value of variable x in member i

Upper Case Characters

$\underset{\sim}{A}$ matrix used to define the consistent predictor

$\underset{\sim}{B}$ the strain displacement matrix

B_i the bulk modulus multiplier

B_i^* the deviatoric strain displacement tensor

$\underset{\sim}{D}$ the elastic constitutive matrix

E Young's modulus

F the strain energy

F_i the body force tensor

$\underset{\sim}{F}$ prescribed force vector

G the shear modulus

$\underset{\sim}{H}$ a submatrix defined in the text

J the integral of the creep strain rate

$\underset{\sim}{K}$ the global elastic stiffness matrix

$\underset{\sim}{K}^*$ the modified stiffness matrix

$\underset{\sim}{K}_T$ the tangential stiffness matrix

$\underset{\sim}{L}$ a submatrix defined in the text

$\underset{\sim}{M}$ a constant matrix

N_i the shape function tensor

$\underset{\sim}{N}$ a submatrix defined in the text

P_i surface traction tensor

$\underset{\sim}{P}$ the global load vector evaluated at the nodes

$\underset{\sim}{R}$ the residual force vector

$\underset{\sim}{S}$ a submatrix defined in the text

S_p part of surface with prescribed tractions

S_u part of surface with prescribed displacements

T temperature

U a convex potential functional

U^* a convex potential functional

V the volume of the body

W the potential form of the constitutive law

$\underset{\sim}{X}$ the internal forces acting on the slips

$\underset{\sim}{Z}$ a submatrix defined in the text

Greek

α the time integration constant in the σ_* path

β a stress ratio defined in the text

δ_{ij} the Kronecker delta

$\underset{\sim}{\epsilon}$ the total strain vector

$\underset{\sim}{\epsilon}^c$ the creep part of the strain vector

$\underset{\sim}{\epsilon}^e$ the elastic part of the strain vector

ϵ_{ij} the total strain tensor

ϵ_{kk} the volumetric strain

$\underset{\sim}{\gamma}$ a material matrix defined in the text

∞ infinity

$\underset{\sim}{\lambda}$ the internal variable vector

Λ_m the largest eigenvalue of a system of equations

ν Poisson's ratio

ϕ the yield function for continuum problems

θ the time integration parameter in the t_* path

$\underset{\sim}{\sigma}$ the stress vector

σ_{ij} the stress tensor

σ_{kk} the total volumetric stress

σ_* denotes trapezoidal approximation of the stresses

τ a local truncation error

η a stress ratio defined in the text

Ω complementary work

Ω^O maximum complementary work

Ω^N net complementary work

Subscripts

n discrete instant in time t_n

α trapezoidal approximation of the variable

t value predicted by the t_* path

σ value predicted by the σ_* path

Right Superscripts

E corresponds to the elastic problem

SE the strain energy

T the transpose of a matrix or vector

c the creep part of

e the elastic part of

n discrete instant in time t_n

Left Superscripts

i the iteration number

j the iteration number

CHAPTER 1

INTRODUCTION

1. ISSUES IN THE NUMERICAL SOLUTION OF CREEP PROBLEMS

The rapid growth of the finite element method to analyse complex nonlinear problems can be attributed to the improvements in computer technology as well as the need to safely and economically predict material response under extreme mechanical and environmental loading. The design and analysis of nuclear power plants, pressure vessels and aircraft are typical examples. Analyses of complex problems involving nonlinear time-dependent material behaviour, in particular, can now be conducted on a large number of finite element programs. Meaningful use of such programs, however, relies on an understanding of the modelling techniques, constitutive relations and the numerical solution procedures.

Recent research in the use of the finite element method for the numerical modelling and analysis of time-dependent material response revolves around four central issues. Firstly, the transient or time-dependent nature of the material behaviour necessitates discretisation of the time domain as well as the usual spatial discretisation of the finite element method. Secondly, in any numerical procedure, the material response is determined at discrete instants in time and integrated over the intervening time intervals to achieve an accurate solution history. Appropriate time integration techniques are essential for reliable analysis procedures. In

particular, integration schemes used to solve first order differential equations are relevant for creep problems. The successful use of the time integration schemes in numerical analysis procedures requires an understanding of the nature of the scheme and the restrictions on its applications. These are concerned with the stability and accuracy of the resultant numerical algorithms.

Thirdly, besides the integration procedure and its limitations, the formulation of solution algorithms and computational strategies for use in finite element programs requires attention. Numerical solution algorithms must be robust and accurate for implementation in finite element methods. Finally, sophisticated constitutive laws for the transient response of time-dependent materials must be developed. Complex mathematical models for specific materials under extreme operating and environmental conditions are used to define the material behaviour. Early creep models have been extended to include modern fracture and damage mechanics concepts.

In this thesis we are concerned specifically with issues in the numerical solution of nonlinear creep problems by finite element methods. Spatial discretisation is achieved by standard techniques. Our interest is confined to the time discretisation, and we focus on the selection and application of appropriate time integration schemes. The discussion is restricted to quasi-static problems: dynamic effects are not included. The emphasis is also on simple structures and we adopt simple constitutive laws, which are adequate for our purposes.

1.2 MATHEMATICAL PRELIMINARIES

Zienkiewicz [1] produced a state-of-the-art survey of finite elements in the general time domain. We are concerned only in establishing appropriate techniques for finite element analysis of creep problems, a nonlinear time dependent material phenomenon. The standard formulation of creep problems leads to first order ordinary differential equations in the kinematic variables. In this section we consider briefly the issues involved in the numerical solution of these equations. This serves as both an introduction to the concepts discussed in later chapters and presents an introduction to the numerical solution of the related creep problem.

First order ordinary nonlinear differential equations of the class of interest in creep can be represented by the generic equation

$$\dot{\underset{\sim}{u}} + \underset{\sim}{g}(\underset{\sim}{M}\,\underset{\sim}{u} - \underset{\sim}{F}(t)) = 0 \quad , \tag{1.1}$$

where $\dot{\underset{\sim}{u}}$ is the time derivative of the variable $\underset{\sim}{u}$, $\underset{\sim}{g}$ a nonlinear operator, $\underset{\sim}{M}$ a constant matrix and $\underset{\sim}{F}(t)$ is a prescribed function defined for $t \in [0,T]$. Initial conditions are given by

$$\underset{\sim}{u}(0) = \underset{\sim}{u}_0 \quad . \tag{1.2}$$

The function $\underset{\sim}{g}(\underset{\sim}{M}\,\underset{\sim}{u} - \underset{\sim}{F}(t)) = \underset{\sim}{M}\,\underset{\sim}{u} - \underset{\sim}{F}(t)$ is the special linear case. The initial value problem consists of finding $\underset{\sim}{u}(t)$ such that equations (1.1) and (1.2) are satisfied.

In general it is not possible to determine the solutions analytically, and we introduce a time discretisation to achieve numerical solutions. We determine the solution at the discrete instants $t_0 = 0$, t_1, t_2, ... t_{n-1}, t_n , ... $t_N = T$. The solution must satisfy the differential equation (1.1) at each discrete instant, so that at the generic instant t_n we have

$$\dot{\underset{\sim}{u}}_n + \underset{\sim}{g}(\underset{\approx}{M}\,\underset{\sim}{u}_n - \underset{\sim}{F}(t_n)) = 0 \quad . \tag{1.3}$$

Least squares or variational forms of the differential equation can be formulated from the set of numerical solutions spanning the entire time-history. The complete set of unknown discrete solutions are then determined simultaneously. In the finite element context the variables are the nodal displacements and internal variables associated with each element; typically the total number of variables is very large. The solution techniques based on variational forms of the differential equations are therefore not suitable in the context of finite element analysis, because of the requirement of simultaneously solving for a very large number of variables. For this reason, in finite element approaches to time-dependent structural problems, a step-wise marching approach from the start to the end of the solution history has been adopted.

In a step-wise marching scheme, we assume that the values $\underset{\sim}{u}_{n-1}$, $\underset{\sim}{u}_{n-2}$ ..., $\underset{\sim}{u}_0$ are known, and we need to determine $\underset{\sim}{u}_n$ at the generic instant t_n . A numerical procedure to solve equation (1.3) can be established by using difference equations relating $\dot{\underset{\sim}{u}}_n$ to the known values $\underset{\sim}{u}_{n-1}$, $\underset{\sim}{u}_{n-2}$, ..., $\underset{\sim}{u}_0$ and the unknown value of $\underset{\sim}{u}_n$. The difference equations are then substituted into equation (1.3) to solve for $\underset{\sim}{u}_n$.

The accuracy of the solution $\underset{\sim}{u}_n$ will depend on the order and number of terms in the difference equations; the higher the order, the greater the accuracy. Storing and recalling of solutions at successive instants is again computationally expensive and prohibitive in large scale nonlinear finite element analyses, because of the number of variables involved. This puts multi-point recurrence schemes and higher order integration methods at a disadvantage and results in the widespread use of two-point schemes. These schemes require that only one set of data be held in core; that for the solution at the previous instant in time.

The general trapezoidal family of methods is the most widely used two-point recurrence scheme. In the trapezoidal rule we write

$$\underset{\sim}{u}_n = \underset{\sim}{u}_{n-1} + \Delta t\left\{(1 - \theta)\, \dot{\underset{\sim}{u}}_{n-1} + \theta\, \dot{\underset{\sim}{u}}_n\right\} \quad , \quad 0 \leq \theta \leq 1$$

where

$$\Delta t = t_n - t_{n-1} \quad . \tag{1.4}$$

We write the governing equations at times t_{n-1} and t_n ,

$$\dot{\underset{\sim}{u}}_{n-1} = - \underset{\sim}{g}(\underset{\sim}{M}\, \underset{\sim}{u}_{n-1} - \underset{\sim}{F}(t_{n-1})) \tag{1.5a}$$

and

$$\dot{\underset{\sim}{u}}_n = - \underset{\sim}{g}(\underset{\sim}{M}\, \underset{\sim}{u}_n - \underset{\sim}{F}(t_n)) \quad . \tag{1.5b}$$

Substituting equations (1.5a,b) into the trapezoidal rule we get

$$\underset{\sim}{u}_n = \underset{\sim}{u}_{n-1} - \Delta t\left\{(1 - \theta)\, \underset{\sim}{g}\, (\underset{\sim}{M}\, \underset{\sim}{u}_{n-1} - \underset{\sim}{F}(t_{n-1})) + \theta\, \underset{\sim}{g}\, (\underset{\sim}{M}\, \underset{\sim}{u}_n - \underset{\sim}{F}(t_n))\right\} \quad , \tag{1.6}$$

which gives

$$\underset{\sim}{u}_n + \theta\Delta t\, \underset{\sim}{g}\,(\underset{\sim}{M}\,\underset{\sim}{u}_n - \underset{\sim}{F}(t_n)) = \underset{\sim}{u}_{n-1} - (1 - \theta)\,\Delta t\, \underset{\sim}{g}(\underset{\sim}{M}\,\underset{\sim}{u}_{n-1} - \underset{\sim}{F}(t_{n-1})) \quad . \tag{1.7}$$

Equation (1.7) presents a simple framework for numerical solution algorithms. These algorithms are divided into two categories: in the first case we set $\theta = 0$ and equation (1.7) becomes a linear equation in $\underset{\sim}{u}_n$. This is known as an explicit scheme. The solution of equation (1.7) is straightforward because $\underset{\sim}{u}_n$ depends only on known values. The solution at any one time instant can be computed directly from the values at the previous instant. In implicit schemes, where $\theta > 0$, equation (1.7) is in general a nonlinear equation in $\underset{\sim}{u}_n$. In this case, the solution must be computed iteratively.

The choice of specific values of θ leads to particular forms of the generalised trapezoidal rule. These are shown in Table 1.1.

Table 1.1 : Special forms of the general trapezoidal scheme

θ	Method	Type
0	Forward difference, Euler forward	Explicit
1/2	Crank-Nicolson, Mid-point rule	Implicit
2/3	Galerkin	Implicit
1	Backward difference, Euler backward	Implicit

The choice of θ and the time step length Δt between discrete instants dictates the numerical characteristics of resultant solution algorithms. The numerical characteristics of an algorithm are judged

according to the consistency, convergence and the stability of the numerical procedure. We can demonstrate these concepts by looking at the applications of the generalised trapezoidal scheme to solve a system of linear first order ordinary differential equations of the form

$$\dot{\underset{\sim}{u}} + \underset{\sim}{M}\,\underset{\sim}{u} = \underset{\sim}{F} \quad . \tag{1.8}$$

Conditions for stability can be derived (Hughes [2]) by uncoupling the equations through modal decomposition, and considering the modal variable u associated with the largest eigenvalue Λ_m . The homogeneous form of the governing equation is

$$\dot{u} + \Lambda_m u = 0 \quad . \tag{1.9}$$

The appropriate form of equation (1.7) for the linear, homogeneous equation (1.9) is

$$u_n = \left[\frac{1 - (1 - \theta)\,\Lambda_m\,\Delta t}{1 + \theta\,\Lambda_m\,\Delta t}\right] u_{n-1} \quad . \tag{1.10}$$

The stability condition is based on the requirement that

$$|u_n| < |u_{n-1}| \quad , \tag{1.11}$$

and leads to the conditions

$$\frac{(1 - (1 - \theta)\Delta t\,\Lambda_m)}{(1 + \theta\,\Delta t\,\Lambda_m)} < 1 \tag{1.12a}$$

and

$$\frac{(1 - (1 - \theta)\Delta t\, \Lambda_m)}{(1 + \theta\, \Delta t\, \Lambda_m)} > -1 \quad . \tag{1.12b}$$

Equation (1.12a) is satisfied for all allowable values of the parameters while equation (1.12b) is satisfied for all values of $\theta \geq 1/2$. For values of $\theta < 1/2$, equation (1.12b) requires

$$\Delta t < \frac{2}{(1 - 2\theta)\, \Lambda_m} \quad . \tag{1.13}$$

This means that an upper limit is imposed on the time step length for stability of the time integration scheme. The scheme is therefore only conditionally stable if $\theta < 1/2$.

For $\theta < 1/2$, the restriction imposed by the largest eigenvalue of the system becomes severe in large systems of equations. Irons [3] demonstrated that Λ_m is conservatively bounded by the maximum eigenvalue of an individual element in a finite element formulation. The scheme is unconditionally stable if $\theta \geq 1/2$. Unconditional stability means that the scheme is stable for any time step length, but in practice the time step must still be restricted to maintain reasonable numerical accuracy.

It must however be noted that the above stability conditions for the trapezoidal rule applies to linear first order differential equations where the solution $\underset{\sim}{u}_n$ can be determined from equation (1.7) in a direct method. In the general nonlinear case this is no longer relevant, because iterative solution schemes are required to solve equation (1.7). The solution of nonlinear first order ordinary differential

equations by more sophisticated methods also lead to stability and convergence criteria involving the eigenvalue of highest magnitude. For the nonlinear systems, this requires the computation of the largest eigenvalue Λ_m or at least an upper bound to Λ_m at every time step.

In a consistent integration scheme the numerical solution must satisfy the governing equations at every discrete instant. Since local truncation errors are not accumulated in the trapezoidal scheme, it is consistent for any choice of θ . A time integration scheme converges if, for successive reductions in the time step length, the numerical solution tends to the true solution. The convergence of a scheme is assured once consistency and stability are verified. The use of the trapezoidal scheme in numerical procedures to solve linear first order differential equations will result in stable convergent algorithms if $\theta \geq 1/2$ and if the time steps are restricted to critical lengths when $\theta < 1/2$ is employed. This, however, does not guarantee the accuracy of the solution.

The local truncation error, τ , introduced by the difference equation for the generalised trapezoidal methods over any one step can be written as

$$|\tau| \leq c\, \Delta t^{k+1} \quad , \tag{1.14}$$

where c is a constant independent of Δt and k is the order of accuracy. For the general nonlinear first order differential equation contained in equation (1.1) we can find the truncation error by simple Taylor series expansion. We can show that, for the general trapezoidal rule, $k = 1$ for all $\theta \in [0,1]$ except when $\theta = 1/2$ in which case $k = 2$. This

shows that the trapezoidal rule is consistent and consecutive reductions in the step lengths will lead to numerical solutions which approach the correct solution. In general, the restrictions placed on the step lengths for stability are sufficient to achieve reasonable accuracy for explicit schemes. In implicit schemes where $\theta \geq 1/2$ the step sizes are bounded by accuracy considerations only.

1.3 SCOPE OF THE THESIS

The purpose of this thesis is to study the time discretisation of nonlinear creep problems. Recent work [4] aimed at the improvement of the accuracy and stability of the numerical algorithms in plasticity explores the fundamental relationship between the nature of the integration algorithm and the mechanical principles of the problem. In this thesis we will attempt to extend this understanding to time-dependent problems. It is sufficient for our purposes to consider simple creep constitutive relations, and to focus on uniaxial creep; results are easily generalised to the continuous problem. The use of an internal variable formulation allows us to explore links between a consistent mathematical programming formulation of the incremental creep problem and the conventional Newton-Raphson iterative solution procedures. This framework allows further examination of consistent bases for the choice of appropriate forms of trapezoidal integration schemes.

In the next chapter we introduce simple creep constitutive laws in the uniaxial framework. The essential nature of the creep problem is presented in different formulations of the uniaxial problem. The traditional finite element formulation, based on a trapezoidal

approximation of the stresses over a step and the resultant solution algorithms is discussed. The problem is recast in an internal variable formulation showing that, in both a coupled and uncoupled form, the only time derivatives which appear in the differential equations of the creep problem are the creep strain rates. This suggests that the trapezoidal rule should be applied to this variable. Further, we show that the incremental creep problem can be formulated as a nonlinear programming problem and written as a minimum principle in the incremental creep strains and displacements. Finally we generalise the uniaxial formulation to a finite element model of a continuum.

An implicit algorithm for the solution of the incremental problem, using the internal variable approach, is developed in Chapter 3. Successive minimum principles are used to arrive at a Newton-Raphson scheme, employing a predictor-corrector strategy to iterate to the correct solution. Whilst the solution algorithm is cast in a completely general framework, special attention is given to the trapezoidal approximation of the creep strains and simple power creep laws. Studies on the optimal form of this integration scheme are performed. In addition two structures exhibiting typical creep redistribution characteristics are analysed to illustrate the stability and the accuracy of the solution algorithm.

The solution algorithm in Chapter 3 uses a trapezoidal approximation of the creep strains while the traditional approach applies the trapezoidal rule to the stresses. The two approaches thus differ in the difference equations used to discretise the time domain. In Chapter 4 we investigate the relationship between these two sets of difference

equations. Each scheme is shown to imply its own stress and strain path over the time intervals between discrete solutions. The paths are distinct. The question of whether the choice of approximating path can be based on the mechanics of the problem, is also addressed. This leads to a maximum net complementary work path. The different paths are adopted in the framework developed in earlier chapters and we shall present some numerical results for simple truss structures.

Finally, the issue of appropriate choices of the integration parameters in both forms of the trapezoidal rule is further explored in Chapter 5. We consider ways in which the parameters can be selected to exactly reproduce any assumed stress-history over a time step. Linear and bilinear approximations of the stress-history are shown to lead to selection criteria which are simple and easy to implement in standard finite element analysis codes. These studies reinforce earlier results regarding the appropriate theoretical forms of the trapezoidal time integration scheme in creep problems.

CHAPTER 2

FORMULATIONS OF THE CREEP PROBLEM

2.1 INTRODUCTION

The objective of this chapter is to explore the ways in which the creep problem can be formulated, and the implications of the formulation for the application of the trapezoidal rule. In order to focus on basic issues, we shall initially consider a truss problem where the constitutive law is simply uniaxial. For simplicity we adopt a Maxwell model for creep, with the dashpot governed by Norton's law.

First we summarise the traditional finite element formulation of the creep problem. This is based on the equilibrium equations and the application of the trapezoidal rule to the stresses in order to obtain the change of creep strain over the time interval. We then describe the standard solution algorithm. Second, as a contrast, we reformulate the problem in the internal variable framework. This permits a set of ordinary nonlinear differential equations to be written in terms of node displacements and element creep strains. A simple transformation allows the equations to be written in uncoupled form.

We note that, in either the coupled or uncoupled form, the only time derivatives which appear in these equations are the creep strain rates, suggesting that this is the variable to which the trapezoidal rule should be applied. We show that the incremental problem can be equivalently formulated as a nonlinear programming problem. This

implies that the incremental creep problem is equivalent to a nonlinear elastic problem.

We then return to the coupled internal variable formulation and recast it as an incremental problem in terms of displacement increments and creep strain increments. A minimum principle for the incremental problem can be written, again demonstrating the holonomic nature of the problem.

Finally we generalise the coupled, incremental truss formulation to a finite element model of a continuum.

2.2 UNIAXIAL CREEP CONSTITUTIVE EQUATIONS

The constitutive equation provides a relationship between the stress history $\underset{\sim}{\sigma}(t)$ and the strain history $\underset{\sim}{\epsilon}(t)$ at a particular material sampling point. In a uniaxial framework we have only a single axial component of stress and strain in each structural member.

The total strain ϵ is assumed to be divided into an elastic strain ϵ^e and an inelastic creep strain ϵ^c such that

$$\epsilon = \epsilon^e + \epsilon^c \quad . \tag{2.1}$$

The stress is related to the elastic strain according to

$$\sigma = E\ \epsilon^e \quad , \tag{2.2}$$

where E is the elastic modulus. The inelastic strain rate is a function of several variables,

$$\dot{\epsilon}^c = f(\sigma, T, \underline{\eta}) \quad , \tag{2.3}$$

where T is the temperature and $\underline{\eta}$ represents additional state variables. Restricting discussion to isothermal creep, the simplest constitutive model is one in which the creep strain rate depends only on the current stress and hence

$$\dot{\epsilon}^c = f(\sigma) \quad . \tag{2.4}$$

We shall adopt Norton's law for metallic creep, such that

$$\dot{\epsilon}^c = k\ \sigma^m \quad , \tag{2.5}$$

where k and m are material constants. The material response is thus described by

$$\dot{\epsilon} = \dot{\sigma}/E + k\ \sigma^m \quad . \tag{2.6}$$

Equation (2.6) corresponds to the response of a Maxwell rheological model in which the mechanical behaviour is represented by a spring and a nonlinear dashpot in series. The spring element describes the instantaneous elastic response and the time-dependent response is represented by the dashpot.

This simple creep constitutive law is adequate for our purposes. The relationship can be generalised to include additional features such as primary creep, damage and viscoplasticity.

2.3 THE STRUCTURAL FORMULATION FOR TRUSS PROBLEMS

In this section the structural creep problem is developed for uniaxial (truss) problems. These problems are easy to formulate and they are a convenient vehicle to illustrate many aspects of creep behaviour. The essential nature of the creep problem can be explored by considering such formulations. We use the virtual work approach to formulate a global equilibrium condition which serves as basis for the current numerical solution strategies.

A truss structure consists of an assemblage of bars with uniform cross-sections and pinned joints which are free to rotate. External loads are applied only at the joints. The axial stress σ is the only non-zero component of stress in each member and is uniform along the member. Similarly the axial strain ϵ is the only strain component and is uniform along each member. Since a variety of single bar coordinate systems are present in an assemblage of bars, it is convenient to introduce a displacement vector $\underset{\sim}{u}$ of joint displacements in a global coordinate system. The external loads acting on these joints are represented by the load vector $\underset{\sim}{P}$. In the same way, we group the individual bar stresses and strains into the respective global vectors $\underset{\sim}{\sigma}$ and $\underset{\sim}{\epsilon}$. The strains and displacements are compatible, so that

$$\underset{\sim}{\epsilon} = \underset{\sim}{B}\,\underset{\sim}{u} \quad , \tag{2.7}$$

where $\underset{\sim}{B}$ is the deformation matrix which consists of linear spatial differential operators.

Furthermore, we can relate the total stress to the current displacements through the elastic relation

$$\begin{aligned} \underset{\sim}{\sigma} &= \underset{\sim}{D}\ \underset{\sim}{\epsilon}^{e} = \underset{\sim}{D}(\underset{\sim}{\epsilon} - \underset{\sim}{\epsilon}^{c}) \\ &= \underset{\sim}{D}\ \underset{\sim}{B}\ \underset{\sim}{u} - \underset{\sim}{D}\ \underset{\sim}{\epsilon}^{c} \quad , \end{aligned} \tag{2.8}$$

where $\underset{\sim}{D}$ is the elasticity matrix consisting on individual contributions of the Young's moduli of the bars in the structure.

The principle of virtual work can be applied to statically and kinematically admissible fields. For virtual displacements $\delta\underset{\sim}{u}$ and compatible strains $\delta\underset{\sim}{\epsilon}$, we have

$$\int_{V} \delta\underset{\sim}{\epsilon}^{T}\ \underset{\sim}{\sigma}\ dV - \delta\underset{\sim}{u}^{T}\ \underset{\sim}{P} = 0 \quad , \tag{2.9}$$

with V denoting the integration over all members in the structure. The external nodal forces are represented by the vector $\underset{\sim}{P}$. Upon substitution of equations (2.7) and (2.8) into (2.9) we get

$$\delta\underset{\sim}{u}^{T}\left[\int_{V} \underset{\sim}{B}^{T}\ \underset{\sim}{\sigma}\ dV - \underset{\sim}{P} \right] = 0 \quad . \tag{2.10}$$

The standard form of the equilibrium equation for stresses and externally applied loads then becomes

$$\int_{V} \underset{\sim}{B}^{T}\ \underset{\sim}{\sigma}\ dV = \underset{\sim}{P} \quad . \tag{2.11}$$

This equilibrium equation, in combination with the governing constitutive relations

$$\underset{\sim}{\sigma} = \underset{\sim}{D}\,\underset{\sim}{B}\,\underset{\sim}{u} - \underset{\sim}{D}\,\underset{\sim}{\epsilon}^{c} \quad , \tag{2.12a}$$

$$\dot{\underset{\sim}{\epsilon}}^{c} = \underset{\sim}{f}(\underset{\sim}{\sigma}) \tag{2.12b}$$

defines the structural response to given loads $\underset{\sim}{P}$.

2.4 THE STANDARD SOLUTION ALGORITHM

The equilibrium and the constitutive equations are usually cast in an incremental form, and iterative incremental solution procedures are developed on the basis of a Newton-Raphson approach. This leads to the common creep solution algorithms which appear in the literature using explicit or implicit procedures [5,6,7]. Several variations on the formulation and development of the algorithms have been presented [8-16], but they are all based on the same governing equations.

In this section we present a brief summary of the standard approach, in the context of the truss problem.

To determine the response of the structure under any loading program, the time domain must be discretised. The response is evaluated at discrete instants $t_0, t_1, \ldots, t_N$. For the n-th interval

$$t_n = t_{n-1} + \Delta t_n \quad . \tag{2.13}$$

Creep problems are rate and time-dependent so that the time parameter t measures real time. The initial conditions are assumed to be known at

the outset of the analysis:

$$\underset{\sim}{u}(0) = \underset{\sim}{u}_0 \ , \ \underset{\sim}{\varepsilon}^c(0) = \underset{\sim}{\varepsilon}^c_0 \text{ and } \underset{\sim}{P}(0) = \underset{\sim}{P}_0 \quad . \tag{2.14}$$

The equilibrium equation must be satisfied at each of the discrete instants at which the solution is determined. At time t_n , the equilibrium equation is

$$\int_V \underset{\sim}{B}^T \underset{\sim}{\sigma}_n \, dV = \underset{\sim}{P}_n \quad . \tag{2.15}$$

It is assumed that an equilibrated solution is known for time t_{n-1} . The stress increment over the time step, $\Delta t_n = t_n - t_{n-1}$, from equation (2.12a) may be written as

$$\Delta\underset{\sim}{\sigma}_n = \underset{\sim}{\sigma}_n - \underset{\sim}{\sigma}_{n-1} = \underset{\sim}{D} \, \underset{\sim}{B}(\underset{\sim}{u}_n - \underset{\sim}{u}_{n-1}) - \underset{\sim}{D}(\underset{\sim}{\varepsilon}^c_n - \underset{\sim}{\varepsilon}^c_{n-1}) \quad . \tag{2.16}$$

The creep strain increment $\Delta\underset{\sim}{\varepsilon}^c_n$ over interval is approximated by assuming that a fixed weighted average value of stresses at the beginning and end of the interval may be substituted in equation (2.12b). Thus

$$\Delta\underset{\sim}{\varepsilon}^c_n = \underset{\sim}{\varepsilon}^c_n - \underset{\sim}{\varepsilon}^c_{n-1} = \Delta t_n \, \underset{\sim}{f}(\underset{\sim}{\sigma}_{n\alpha}) \tag{2.17a}$$

where

$$\begin{aligned} \underset{\sim}{\sigma}_{n\alpha} &= (1 - \alpha)\underset{\sim}{\sigma}_{n-1} + \alpha\underset{\sim}{\sigma}_n \\ &= \underset{\sim}{\sigma}_{n-1} + \alpha\Delta\underset{\sim}{\sigma}_n \quad , \quad 0 \le \alpha \le 1 \quad , \end{aligned} \tag{2.17b}$$

and

$$\underset{\sim}{f}(\underset{\sim}{\sigma}_{n\alpha}) = \underset{\sim}{k} \, \underset{\sim}{\sigma}^m_{n\alpha} \quad . \tag{2.17c}$$

In equation (2.17c), $\underset{\sim}{k}$ is a diagonal matrix made up of the appropriate constants k for each member, and $\underset{\sim}{\sigma}^{m}_{na}$ is a vector in which each component of $\underset{\sim}{\sigma}_{na}$ is raised to be power m . Equation (2.17b) indicates that the trapezoidal rule is used to compute the fixed weighted average value of stress.

Substituting equation (2.17a) into equation (2.16), a relation between stress increments $\Delta\underset{\sim}{\sigma}_n$ and the displacement increment $\Delta\underset{\sim}{u}_n = \underset{\sim}{u}_n - \underset{\sim}{u}_{n-1}$ is obtained:

$$\Delta\underset{\sim}{\sigma}_n = \underset{\sim}{D}\,\underset{\sim}{B}\,\Delta\underset{\sim}{u}_n + \Delta t_n\,\underset{\sim}{D}\,\underset{\sim}{f}(\underset{\sim}{\sigma}_{na}) \quad . \tag{2.18}$$

This equation is linear in the explicit case ($a = 0$) , and nonlinear in the implicit case ($a > 0$) .

The equilibrium equation (2.15) is also written in incremental form as

$$\begin{aligned}\int_V \underset{\sim}{B}^T\,\Delta\underset{\sim}{\sigma}_n\,dV &= \underset{\sim}{P}_n - \int_V \underset{\sim}{B}^T\,\underset{\sim}{\sigma}_{n-1}\,dV \\ &= \underset{\sim}{R}_n \quad .\end{aligned} \tag{2.19}$$

In the explicit case, substitution of equation (2.18) into equation (2.19) leads to a linear equation in $\Delta\underset{\sim}{u}_n$:

$$\underset{\sim}{K}\,\Delta\underset{\sim}{u}_n = \underset{\sim}{R}_n - \Delta t_n \int_V \underset{\sim}{B}^T\,\underset{\sim}{D}\,\underset{\sim}{f}(\underset{\sim}{\sigma}_{n-1})\,dV \tag{2.20}$$

where

$$\underset{\sim}{K} = \int_V \underset{\sim}{B}^T\,\underset{\sim}{D}\,\underset{\sim}{B}\,dV$$

is the elastic stiffness matrix. The corresponding stress increment $\Delta\underset{\sim}{\sigma}_n$ is easily determined from equation (2.18). The resulting explicit solution procedure, an extension of the algorithms given by Mendelson *et al.* [17] and Greenbaum *et al.* [18], is widely used for finite element analysis of creep problems. Because the material nonlinearities appear as effective loads, they are also referred to as initial strain or residual force methods.

The explicit solution algorithm is computationally efficient because the elastic stiffness matrix is used throughout the solution history. While the problem is not posed in the generic form used in Chapter 1, we are in fact solving a system of nonlinear first order ordinary differential equations. To use the above explicit approach, the time step length between successive discrete solutions must be restricted to a critical time step length Δt_{cr} to ensure the stability of the solution procedure. The critical step length is based on the largest eigenvalue of the system (Λ_m) for every step. In practice it is easier to determine a bound on Λ_m for every time step so that Δt_{cr} can be estimated without recalculating Λ_m . Cormeau [19] showed that the bound on Λ_m can be expressed in terms of the creep laws and current stress state of the structure so that analytical expressions for Δt_{cr} can be derived for different creep laws.

In the implicit case, the nonlinearity of equation (2.18) necessitates the use of an iterative procedure to determine the incremental displacements and stresses. In a standard Newton-Raphson approach, successive corrections $\Delta\hat{\underset{\sim}{u}}_n$ and $\Delta\hat{\underset{\sim}{\sigma}}_n$ are computed in the i-th iteration

to update the previous estimates:

$$^{i+1}\Delta\underset{\sim}{u}_n = {}^{i}\Delta\underset{\sim}{u}_n + \Delta\hat{\underset{\sim}{u}}_n \quad , \tag{2.21a}$$

$$^{i+1}\Delta\underset{\sim}{\sigma}_n = {}^{i}\Delta\underset{\sim}{\sigma}_n + \Delta\hat{\underset{\sim}{\sigma}}_n \quad . \tag{2.21b}$$

By adopting a truncated Taylor series expansion for $\underset{\sim}{f}(\underset{\sim}{\sigma}_{n\alpha})$, so that

$$\underset{\sim}{f}(^{i+1}\underset{\sim}{\sigma}_{n\alpha}) = \underset{\sim}{f}(^{i}\underset{\sim}{\sigma}_{n\alpha}) + \Delta\hat{\underset{\sim}{\sigma}}^{T}_{n\alpha} \left.\frac{\partial \underset{\sim}{f}}{\partial \underset{\sim}{\sigma}_{n\alpha}}\right|_{i_{\underset{\sim}{\sigma}_{n\alpha}}} \quad , \tag{2.22a}$$

with

$$^{i}\Delta\underset{\sim}{\sigma}_{n\alpha} = (1 - \alpha)\ \underset{\sim}{\sigma}_{n-1} + \alpha\ ^{i}\underset{\sim}{\sigma}_n \quad . \tag{2.22b}$$

Equation (2.18) can then be reformulated to become

$$\Delta\hat{\underset{\sim}{\sigma}}_n + \underset{\sim}{D}\ \underset{\sim}{B}\ \Delta\hat{\underset{\sim}{u}}_n + \underset{\sim}{D}\ \alpha\Delta t_n\ \Delta\hat{\underset{\sim}{\sigma}}_n\ ^{i}\underset{\sim}{S}_n = 0 \quad , \tag{2.23a}$$

where

$$^{i}\underset{\sim}{S}_n = \left.\frac{\partial \underset{\sim}{f}}{\partial \underset{\sim}{\sigma}_{n\alpha}}\right|_{i_{\underset{\sim}{\sigma}_{n\alpha}}} \quad . \tag{2.23b}$$

After premultiplying by $\underset{\sim}{D}^{-1}$, equation (2.23a) permits us to express $\Delta\hat{\underset{\sim}{\sigma}}_n$ in terms of $\Delta\hat{\underset{\sim}{u}}_n$;

$$\begin{aligned}\Delta\hat{\underset{\sim}{\sigma}}_n &= \left[\underset{\sim}{D}^{-1} + \alpha\Delta t_n\ ^{i}\underset{\sim}{S}_n\right]^{-1} \underset{\sim}{B}\ \Delta\hat{\underset{\sim}{u}}_n \\ &= {}^{i}\underset{\sim}{D}_T\ \underset{\sim}{B}\ \Delta\hat{\underset{\sim}{u}}_n \quad .\end{aligned} \tag{2.24}$$

Substitution of equations (2.21b) and (2.24) into the equilibrium equation (2.19) leads to a predictor equation for $\Delta\hat{\underset{\sim}{u}}_n$;

$$ {}^{i}\underset{\sim}{K}_T \, \Delta\hat{\underset{\sim}{u}}_n = {}^{i}\underset{\sim}{R}_n \qquad (2.25a) $$

where

$$ {}^{i}\underset{\sim}{K}_T = \int_V \underset{\sim}{B}^T \, {}^{i}\underset{\sim}{D}_T \, \underset{\sim}{B} \, dV \quad , \qquad (2.25b) $$

$$ {}^{i}\underset{\sim}{R}_n = \underset{\sim}{P}_n - \int \underset{\sim}{B}^T (\underset{\sim}{\sigma}_{n-1} + {}^{i}\Delta\underset{\sim}{\sigma}_n) \, dV \quad . \qquad (2.25c) $$

The tangential stiffness matrix ${}^{i}\underset{\sim}{K}_T$ is based on the current stress state and the residual force vector ${}^{i}\underset{\sim}{R}_n$ describes the out-of-equilibrium nodal forces for this stress state. Once $\Delta\hat{\underset{\sim}{u}}_n$ is computed, the corrected stress increment ${}^{i+1}\Delta\underset{\sim}{\sigma}_n$ can be determined from equations (2.24) or, more conveniently for finite element computations, from equation (2.16). The iterative cycle is repeated until the residual force ${}^{i}\underset{\sim}{R}_n$ becomes tolerably small.

The implicit (tangential stiffness) creep solution procedures thus account for the material nonlinearities in a modified stiffness matrix and force vector. The successive reformation of the tangential stiffness matrix results in considerable computational effort for each iteration within a time step. This can be reduced by using selective reformation of $\underset{\sim}{K}_T$ and employing accelerating techniques to reduce the number of iterations within each time step.

It can, however, be shown that time integration schemes used in equation (2.17) results in an unconditionally stable scheme for any $\alpha \geq 1/2$ (Hughes and Taylor [20]). This allows the use of time step

lengths far larger than those imposed by the stability conditions in the explicit formulation. The use of large time steps through the solution history offsets the computational effort involved in the reformation of the tangential stiffness matrix in the implicit approach.

In practice the choice of Δt is bounded by accuracy considerations. In particular, if a reasonably smooth load history $\underset{\sim}{P}(t)$ is present, large time steps can be selected. The accuracy of the discrete solution is then affected by the choice of the parameter α in the trapezoidal scheme. No consistent basis for the choice of α in implicit creep solution algorithms has been proposed and it is based on numerical experience only [5,6].

The choice between an implicit or explicit scheme is not straightforward and depends on the particular problem under consideration. Both forms of the standard solution algorithm are in wide-spread use and appear in most nonlinear finite element codes. Much research revolves around several refinements to the basic formulations: for example effective stress [12] and sub-incrementation algorithms [15] have been used to enhance the performance and robustness of the methods. Several authors [6,9,22-25] also contributed towards improved numerical integration schemes through theoretical and numerical studies. Explicit and implicit techniques may be combined in an algorithm so that mixed implicit-explicit schemes can be used to obtain economic solutions [16]. In problems where different materials lead to very different permissible step lengths within the same mesh, regions of small step sizes are evaluated implicitly and remaining regions explicitly integrated.

2.5 AN INTERNAL VARIABLE FORMULATION FOR TRUSS PROBLEMS

In order to explore the essential nature of the creep problem we cast the formulation of the creep problem into a more general framework. The internal variable formulation provides a simple framework which can be applied directly to a finite element analysis. This allows us to formulate the general inelastic problem for a broad class of material laws. Specific forms of material responses may be adopted to specialise this general framework to a particular class of problems such as creep or plasticity. The thermodynamic basis and formulation of the internal variable theory is discussed by Martin [26]. We present here a form of the internal variable formulation that is appropriate for truss structures and Norton creep material models.

Let the displacements of the truss structure be represented by a displacement vector $\underset{\sim}{u}$, and the inelastic behaviour be described by a vector of internal variables $\underset{\sim}{\lambda}$. For our purposes we consider the inelastic (creep) strains in individual bars to be the internal variables. The strain energy F of the structure is assumed to be a homogeneous quadratic function of $\underset{\sim}{u}$ and $\underset{\sim}{\lambda}$. For small changes in the kinematic variables

$$\begin{aligned} dF &= d\underset{\sim}{u}^T \frac{\partial F}{\partial \underset{\sim}{u}} + d\underset{\sim}{\lambda}^T \frac{\partial F}{\partial \underset{\sim}{\lambda}} \\ &= d\underset{\sim}{u}^T \underset{\sim}{R} - d\underset{\sim}{\lambda}^T \underset{\sim}{X} \quad , \end{aligned} \tag{2.26}$$

where

$$\underset{\sim}{R} = \frac{\partial F}{\partial \underset{\sim}{u}} \quad , \quad \underset{\sim}{X} = - \frac{\partial F}{\partial \underset{\sim}{\lambda}} \quad . \tag{2.27}$$

The vector $\underset{\sim}{R}$ is identified as the vector of internal nodal forces, while $\underset{\sim}{X}$, in view of the negative sign in equation (2.27) is the vector of internal forces acting on the internal variables. Since $\partial^2 F/\partial \underset{\sim}{u}\ \partial \underset{\sim}{\lambda} = \partial^2 F/\partial \underset{\sim}{\lambda}\ \partial \underset{\sim}{u}$, we can write

$$\underset{\sim}{R} = \underset{\sim}{K}' \underset{\sim}{u} + \underset{\sim}{L}\ \underset{\sim}{\lambda} \tag{2.28a}$$

and

$$-\ \underset{\sim}{X} = \underset{\sim}{L}^T \underset{\sim}{u} + \underset{\sim}{H}\ \underset{\sim}{\lambda} \quad . \tag{2.28b}$$

This means the strain energy may be written as

$$F = \frac{1}{2}\ \underset{\sim}{u}^T \underset{\sim}{K}\ \underset{\sim}{u} + \underset{\sim}{u}^T \underset{\sim}{L}\ \underset{\sim}{\lambda} + \frac{1}{2}\ \underset{\sim}{\lambda}^T \underset{\sim}{H}\ \underset{\sim}{\lambda}$$

$$= \frac{1}{2} \begin{Bmatrix} \underset{\sim}{u} \\ \underset{\sim}{\lambda} \end{Bmatrix}^T \begin{bmatrix} \underset{\sim}{K} & \underset{\sim}{L} \\ \underset{\sim}{L}^T & \underset{\sim}{H} \end{bmatrix} \begin{Bmatrix} \underset{\sim}{u} \\ \underset{\sim}{\lambda} \end{Bmatrix} \quad . \tag{2.29}$$

In general, we may identify $\underset{\sim}{K}$ as the positive definite elastic stiffness matrix. The matrix $\underset{\sim}{H}$ will be positive semi-definite, in view of the fact that in most circumstances it will be possible for changes in $\underset{\sim}{\lambda}$ to occur without changes in F .

External equilibrium demands that the externally applied forces $\underset{\sim}{P}(t)$ should be equal to the internal nodal forces $\underset{\sim}{R}$. The formulation is completed by the introduction of a kinetic equation relating the internal variable rates $\dot{\underset{\sim}{\lambda}}$ and the internal slip forces $\underset{\sim}{X}$. This we take to be of the form

$$\underset{\sim}{X} = \underset{\sim}{X}(\dot{\underset{\sim}{\lambda}}) \quad . \tag{2.30}$$

The governing equations thus become

$$\underset{\sim}{K}\,\underset{\sim}{u}(t) + \underset{\sim}{L}\,\underset{\sim}{\lambda}(t) = \underset{\sim}{P}(t) \quad , \tag{2.31a}$$

$$\underset{\sim}{L}^{T}\underset{\sim}{u}(t) + \underset{\sim}{H}\,\underset{\sim}{\lambda}(t) = -\,\underset{\sim}{X}(\underset{\sim}{\lambda}) \quad , \tag{2.31b}$$

with $\underset{\sim}{P}(t)$ prescribed and initial conditions $\underset{\sim}{\lambda}(0) = \underset{\sim}{\lambda}_0$ given. The structure of these equations should be noted. In equation (2.31a), $\underset{\sim}{K}$ will be a banded matrix, and must be regarded as a global set of equations in $\underset{\sim}{u}$. In equation (2.31b), $\underset{\sim}{H}$ will be a diagonal matrix for the truss problem, and thus these equations can be regarded as a set of independent member equations which are uncoupled in $\underset{\sim}{\lambda}$ and $\underset{\sim}{X}$.

The more conventional truss formulation given in Section 2.3 can be identified with the internal variable formulation through equation (2.8)

$$\underset{\sim}{\sigma} = \underset{\sim}{D}\,\underset{\sim}{B}\,\underset{\sim}{u} - \underset{\sim}{D}\,\underset{\sim}{\epsilon}^{c} \tag{2.32}$$

and equation (2.11)

$$\int_V \underset{\sim}{B}^{T}\,\underset{\sim}{\sigma}\,dV = \underset{\sim}{P} \quad . \tag{2.33}$$

Substituting equation (2.32) into (2.33), we get

$$\left[\int_V \underset{\sim}{B}^{T}\underset{\sim}{D}\,\underset{\sim}{B}\,dV\right]\underset{\sim}{u} - \left[\int_V \underset{\sim}{B}^{T}\underset{\sim}{D}\,dV\right]\underset{\sim}{\epsilon}^{c} = \underset{\sim}{P} \quad , \tag{2.34a}$$

and integrating equation (2.32) over the volume

$$- \left[\int_V \underset{\sim}{D}\,\underset{\sim}{B}\, dV\right]\underset{\sim}{u} + \left[\int_V \underset{\sim}{D}\, dV\right]\underset{\sim}{\epsilon}^c = - \left[\int_V \underset{\sim}{\sigma}\, dV\right] \quad . \qquad (2.34b)$$

For the particular case of the truss, integration over the volume of the structure implies multiplying each element or member contribution by the length and cross-sectional area of the bar.

Equations (2.34) are equivalent to equations (2.31): hence we see that

$$\underset{\sim}{\epsilon}^c \equiv \underset{\sim}{\lambda} \quad , \quad \underset{\sim}{X} \equiv \int_V \underset{\sim}{\sigma}\, dV \qquad (2.35a)$$

and

$$\underset{\sim}{K} = \int_V \underset{\sim}{B}^T \underset{\sim}{D}\,\underset{\sim}{B}\, dV \ , \ \underset{\sim}{L} = - \int_V \underset{\sim}{B}^T \underset{\sim}{D}\, dV \ , \ \underset{\sim}{H} = \int_V \underset{\sim}{D}\, dV \quad . \qquad (2.35b)$$

The uniaxial form of the kinetic equation is given by equation (2.5) as

$$\dot{\epsilon}^c = k\, \sigma^m \quad . \qquad (2.36a)$$

Recasting this equation, we write

$$\int_V \underset{\sim}{\sigma}\, dV = \underset{\sim}{\chi}(\dot{\underset{\sim}{\epsilon}}^c)^{1/m} \qquad (2.36b)$$

where $\underset{\sim}{\chi}$ is a diagonal matrix whose entries are $(k)^{1/m}$ multiplied by the volume of the bar.

Equations (2.31) and (2.34) can be uncoupled. Equation (2.31a) is written as

$$\begin{aligned} \underset{\sim}{u} &= \underset{\sim}{K}^{-1}\,\underset{\sim}{P} - \underset{\sim}{K}^{-1}\,\underset{\sim}{L}\,\underset{\sim}{\lambda} \\ &= \underset{\sim}{u}^{E} + \underset{\sim}{u}^{c} \end{aligned} \qquad (2.37a)$$

where

$$\underset{\sim}{u}^{E} = \underset{\sim}{K}^{-1}\,\underset{\sim}{P} \qquad (2.37b)$$

$$\underset{\sim}{u}^{c} = -\,\underset{\sim}{K}^{-1}\,\underset{\sim}{L}\,\underset{\sim}{\lambda} = \underset{\sim}{N}\,\underset{\sim}{\lambda} \quad . \qquad (2.37c)$$

Substituting equation (2.37b) into equation (2.31b), we obtain

$$\underset{\sim}{X} + \underset{\sim}{Z}\,\underset{\sim}{\lambda} = \underset{\sim}{X}^{E} \qquad (2.38a)$$

where

$$\underset{\sim}{Z} = \underset{\sim}{H} - \underset{\sim}{N}^{T}\,\underset{\sim}{K}\,\underset{\sim}{N} \qquad (2.38b)$$

$$\underset{\sim}{X}^{E} = \underset{\sim}{N}^{T}\,\underset{\sim}{P} \quad . \qquad (2.38c)$$

Thus, in the variables $\underset{\sim}{u}^{E}$, $\underset{\sim}{\lambda}$, equations (2.37b) and (2.38a) provide two uncoupled equations. The displacements $\underset{\sim}{u}$ are recovered from equation (2.37a). The solution of equation (2.37b) is straightforward, and is simply a linear elastic problem.

The essential nature of the creep problem is thus expressed by equations (2.38). For the particular case of the truss problem with Norton creep, equation (2.38a) becomes

$$\underset{\sim}{\gamma}(\dot{\underset{\sim}{\epsilon}}^{c})^{1/m} + \underset{\sim}{Z}\,\underset{\sim}{\epsilon}^{c} = \underset{\sim}{X}^{E} \quad . \qquad (2.39)$$

Equation (2.39) is a set of differential equations for the creep problem in a truss, in a form directly comparable with the generic equation (1.3) introduced in Chapter 1. Presented with this equation, it would appear that in setting up the time discretisation we should apply the time integration techniques directly to the creep strain history, rather than to the stress history.

Thus, for the n-th time increment, we put

$$\epsilon^c_n - \epsilon^c_{n-1} = \theta\Delta t\ \dot{\epsilon}^c_n + (1 - \theta)\ \Delta t\ \dot{\epsilon}^c_{n-1}\ ,\ 0 \leq \theta \leq 1 \quad . \tag{2.40}$$

We also write equation (2.39) at time t_n as

$$\gamma(\dot{\underset{\sim}{\epsilon}}^c_n)^{1/m} + \underset{\sim}{Z}\ \underset{\sim}{\epsilon}^c_n = \underset{\sim}{X}^E_n \quad . \tag{2.41}$$

For the implicit case, $\theta > 0$, which will be our prime interest, we substitute $\dot{\underset{\sim}{\epsilon}}^c_n$ from equation (2.40) into equation (2.41), to get

$$\gamma\left\{\frac{1}{\theta\Delta t}\left[\underset{\sim}{\epsilon}^c_n - \underset{\sim}{\epsilon}^c_{n-1}\right] - \left[\frac{1 - \theta}{\theta}\right]\dot{\underset{\sim}{\epsilon}}^c_{n-1}\right\}^{1/m} + \underset{\sim}{Z}\ \underset{\sim}{\epsilon}^c_n = \underset{\sim}{X}^E_n \quad . \tag{2.42}$$

This is a nonlinear equation in $\underset{\sim}{\epsilon}^c_n$, with $\dot{\underset{\sim}{\epsilon}}^c_{n-1}$ given by

$$\dot{\underset{\sim}{\epsilon}}^c_{n-1} = \left[\gamma\left[\underset{\sim}{X}^E_{n-1} - \underset{\sim}{Z}\ \underset{\sim}{\epsilon}^c_{n-1}\right]\right]^m \quad . \tag{2.43}$$

It is of interest to note the solution of equation (2.42) is equivalent to the solution of an unconstrained convex nonlinear programming

problem. Thus

$$\underset{\sim}{\varepsilon}_n^c = \min_{\underset{\sim}{\varepsilon}^c} U_n \tag{2.44}$$

where

$$U_n = \frac{1}{2}\,\underset{\sim}{\varepsilon}^{cT}\,\underset{\sim}{Z}\,\underset{\sim}{\varepsilon}^c + \frac{m\,\theta\Delta t}{m+1}\,\chi\left\{\frac{1}{\theta\Delta t}\left[\underset{\sim}{\varepsilon}^c - \underset{\sim}{\varepsilon}_{n-1}^c\right] - \left[\frac{1-\theta}{\theta}\right]\dot{\underset{\sim}{\varepsilon}}_{n-1}^c\right\}^{\frac{m+1}{m}} - \underset{\sim}{\varepsilon}^{cT}\,\underset{\sim}{X}_n^E \quad . \tag{2.45}$$

The convex nonlinear programming problem, or minimum principle, is an important one in studying the nature of the implicit creep problem, and we shall make use of it in setting up the iterative algorithm and in comparing various assumptions regarding the time integration algorithms. However, finite element analysis is conventionally carried out in terms of solutions for nodal displacement increments and creep strain increments. For this reason we shall use the coupled form of the equations (2.34) rather than the uncoupled form. Further, we shall cast the equations in terms of increments $\Delta\underset{\sim}{u}_n$, $\Delta\underset{\sim}{\varepsilon}_n^c$ rather than in terms of total quantities $\underset{\sim}{u}_n$, $\underset{\sim}{\varepsilon}_n^c$. This will be done in the next section.

2.6 THE INCREMENTAL PROBLEM

We consider the governing equations for the coupled problem given in equations (2.31a), (2.31b) and (2.36b), and write them at time t_n in

the form

$$\underset{\sim}{K}\,\underset{\sim}{u}_n + \underset{\sim}{L}\,\underset{\sim}{\epsilon}^c_n = \underset{\sim}{P}_n \quad , \tag{2.46a}$$

$$\underset{\sim}{L}^T\underset{\sim}{u}_n + \underset{\sim}{H}\,\underset{\sim}{\epsilon}^c_n = -\,\underset{\sim}{X}_n \quad , \tag{2.46b}$$

and

$$\underset{\sim}{X}_n = \underset{\sim}{X}(\dot{\underset{\sim}{\epsilon}}^c_n) \quad . \tag{2.46c}$$

In the incremental problem we write

$$\underset{\sim}{u}_n = \underset{\sim}{u}_{n-1} + \Delta\underset{\sim}{u}_n \quad , \tag{2.47a}$$

$$\underset{\sim}{\epsilon}^c_n = \underset{\sim}{\epsilon}^c_{n-1} + \Delta\underset{\sim}{\epsilon}^c_n \quad . \tag{2.47b}$$

Substituting equations (2.47) into equations (2.46a) and (2.46b), we obtain

$$\begin{aligned}\underset{\sim}{K}\,\Delta\underset{\sim}{u}_n + \underset{\sim}{L}\,\Delta\underset{\sim}{\epsilon}^c_n &= \underset{\sim}{P}_n - (\underset{\sim}{K}\,\underset{\sim}{u}_{n-1} + \underset{\sim}{L}\,\underset{\sim}{\epsilon}^c_{n-1}) \\ &= \underset{\sim}{R}_n \quad ,\end{aligned} \tag{2.48a}$$

$$\underset{\sim}{L}^T\Delta\underset{\sim}{u}_n + \underset{\sim}{H}\,\Delta\underset{\sim}{\epsilon}^c_n = -\,\underset{\sim}{X}_n - (\underset{\sim}{L}^T\underset{\sim}{u}_{n-1} + \underset{\sim}{H}\,\underset{\sim}{\epsilon}^c_{n-1}) \quad . \tag{2.48b}$$

In the <u>explicit case</u> ($\theta = 0$) , we put

$$\Delta\underset{\sim}{\epsilon}^c_n = \underset{\sim}{\epsilon}^c_n - \underset{\sim}{\epsilon}^c_{n-1} = \Delta t\ \dot{\underset{\sim}{\epsilon}}^c_{n-1} \quad . \tag{2.49}$$

From equation (2.46c), written at time t_{n-1} , we may thus write

$$\Delta\underset{\sim}{\epsilon}^c_n = \Delta t\left[\underset{\sim}{\gamma}^{-1}\,\underset{\sim}{X}_{n-1}\right]^m \quad . \tag{2.50}$$

This implies that equations (2.48a) and (2.48b) are effectively uncoupled: we write these equations as

$$\underset{\sim}{K}\,\Delta\underset{\sim}{u}_n = \underset{\sim}{R}_n - \Delta t\,\underset{\sim}{L}\left[\gamma^{-1}\,\underset{\sim}{X}_{n-1}\right]^m \quad , \tag{2.51a}$$

$$\underset{\sim}{X}_n = -\left(\underset{\sim}{L}^T\underset{\sim}{u}_n + \underset{\sim}{H}\,\underset{\sim}{\epsilon}^c_n\right) \quad , \tag{2.51b}$$

and may then proceed to the next time step.

In the <u>implicit case</u> ($\theta > 0$) , the trapezoidal rule gives

$$\Delta\underset{\sim}{\epsilon}^c_n = \underset{\sim}{\epsilon}^c_n - \underset{\sim}{\epsilon}^c_{n-1} = (1-\theta)\,\Delta t\,\dot{\underset{\sim}{\epsilon}}^c_{n-1} + \theta\Delta t\,\dot{\underset{\sim}{\epsilon}}^c_n \quad , \tag{2.52}$$

and hence

$$\dot{\underset{\sim}{\epsilon}}^c_n = \frac{1}{\theta\Delta t}\,\Delta\underset{\sim}{\epsilon}^c_n - \left[\frac{1-\theta}{\theta}\right]\dot{\underset{\sim}{\epsilon}}^c_{n-1} \quad . \tag{2.53}$$

Equation (2.46c) thus becomes

$$\underset{\sim}{X}_n = \gamma\left[\frac{1}{\theta\Delta t}\,\Delta\underset{\sim}{\epsilon}^c_n - \left[\frac{1-\theta}{\theta}\right]\dot{\underset{\sim}{\epsilon}}^c_{n-1}\right]^{1/m} \quad . \tag{2.54}$$

This equation is a one-to-one relation between $\underset{\sim}{X}_n$ and $\Delta\underset{\sim}{\epsilon}^c_n$ which can be regarded as equivalent to a nonlinear elastic (or holonomic) constitutive equation. Its one dimensional representation is shown in Figure 2.1. It is convenient to define a potential function $W_n(\Delta\underset{\sim}{\epsilon}^c)$, and to

write equation (2.54) in the form

$$\underset{\sim}{X}_n = \left.\frac{\partial W_n}{\partial \Delta \underset{\sim}{\epsilon}^c}\right|_{\Delta \underset{\sim}{\epsilon}^c_n} , \tag{2.55a}$$

where

$$W_n = \left[\frac{m}{m+1}\right] \theta \Delta t \, \chi \left[\frac{1}{\theta \Delta t} \Delta \underset{\sim}{\epsilon}^c - \left[\frac{1-\theta}{\theta}\right] \dot{\underset{\sim}{\epsilon}}^c_{n-1}\right]^{\frac{m+1}{m}} . \tag{2.55b}$$

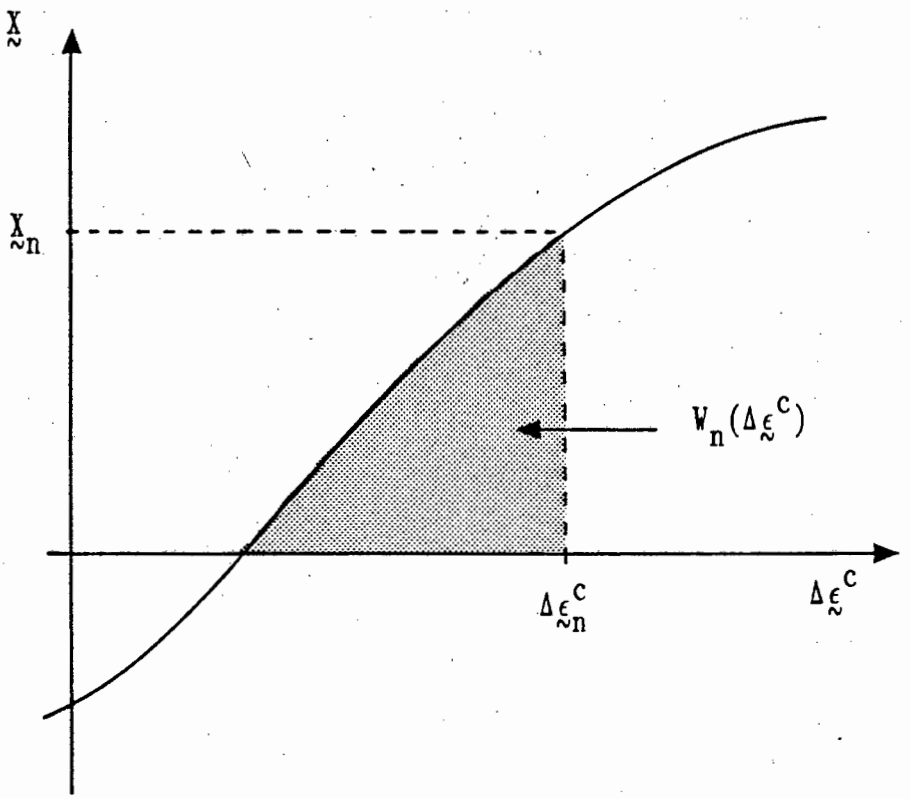

Figure 2.1 : One dimensional representation of equations (2.54) and (2.55)

The potential function W_n is the strain energy associated with the hypothetical elastic material, as shown in Figure 2.1, and is convex.

We now evaluate equations (2.48a) and (2.48b) in the form

$$\underset{\sim}{K}\,\Delta\underset{\sim}{u}_n + \underset{\sim}{L}\,\Delta\underset{\sim}{\epsilon}^c_n = \underset{\sim}{R}_n \qquad (2.56a)$$

$$\underset{\sim}{L}^T\Delta\underset{\sim}{u}_n + \underset{\sim}{H}\,\Delta\underset{\sim}{\epsilon}^c_n + \left.\frac{\partial W_n}{\partial \Delta\underset{\sim}{\epsilon}^c}\right|_{\Delta\underset{\sim}{\epsilon}^c_n} = -\,(\underset{\sim}{L}^T\underset{\sim}{u}_{n-1} + \underset{\sim}{H}\,\underset{\sim}{\epsilon}^c_{n-1}) \quad . \qquad (2.56b)$$

These equations are coupled and nonlinear, and must be solved to provide the solution for the n-th increment.

We can cast the solution as a nonlinear, unconstrained programming problem, in a similar manner to that presented in the previous section. We define

$$U_n = \frac{1}{2}\begin{Bmatrix}\Delta\underset{\sim}{u}\\ \Delta\underset{\sim}{\epsilon}^c\end{Bmatrix}^T\begin{bmatrix}\underset{\sim}{K} & \underset{\sim}{L}\\ \underset{\sim}{L}^T & \underset{\sim}{H}\end{bmatrix}\begin{Bmatrix}\Delta\underset{\sim}{u}\\ \Delta\underset{\sim}{\epsilon}^c\end{Bmatrix} + W(\Delta\underset{\sim}{\epsilon}^c)$$

$$- \Delta\underset{\sim}{u}^T\,\underset{\sim}{R}_n + \Delta\underset{\sim}{\epsilon}^{cT}(\underset{\sim}{L}^T\underset{\sim}{u}_{n-1} + \underset{\sim}{H}\,\underset{\sim}{\epsilon}^c_{n-1}) \quad . \qquad (2.57)$$

Then, $\Delta\underset{\sim}{u}_n$ and $\Delta\underset{\sim}{\epsilon}^c_n$ are given by

$$\min_{\Delta\underset{\sim}{u}\,,\ \Delta\underset{\sim}{\epsilon}^c} \quad U_n \quad . \qquad (2.58)$$

The function U_n is convex, and the only term which is neither linear nor quadratic is $W(\Delta\underset{\sim}{\epsilon}^c)$.

In the next section we shall show that the basic form of this minimum principle holds for a finite element discretisation of a continuous body.

2.7 FINITE ELEMENT FORMULATION FOR MULTI-AXIAL PROBLEMS

Our purpose in this section is to show that the truss formulation described in the previous sections of this chapter may be generalised directly to a finite element discretisation of a three-dimensional continuous body. We shall demonstrate this without a fully rigorous argument, with the object of simply establishing how the various terms in equations (2.56) and (2.57) are interpreted in the continuous case.

In the multi-axial case, we shall assume that the material is isotropic and that creep is associated only with deviatoric components. The constitutive equations for the generalisation of the Norton creep law will thus be written in the form

$$\sigma_{ij} = s_{ij} + \frac{1}{3}\,\delta_{ij}\,\sigma_{kk} \tag{2.59a}$$

$$\epsilon_{ij} = e_{ij} + \frac{1}{3}\,\delta_{ij}\,\epsilon_{kk} \tag{2.59b}$$

$$\sigma_{kk} = 3K\,\epsilon_{kk} \tag{2.59c}$$

$$e_{ij} = e^{e}_{ij} + e^{c}_{ij} \tag{2.59d}$$

$$s_{ij} = 2G\,e^{e}_{ij} \tag{2.59e}$$

$$s_{ij} = \gamma\,\phi^{1/m}\,\frac{\partial\phi}{\partial\dot{e}^{c}_{ij}} = \frac{m}{(m+1)}\,\gamma\,\frac{\partial}{\partial\dot{e}^{c}_{ij}}\,(\phi)^{\frac{m+1}{m}} \tag{2.59f}$$

where

$$\phi = (2\dot{e}^c_{ij}\ \dot{e}^c_{ij})^{1/2} \quad . \tag{2.59g}$$

For the implicit case ($\theta > 0$) , we put, following equation (2.53),

$$\dot{e}^{cn}_{ij} = \frac{1}{\theta\Delta t}\,\Delta e^{cn}_{ij} - \left[\frac{1 - \theta}{\theta}\right]\dot{e}^{c(n-1)}_{ij} \quad , \tag{2.59h}$$

where the superscripts n,(n-1) indicate values at times t_n , t_{n-1} respectively. With this assumption, we may substitute into equation (2.59f) and write

$$s^n_{ij} = \left.\frac{\partial W_n}{\partial \Delta e^c_{ij}}\right|_{\Delta e^{cn}_{ij}} \quad , \tag{2.60a}$$

where

$$W_n(\Delta e^c_{ij}) = \frac{m}{(m+1)}\,\gamma\,\theta\Delta t\,\phi^{\frac{m+1}{m}} \tag{2.60b}$$

$$\phi = \left\{2\left[\frac{1}{\theta\Delta t}\,\Delta e^c_{ij} - \left[\frac{1 - \theta}{\theta}\right]\dot{e}^{c(n-1)}_{ij}\right]\left[\frac{1}{\theta\Delta t}\,\Delta e^c_{ij} - \left[\frac{1 - \theta}{\theta}\right]\dot{e}^{c(n-1)}_{ij}\right]\right\}^{1/2} \quad . \tag{2.60c}$$

We also write corresponding incremental forms of equations (2.59c) and (2.59e);

$$\sigma^n_{kk} = 3K\,\Delta\epsilon^n_{kk} + \sigma^{(n-1)}_{kk} \tag{2.60d}$$

$$s^n_{ij} = 2G\,\Delta e^{en}_{ij} + s^{n-1}_{ij} \quad . \tag{2.60e}$$

We thus arrive at the appropriate form of the constitutive relations.

Assume now that the continuous body which we wish to analyse occupies volume V and has surface S . For simplicity, we assume that the surface S is divided into time independent subregions S_p and S_u . The tractions are prescribed on S_p and the displacements are specified as equal to zero on S_u . Let surface tractions $P_i(x_i,t)$ be given on S_p , and body forces $F_i(x_i,t)$ on V . The displacements, stresses and strains are denoted by $u_i(x_i,t)$, $\sigma_{ij}(x_i,t)$, $\epsilon_{ij}(x_i,t)$.

The body is discretised in a finite element mesh, with global nodal displacements denoted by $u_a(t)$, $a = 1$, ..., M . We then write

$$u_i(x_i,t) = N_{ia}(x_i)\, u_a(t) \quad , \tag{2.61a}$$

$$\epsilon_{ij}(x_i,t) = B_{ija}(x_i)\, u_a(t) \quad , \tag{2.61b}$$

$$e_{ij}(x_i,t) = B^{*}_{ija}(x_i)\, u_a(t) \quad , \tag{2.61c}$$

where N_{ia} are shape functions and B_{ija} , B^{*}_{ija} are deformation tensors derived from the shape functions.

At time t_n the elastic potential of the body can be written as

$$U^e_n = \int_V \frac{3}{2} K\, \epsilon^2_{kk}\, dV + \int_V G(e_{ij} - e^c_{ij})(e_{ij} - e^c_{ij})\, dV$$

$$- \int_{S_p} P^n_i\, u_i\, dS - \int_V F^n_i\, u_i\, dV \quad . \tag{2.62}$$

Introducing the shape functions and deformation tensors of equations (2.61), the discretised finite element form of the potential is

$$U_n^e = \int_V \frac{3}{2} K B_{kk\alpha} B_{kk\beta} u_\alpha u_\beta \, dV$$

$$+ \int_V G(B_{ij\alpha} u_\alpha - e_{ij}^c)(B_{ij\beta} u_\beta - e_{ij}^c) u_\alpha u_\beta \, dV$$

$$- \int_{S_p} P_i^n N_{ij\alpha} u_\alpha \, dV - \int_V F_i^n N_{ij\alpha} u_\alpha \, dV \quad . \qquad (2.63)$$

Integration is carried out on an element by element basis using Gauss quadrature. We define the creep strains only at the Gauss points, and, changing to vector notation, may write equation (2.63) as

$$U_n^e = \frac{1}{2} \underset{\sim}{u}^T \underset{\sim}{K} \underset{\sim}{u} + \underset{\sim}{u}^T \underset{\sim}{L} \underset{\sim}{\epsilon}^c + \frac{1}{2} \underset{\sim}{\epsilon}^{cT} \underset{\sim}{H} \underset{\sim}{\epsilon}^c - \underset{\sim}{u}^T \underset{\sim}{P}_n \qquad (2.64)$$

where $\underset{\sim}{u}$, $\underset{\sim}{\epsilon}^c$ denote global vectors of nodal displacements and Gauss point creep strains, and $\underset{\sim}{K}$, $\underset{\sim}{L}$, $\underset{\sim}{H}$ and the nodal loads $\underset{\sim}{P}_n$ are defined through equation (2.63).

The stationary value of U_n^e with respect to $\underset{\sim}{u}$ gives the global equilibrium equation corresponding to equation (2.46a). This may be cast in incremental form by the same process as that described in the previous section to give

$$\underset{\sim}{K} \Delta \underset{\sim}{u}_n + \underset{\sim}{L} \Delta \underset{\sim}{\epsilon}_n^c = \underset{\sim}{R}_n \quad . \qquad (2.65)$$

The second equation in the coupled set of internal variable equations (equation (2.46b) or (2.56b)) essentially expresses the requirement

that s_{ij}^{n} computed from equations (2.60a) and (2.60e) should be the same. Thus we start with the condition

$$2G\,\Delta e_{ij}^{en} + s_{ij}^{n-1} = \left.\frac{\partial W_n}{\partial \Delta e_{ij}^{c}}\right|_{\Delta e_{ij}^{cn}} , \tag{2.66a}$$

and rewrite it as

$$-\,2G\,\Delta e_{ij}^{n} + 2G\,\Delta e_{ij}^{cn} + \left.\frac{\partial W_n}{\partial \Delta e_{ij}^{c}}\right|_{\Delta e_{ij}^{cn}} = -\,(-\,2G\,e_{ij}^{n-1} + 2G\,e_{ij}^{c(n-1)}) \quad . \tag{2.66b}$$

We now introduce the deformation tensor B_{ija}^{*} and integrate over the body, element by element using Gaussian quadrature. Introducing vector notation, this leads to

$$\underset{\sim}{L}^{T}\Delta u_{n} + \underset{\sim}{H}\,\Delta \underset{\sim}{\epsilon}_{n}^{c} + \left.\frac{\partial W_n}{\partial \Delta \underset{\sim}{\epsilon}^{c}}\right|_{\Delta \underset{\sim}{\epsilon}_{n}^{c}} = -\,(\underset{\sim}{L}^{T}\underset{\sim}{u}_{n-1} + \underset{\sim}{H}\,\underset{\sim}{\epsilon}_{n-1}^{c}) \quad . \tag{2.67}$$

In this integration process $\underset{\sim}{L}$ and $\underset{\sim}{H}$ are defined ($\underset{\sim}{L}$ being the same matrix that appears in equation 2.65); however we modify W_n to become

$$W_n = \frac{m}{(m+1)}\,\theta\Delta t\,\chi\,\phi^{\frac{m+1}{m}} , \tag{2.68a}$$

$$\phi = \left\{2\left[\frac{1}{\theta\Delta t}\,\Delta \underset{\sim}{\epsilon}^{c} - \left[\frac{1-\theta}{\theta}\right]\dot{\underset{\sim}{\epsilon}}_{n-1}^{c}\right]^{T}\left[\frac{1}{\theta\Delta t}\,\Delta \underset{\sim}{\epsilon}^{c} - \left[\frac{1-\theta}{\theta}\right]\dot{\underset{\sim}{\epsilon}}_{n-1}^{c}\right]\right\}^{1/2} . \tag{2.68b}$$

The matrix χ is a diagonal matrix whose entries consist of the value of γ at each Gauss point multiplied by the Gauss point weight.

It should be noted, however, that in equation (2.67) each Gauss point is uncoupled from any other; this is evident from equation (2.66a), which is a pointwise relation.

Equations (2.65) and (2.67) are identical to equations (2.56a) and (2.56b), and indicate that with a suitable re-interpretation of the terms the formulation given for the truss is generally applicable. In particular, the minimum principle of equations (2.57) and (2.58) may be applied to a finite element discretisation of a continuous body.

2.8 CONCLUSION

A uniaxial framework was adopted to demonstrate different approaches to the formulation of the creep problem. The spatial discretisation techniques of the finite element method are combined with a suitable time discretisation scheme to formulate governing equations. At any discrete instant in time, the overall equilibrium conditions must be satisfied and the internal variables (creep strains) updated according to the kinetic relations. This can however only be achieved through an approximation of the solution history between consecutive solution instants, because the rate form of the creep laws leads to a differential equation for the creep problem. The time integration scheme which represents the selected approximation of the transient response over the step is combined with the governing equilibrium and kinetic equation to form the basis of the numerical solution procedures.

In the standard solution procedures, a constant weighted average value of the stress over any time step is assumed. This assumption, and the weighting parameter α , is used to derive a general creep solution algorithm. If a forward difference relation for the stress change is assumed, an explicit procedure is formulated. While the explicit procedure is computationally efficient because the elastic stiffness matrix is used throughout, it is limited by severe time step length restrictions to ensure stability of the procedure. An implicit difference relation for the stresses requires a Newton-Raphson iterative procedure to solve the resulting system of nonlinear equations in the kinematic variables. These schemes require continuous reformation of the stiffness matrix, but are bounded in time step sizes by the accuracy considerations only.

The internal variable formulation provided a general framework, applicable to uniaxial and multi-axial problems, in which the essential nature of the creep problem was explored. The creep problem was cast as a coupled problem in displacements and creep strains, or alternatively it was shown to be a fully uncoupled problem in the elastic displacements and the creep strains. We found that, in both forms, the creep response was contained in a nonlinear first order ordinary differential equation in the creep strains only. This result is significant because it shows that an integration scheme which approximates the creep strain history, rather than the stresses, is appropriate.

Furthermore, the creep problem was cast in an incremental form, equivalent to that of a nonlinear elastic material. This demonstrated the holonomic nature of the creep problem. The solution of the

incremental problem is identical to that of a nonlinear, unconstrained mathematical programming problem. The minimum principle, shown to be equally applicable to uniaxial and continuous bodies, can be exploited in a numerical solution algorithm. This is done in the next chapter.

CHAPTER 3

A NUMERICAL ALGORITHM FOR THE SOLUTION OF CREEP PROBLEMS BY THE FINITE ELEMENT METHOD

3.1 INTRODUCTION

The creep problem has been posed as a system of nonlinear equations in the kinematic variables (displacements and creep strains). We have formulated an incremental form of the two governing equations: the first enforcing a global equilibrium condition and the second relating to the internal state of the body or structure. The standard numerical strategies for the solution of these equations are usually based on Newton-Raphson incremental approaches in which improved estimates of the incremental solutions are determined iteratively. One such strategy is to use one equation to predict the displacements $\Delta \underset{\sim}{u}$ and the other to improve the creep strains $\Delta \underset{\sim}{\varepsilon}^{c}$. This follows the thrust of algorithms which are widely used to solve creep problems in finite element analysis [5,6,7].

Alternatively, we have posed the solution of the incremental problem as a nonlinear, unconstrained mathematical programming problem. The numerical solution algorithm can therefore be formulated as a mathematical programming problem resulting from the minimisation of a convex potential function. In this chapter we show how this approach leads to a framework that is equivalent to that of the Newton-Raphson methods. The formulation is developed to present a general solution algorithm in which consistent predictors for different integration schemes and constitutive laws are easily implemented [27].

The algorithm has been developed for the uniaxial and continuum framework developed in Chapter 2. Uniaxial creep is again governed by Norton's power law, while multi-axial creep is governed by a von Mises type potential function. These simple models have been chosen for illustrative purposes: any form of the creep constitutive relationship can be accommodated. The solution algorithm has been coded and implemented in the finite element package NOSTRUM [28], developed by the Applied Mechanics Research Unit at the University of Cape Town.

Simple uniaxial problems are analysed to examine the effects of the time integration parameters. A particular form of the integration parameter is demonstrated to be more accurate and efficient. Further uniaxial and multi-axial problems exhibiting typical creep behaviour are analysed to illustrate the numerical characteristics of the proposed solution algorithm.

3.2 THE MATHEMATICAL PROGRAMMING PROBLEM

In Section 2.6 we showed that the solution to the creep problem corresponds to the minimisation of a potential function. At any time t_n , the incremental displacements $\Delta \underset{\sim}{u}_n = \underset{\sim}{u}_n - \underset{\sim}{u}_{n-1}$ and incremental creep strains $\Delta \underset{\sim}{\epsilon}^c_n = \underset{\sim}{\epsilon}^c_n - \underset{\sim}{\epsilon}^c_{n-1}$ are given by

$$\min_{\Delta \underset{\sim}{u} \, , \, \Delta \underset{\sim}{\epsilon}^c} \quad U_n \quad , \tag{3.1a}$$

where

$$U_n = \frac{1}{2}\begin{Bmatrix}\Delta u_n \\ \Delta \epsilon_n^c\end{Bmatrix}^T \begin{bmatrix} K & L \\ L^T & H \end{bmatrix} \begin{Bmatrix}\Delta u_n \\ \Delta \epsilon_n^c\end{Bmatrix} + W_n(\Delta \epsilon_n^c)$$

$$- \Delta u^T \left\{ P_n - K\, u_{n-1} - L\, \epsilon_{n-1}^c \right\} + \Delta \epsilon^{cT} \left\{ L^T u_{n-1} + H\, \Delta \epsilon_{n-1}^c \right\} \quad . \tag{3.1b}$$

The function U_n is convex and $W(\Delta \epsilon^c)$ is the only term which is not linear nor quadratic in Δu and $\Delta \epsilon^c$. Specific forms of W_n have been formulated in equation (2.55b) for uniaxial and in equation (2.60b) for uniaxial and multi-axial problems respectively.

Let us start with the i-th estimates ${}^i\Delta u_n$ and ${}^i\Delta \epsilon_n^c$ of the solution at time t_n and put

$${}^{i+1}\Delta u_n = {}^i\Delta u_n + \Delta \hat{u} \quad , \tag{3.2a}$$

$${}^{i+1}\Delta \epsilon_n^c = {}^i\Delta \epsilon_n^c + \Delta \hat{\epsilon}^c \quad . \tag{3.2b}$$

When we substitute these expressions into equation (3.1b) the convex functional becomes

$$U_n = \frac{1}{2}\begin{Bmatrix}\Delta \hat{u} \\ \Delta \hat{\epsilon}^c\end{Bmatrix}^T \begin{bmatrix} K & L \\ L^T & H \end{bmatrix} \begin{Bmatrix}\Delta \hat{u} \\ \Delta \hat{\epsilon}^c\end{Bmatrix} + \frac{1}{2}\begin{Bmatrix}{}^i\Delta u_n \\ {}^i\Delta \epsilon_n^c\end{Bmatrix}^T \begin{bmatrix} K & L \\ L & H \end{bmatrix} \begin{Bmatrix}{}^i\Delta u_n \\ {}^i\Delta \epsilon_n^c\end{Bmatrix}$$

$$+ W_n\left[{}^i\Delta \epsilon_n^c + \Delta \hat{\epsilon}^c \right] - \Delta \hat{u}^T \left\{ P_n - K\, u_{n-1} + K\, {}^i\Delta u_n - L\, \epsilon_{n-1}^c + L\, {}^i\Delta \epsilon_n^c \right\}$$

$$+ \Delta \hat{\epsilon}^{cT} \left\{ L^T u_{n-1} + L^T\, {}^i\Delta u_n + H\, \Delta \epsilon_{n-1}^c + H\, {}^i\Delta \epsilon_n^c \right\}$$

$$= \frac{1}{2} \begin{Bmatrix} \Delta\hat{\underset{\sim}{u}} \\ \Delta\hat{\underset{\sim}{\epsilon}}^c \end{Bmatrix}^T \begin{bmatrix} \underset{\sim}{K} & \underset{\sim}{L} \\ \underset{\sim}{L}^T & \underset{\sim}{H} \end{bmatrix} \begin{Bmatrix} \Delta\hat{\underset{\sim}{u}} \\ \Delta\hat{\underset{\sim}{\epsilon}}^c \end{Bmatrix} + W\left[{}^i\Delta\underset{\sim}{\epsilon}_n^c + \Delta\hat{\underset{\sim}{\epsilon}}^c\right]$$

$$- \Delta\hat{\underset{\sim}{u}}^T \, {}^i\underset{\sim}{R}_n - \Delta\hat{\underset{\sim}{\epsilon}}^{cT} \, {}^i\underset{\sim}{X}_n \qquad (3.3a)$$

where

$${}^i\underset{\sim}{R}_n = \underset{\sim}{P}_n - \underset{\sim}{K}\left\{\underset{\sim}{u}_{n-1} + {}^i\Delta\underset{\sim}{u}_n\right\} - \underset{\sim}{L}\left\{\underset{\sim}{\epsilon}^c_{n-1} + {}^i\Delta\underset{\sim}{\epsilon}^c_n\right\} \qquad (3.3b)$$

$${}^i\underset{\sim}{X}_n = - \underset{\sim}{L}^T\left\{\underset{\sim}{u}_{n-1} + {}^i\Delta\underset{\sim}{u}_n\right\} - \underset{\sim}{H}\left\{\underset{\sim}{\epsilon}^c_{n-1} + {}^i\Delta\underset{\sim}{\epsilon}^c_n\right\} \quad . \qquad (3.3c)$$

In order to find a consistent approach to the minimisation of U_n for the general case, we adopt a two-step strategy in which a predictor and a corrector step is used. In the predictor step we linearise the problem by using a quadratic approximation of W_n . This allows the computation of $\Delta\hat{\underset{\sim}{u}}$ or ultimately ${}^{i+1}\Delta\underset{\sim}{u}_n$. The corrector step is used to find the associated values of $\Delta\hat{\underset{\sim}{\epsilon}}^c_n$, and hence ${}^{i+1}\Delta\underset{\sim}{\epsilon}^c_n$, and at the same time to evaluate an updated estimate of ${}^{i+1}\underset{\sim}{X}_n$.

3.2.1 The Predictor Step

In order to formulate a consistent predictor for the minimisation of U_n , we write a quadratic approximation of W_n so that

$$W_n\left[{}^{i+1}\Delta\underset{\sim}{\epsilon}^c_n\right] = W_n\left[{}^i\Delta\underset{\sim}{\epsilon}^c_n + \Delta\hat{\underset{\sim}{\epsilon}}^c\right]$$

$$\approx W_n\left[{}^{i}\Delta\underset{\sim}{\epsilon}^{c}_{n}\right] + \Delta\hat{\underset{\sim}{\epsilon}}^{c^T}\left[\left.\frac{\partial W_n}{\partial \Delta\underset{\sim}{\epsilon}^{c}}\right|_{{}^{i}\Delta\underset{\sim}{\epsilon}^{c}}\right]$$

$$+ \frac{1}{2}\,\Delta\hat{\underset{\sim}{\epsilon}}^{c^T}\left[\left.\frac{\partial^2 W_n}{\partial\Delta\underset{\sim}{\epsilon}^{c^T}\partial\Delta\underset{\sim}{\epsilon}^{c}}\right|_{{}^{i}\Delta\underset{\sim}{\epsilon}^{c}_{n}}\right]\Delta\hat{\underset{\sim}{\epsilon}}^{c} + \text{higher order terms}$$

$$\approx W_n\left[{}^{i}\Delta\underset{\sim}{\epsilon}^{c}_{n}\right] + \Delta\hat{\underset{\sim}{\epsilon}}^{c^T}\,{}^{i}\underset{\sim}{X}_{n} + \frac{1}{2}\,\Delta\hat{\underset{\sim}{\epsilon}}^{c^T}\,\underset{\sim}{A}\,\Delta\hat{\underset{\sim}{\epsilon}}^{c} \qquad (3.4a)$$

where

$$\underset{\sim}{A} = \left.\frac{\partial^2 W_n}{\partial\Delta\underset{\sim}{\epsilon}^{c^T}\partial\Delta\underset{\sim}{\epsilon}^{c}}\right|_{{}^{i}\Delta\underset{\sim}{\epsilon}^{c}_{n}} \quad . \qquad (3.4b)$$

The quadratic approximation of the convex functional can now be written as

$$U_n^* = \frac{1}{2}\begin{Bmatrix}\Delta\hat{\underset{\sim}{u}}\\ \Delta\hat{\underset{\sim}{\epsilon}}^{c}\end{Bmatrix}^T\begin{bmatrix}\underset{\sim}{K} & \underset{\sim}{L}\\ \underset{\sim}{L}^T & \underset{\sim}{H}\end{bmatrix}\begin{Bmatrix}\Delta\hat{\underset{\sim}{u}}\\ \Delta\hat{\underset{\sim}{\epsilon}}^{c}\end{Bmatrix} + W_n\left[{}^{i}\Delta\underset{\sim}{\epsilon}^{c}\right]$$

$$+ \frac{1}{2}\,\Delta\hat{\underset{\sim}{\epsilon}}^{c^T}\,\underset{\sim}{A}\,\Delta\hat{\underset{\sim}{\epsilon}}^{c} - \Delta\underset{\sim}{u}^T\,{}^{i}\underset{\sim}{R}_{n} \quad . \qquad (3.5)$$

The least value of U_n^* is then given by the solutions to

$$\underset{\sim}{K}\,\Delta\hat{\underset{\sim}{u}} + \underset{\sim}{L}\,\Delta\hat{\underset{\sim}{\epsilon}}^{c} = {}^{i}\underset{\sim}{R}_{n} \quad , \qquad (3.6a)$$

$$\underset{\sim}{L}^T\Delta\hat{\underset{\sim}{u}} + (\underset{\sim}{H} + \underset{\sim}{A})\Delta\hat{\underset{\sim}{\epsilon}}^{c} = 0 \quad . \qquad (3.6b)$$

By rewriting equation (3.6b) as

$$\Delta\hat{\underset{\sim}{\epsilon}}^{c} = (\underset{\sim}{H} + \underset{\sim}{A})^{-1}\ \underset{\sim}{L}^{T}\Delta\hat{\underset{\sim}{u}} \tag{3.7}$$

we can uncouple the displacements in equation (3.6a) to obtain an expression for the iterative incremental displacements:

$$\underset{\sim}{K}^{*}\ \Delta\hat{\underset{\sim}{u}} = {}^{i}\underset{\sim}{R}_{n} \tag{3.8}$$

where

$$\underset{\sim}{K}^{*} = \left\{\underset{\sim}{K} - \underset{\sim}{L}[\underset{\sim}{H} + \underset{\sim}{A}]^{-1}\ \underset{\sim}{L}^{T}\right\} \tag{3.9}$$

and ${}^{i}\underset{\sim}{R}$ is an out-of-balance nodal force vector defined in equation (3.3b).

Equation (3.8) and the modified stiffness matrix K^{*} can readily be identified as the same form as the tangential stiffness matrix in the implicit solution algorithm in equation (2.25). This minimisation approach, therefore, results in a formulation that is identical to that of standard Newton-Raphson solution algorithms. Of interest is to note that the consistent predictor is contained in the $\underset{\sim}{A}$ matrix in equation (3.9), which is a result of the quadratic approximation of W_n . We will consider the effects of different choices of W_n in the next chapter.

3.2.2 The Corrector Step

The predictor step achieves an improved estimate ${}^{i+1}\Delta\underset{\sim}{u}_{n}$ for a given previous estimate of ${}^{i}\underset{\sim}{\epsilon}^{c}_{n}$. A subsequent corrector step will enable us

to determine updated estimates of ${}^{i}\Delta\underset{\sim}{\epsilon}_n^c$ and ${}^{i}\underset{\sim}{X}_n$ resulting from the new displacements. This step corresponds to minimising $U_n(\Delta\hat{\underset{\sim}{u}}\ ,\ \Delta\hat{\underset{\sim}{\epsilon}}^c)$ with respect to $\Delta\hat{\underset{\sim}{\epsilon}}^c$, holding $\Delta\hat{\underset{\sim}{u}}$ fixed. The minimum is given by

$$\underset{\sim}{L}^T\ {}^{i+1}\Delta\underset{\sim}{u}_n + \underset{\sim}{H}^T\ {}^{i+1}\Delta\underset{\sim}{\epsilon}_n^c + \left.\frac{\partial W_n}{\partial \Delta\underset{\sim}{\epsilon}^c}\right|_{{}^{i+1}\Delta\underset{\sim}{\epsilon}_n^c} + (\underset{\sim}{L}^T\underset{\sim}{u}_{n-1} + \underset{\sim}{H}\ \underset{\sim}{\epsilon}_{n-1}^c) = 0 \quad , \tag{3.10a}$$

that is

$$\left.\frac{\partial W_n}{\partial \Delta\underset{\sim}{\epsilon}^c}\right|_{{}^{i+1}\Delta\underset{\sim}{\epsilon}_n^c} = -\ \underset{\sim}{L}^T(\underset{\sim}{u}_{n-1} + {}^{i+1}\Delta\underset{\sim}{u}_n) - \underset{\sim}{H}(\underset{\sim}{\epsilon}_{n-1}^c + {}^{i+1}\Delta\underset{\sim}{\epsilon}_n^c) \quad . \tag{3.10b}$$

The corrector step, contained in equation (3.10b), is used to update $\underset{\sim}{\epsilon}_n^c$ and $\underset{\sim}{X}_n$ for the latest estimate of displacements ${}^{i+1}\underset{\sim}{u}_n$. It should be noted that equation (3.10b) results from a balance of the internal force state of the body or structure. The left-hand side corresponds to the potential form of the creep law defined in equation (2.55) as

$${}^{i+1}\underset{\sim}{X}_n = \left.\frac{\partial W_n}{\partial \Delta\underset{\sim}{\epsilon}^c}\right|_{{}^{i+1}\Delta\underset{\sim}{\epsilon}^c} \tag{3.11}$$

while the right-hand side of equation (3.10b) satisfies the elastic relation

$$-\ {}^{i+1}\underset{\sim}{X}_n = \underset{\sim}{L}^T\ {}^{i+1}\underset{\sim}{u}_n + \underset{\sim}{H}\ {}^{i+1}\underset{\sim}{\epsilon}_n^c \quad . \tag{3.12}$$

The structure of equations (3.10a,b) is such that each sample point is completely uncoupled from the other. For finite element computation it is convenient to consider them as a set of pointwise relations, so that they are solved in a loop over all points in the structure rather than in a global computation. The corrector step is implemented by solving equation (3.10) and updating ${}^{i+1}\underset{\sim}{\sigma}_n$, ${}^{i+1}\underset{\sim}{\epsilon}^c_n$ in an element by element fashion. We evaluate the stresses first. This is done by eliminating ${}^{i+1}\Delta\underset{\sim}{\epsilon}^c_n$ from equation (3.10) through the trapezoidal rule and the constitutive law $\dot{\underset{\sim}{\epsilon}}^c_n = \underset{\sim}{f}(\underset{\sim}{X}_n)$. For a trapezoidal approximation of the creep strain increment

$$ {}^{i+1}\Delta\underset{\sim}{\epsilon}^c_n = (1 - \theta)\Delta t\ \dot{\underset{\sim}{\epsilon}}^c_{n-1} + \theta\Delta t\ {}^{i+1}\dot{\underset{\sim}{\epsilon}}^c_n \qquad (3.13) $$

we find

$$ {}^{i+1}\underset{\sim}{X}_n + \theta\Delta t\ \underset{\sim}{H}\ \underset{\sim}{f}(\underset{\sim}{X}_n) = -\ \underset{\sim}{L}(\underset{\sim}{u}_{n-1} + {}^{i+1}\Delta\underset{\sim}{u}_n) - \underset{\sim}{H}(\underset{\sim}{\epsilon}^c_{n-1} + (1 - \theta)\ \Delta t\ \dot{\underset{\sim}{\epsilon}}^c_{n-1}) \quad . \qquad (3.14) $$

By uncoupling equation (3.14) and omitting volume integrations, the sample point stresses are contained in

$$ {}^{i+1}\underset{\sim}{\sigma}_n + \theta\Delta t\ \underset{\sim}{D}\ \underset{\sim}{f}(\underset{\sim}{\sigma}_n) = \underset{\sim}{D}\ \underset{\sim}{B}(\underset{\sim}{u}_{n-1} + {}^{i+1}\Delta\underset{\sim}{u}_n) $$

$$ - \underset{\sim}{D}(\underset{\sim}{\epsilon}^c_{n-1} + (1 - \theta)\ \Delta t\ \dot{\underset{\sim}{\epsilon}}^c_{n-1}) \quad . \qquad (3.15) $$

This is easily solved through Newton's method or equivalent techniques. Creep strain rates are then updated from the constitutive laws and substituted into the time integration schemes to determine ${}^{i+1}\underset{\sim}{\epsilon}^c_n$.

The updated solutions can now serve as improved estimates for the next sequence of predictor-corrector steps, until the convex functional U_n reaches a minimum.

3.2.3 Convergence Criteria

In the iterative predictor-corrector scheme our objective is to minimise U_n in equations (3.1) or (3.3). These equations provide us with the necessary conditions to monitor the convergence of the algorithm. In fact, assessment of whether the revised estimates provided by each iteration are indeed improvements, are based on whether the value of U_n in equation (3.3) is decreased after the iteration.

In the iterative process, the least value of U_n is achieved when ${}^{i}\underset{\sim}{R} = 0$, which occurs when $\Delta\hat{\underset{\sim}{u}} = 0$ and $\Delta\hat{\underset{\sim}{\epsilon}}^{c} = 0$. The out-of-balance nodal force vector ${}^{i}\underset{\sim n}{R}$ is computed in every iteration and therefore provides a convenient indication of the convergence of the iterative cycle within each time step. If the estimates of displacement ${}^{i+1}\underset{\sim n}{u}$ and internal variables ${}^{i+1}\underset{\sim n}{\epsilon}^{c}$ are sufficiently accurate, the equilibrium conditions are satisfied and ${}^{i}\underset{\sim n}{R}$ vanishes. In practice, because of numerical round-off errors, we apply the condition that $|{}^{i}\underset{\sim n}{R}|$ is small, that is within a specified tolerance. The out-of-balance force therefore provides a natural check on the convergence and on the accuracy of solution algorithms. This convergence criterion is commonly used in nonlinear finite element analysis.

If, however, we apply the condition that $|{}^{i}\underset{\sim n}{R}|$ is tolerably small, it is equivalent to the requirement that $|\Delta\hat{\underset{\sim}{u}}|$ and $|\Delta\hat{\underset{\sim}{\epsilon}}^{c}|$ are small. Within

the iterative cycle, we then require only that successive improvements $|\Delta\hat{\underset{\sim}{u}}|$ and $|\Delta\hat{\underset{\sim}{\varepsilon}}^c|$ become tolerably small. This means that successive updates of ${}^{i+1}\underset{\sim}{u}_n$ and ${}^{i+1}\underset{\sim}{\varepsilon}^c_n$ will remain unchanged. In view of the fact that the predictor displacements will always satisfy equilibrium and that we are actually solving a nonlinear differential equation in the creep strains, the accurate solution of $\underset{\sim}{\varepsilon}^c_n$ provides a sensible convergence criterion. For this reason, the iterative cycle may be considered to have converged if ${}^{i+1}\underset{\sim}{\varepsilon}^c_n \approx {}^{i}\underset{\sim}{\varepsilon}^c_n$, or simply ${}^{i+1}\dot{\underset{\sim}{\varepsilon}}^c_n \approx {}^{i}\dot{\underset{\sim}{\varepsilon}}^c_n$, at every sample point.

3.3 NUMERICAL IMPLEMENTATION

The solution algorithm developed in earlier sections has been implemented in NOSTRUM [28], a general purpose nonlinear finite element package for two-dimensional problems. The following basic capabilities of the program were used:

1. An element library with linear 2-noded elements for uniaxial problems or 4, 8 and 9-noded isoparametric quadrilateral elements with optional 2x2 and 3x3 Gaussian integration;
2. Linear elastic analysis for given loads, including element by element stiffness formulation and the solution of a system of equations with a front solver.

The solution procedure is used for the transient analysis of structures undergoing creep under constant or time-variable loading. The essential steps in the solution algorithm are given below:

1. Perform an elastic analysis for the first load increment to evaluate the initial displacement and stress fields $\underset{\sim}{u}_0$ and $\underset{\sim}{\sigma}_0$.
2. Compute the initial creep strains and creep strain rates according to the constitutive laws in equations (2.5) or (2.59).
3. For the first iteration of a new time step, predict the end of time step values ${}^{i}\underset{\sim}{\epsilon}^{c}_{n}$ and ${}^{i}\underset{\sim}{\dot{\epsilon}}^{c}_{n}$ for steady state creep, assuming no stress redistribution.
4. Formulate modified stiffness matrices $\underset{\sim}{K}^{*}$ and residual force vector ${}^{i}\underset{\sim}{R}$ according to equations (3.9) and (3.3b).
5. Solve for the predicted incremental displacements $\Delta\underset{\sim}{\hat{u}}_n$ and evaluate the updated stresses ${}^{i+1}\underset{\sim}{\sigma}_n$ from the nonlinear expression (3.15).
6. Compute the updated estimates of ${}^{i+1}\underset{\sim}{\dot{\epsilon}}^{c}_{n}$ and ${}^{i+1}\underset{\sim}{\epsilon}^{c}_{n}$.
7. If the creep strain rate ${}^{i+1}\underset{\sim}{\dot{\epsilon}}^{c}_{n}$ has not converged at all sample points, use the updated estimates to iterate from step 4 until ${}^{i+1}\underset{\sim}{\dot{\epsilon}}^{c}_{n} = {}^{i}\underset{\sim}{\dot{\epsilon}}^{c}_{n}$ within the selected tolerance.
8. Once convergence has been achieved, the end of time step results are updated. The next time step is started from step 3.

This analysis procedure is continued until the response over the entire time-history has been computed.

3.4 TIME INTEGRATION PARAMETER STUDIES

The time discretisation has been achieved by adopting the general trapezoidal rule for the creep strain incrementation. The solution

procedure is in essence solving the nonlinear first order differential equation, formulated in equation (2.41) as

$$\underset{\sim}{\gamma}(\dot{\underset{\sim}{\epsilon}}^{c})^{1/m} + \underset{\sim}{Z}(\underset{\sim}{\epsilon}^{c}) = \underset{\sim}{N}^{T}\underset{\sim}{P} \quad , \tag{3.15}$$

by a simple 2-step recurrence scheme. The stability and convergence of the procedure is thus contained in the numerical solution of the above differential problem. For a linear creep law (power index m=1) we will expect the characteristics discussed for linear first order differential equations in the introductory chapter. The choice of the integration parameter θ determines conditional and unconditional stability, accuracy and convergence. For the general nonlinear problem, the choice of θ is again expected to influence the numerical response. We can demonstrate the effects that θ has on the performance of the solution procedure by analysing a simple two-bar truss structure.

3.4.1 Two-bar Truss : Constant Loads

The two-bar truss problem depicted in Figure 3.1 presents simple uniaxial redistribution problems. The effects of θ over a range of nonlinear creep laws is demonstrated. The power index m ranging from 1 to 5 was selected. Elastic and fluidity constants are chosen to give similar redistribution behaviour in each case. Since the material properties are chosen for mathematical convenience, the units are omitted.

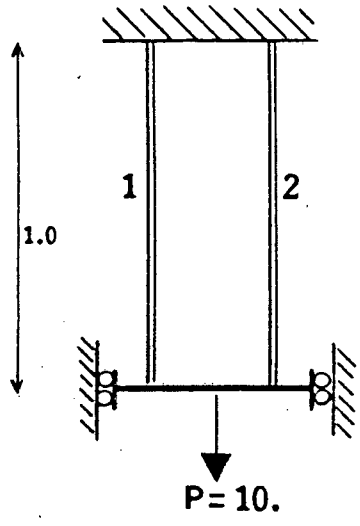

Case	Member	E	k	m
(a)	1	100	0.010	1
	2	50	0.025	1
(b)	1	100	32×10^{-5}	3
	2	50	0.5×10^{-5}	3
(c)	1	100	1024×10^{-8}	5
	2	50	1×10^{-8}	5

All cross-sectional areas = 1.0

Figure 3.1 : Geometric and material parameters for the two-bar truss problem

Table 3.1 : Single step accuracy for the trapezoidal rule. Percentage errors in the prediction of stresses and creep strains in bar 1 (* denotes θ = m/m+1).

CASE	THETA	ERROR PERCENTAGES: e% Stress	Creep Strain
(a) m = 1 (Δt=2.)	0.20	-17.248493	16.138398
	0.30	-11.731527	10.977014
	0.40	-6.904462	6.460198
	* 0.50	-2.645155	2.474716
	0.60	1.140731	-1.067505
	0.70	4.528415	-4.236729
	0.80	7.576984	-7.089281
	0.90	10.335343	-9.670167
	1.00	12.842964	-12.016366
(b) m = 3 (Δt=2.)	0.20	-58.461398	83.596105
	0.30	-43.592368	62.607733
	0.40	-30.241624	43.634158
	0.50	-18.658416	27.099802
	0.60	-8.837424	13.041439
	0.70	-0.602857	1.223226
	* 0.75	2.995286	-3.931085
	0.80	6.288454	-8.659889
	0.90	12.076639	-16.975297
	1.00	16.970924	-24.009964
(c) m = 5 (Δt=2.)	0.20	no result	no result
	0.30	no result	no result
	0.40	-69.354873	117.997312
	0.50	-48.371984	82.288510
	0.60	-28.923772	49.203553
	0.70	-12.728014	21.670021
	0.80	-0.402444	0.729639
	* 0.83	2.944185	-4.954056
	0.90	8.709055	-14.742694
	1.00	15.524858	-26.313337

In each case, the redistribution problem is analysed using a single time step with θ ranging from 0.2 to 1.0 to monitor the predictions of stresses and creep strains. The percentage errors for predictions in member 1 are listed in Table 3.1. The error is computed from

$$e\% = 100 \times \left[\frac{x - \bar{x}}{\bar{x}}\right] \tag{3.16}$$

where x is the numerical prediction and $\bar{x}$ is the baseline solution. In this example no analytical solution was available, so the baseline solution was obtained from numerical analyses using very small time steps.

The trends in Table 3.1 show that no one constant value of θ gives most accurate results. The choice

$$\theta = m/m+1 \tag{3.17}$$

where m is the power index, appears to provide consistently good accuracy. Intuitively, a suitable choice of θ clearly depends on the nonlinearity of the creep law and the redistribution from initial to final stress over the step. The ratio $\theta = m/m+1$ appears to be near optimal in each case.

3.4.2 Two-bar Truss : Variable Loads

The performance of the solution procedure for different choices of θ under variable loads is demonstrated. The stress redistribution

history for the two-bar truss for the case m = 5 (Figure 3.1(c)) is depicted in Figure 3.2 for

(a) a constant load P = 10.0,

(b) an increasing load P = 10.0 + t,

and (c) a decreasing load P = 10.0 - t/2.

In these figures the results obtained for values of θ set to 1/2, 2/3, m/m+1 and 1.0 using Δt = 2.0 are compared to the baseline solution. Again the ratio of θ = m/m+1 consistently showed faster convergence and superior accuracy in predicting the displacements and member stresses.

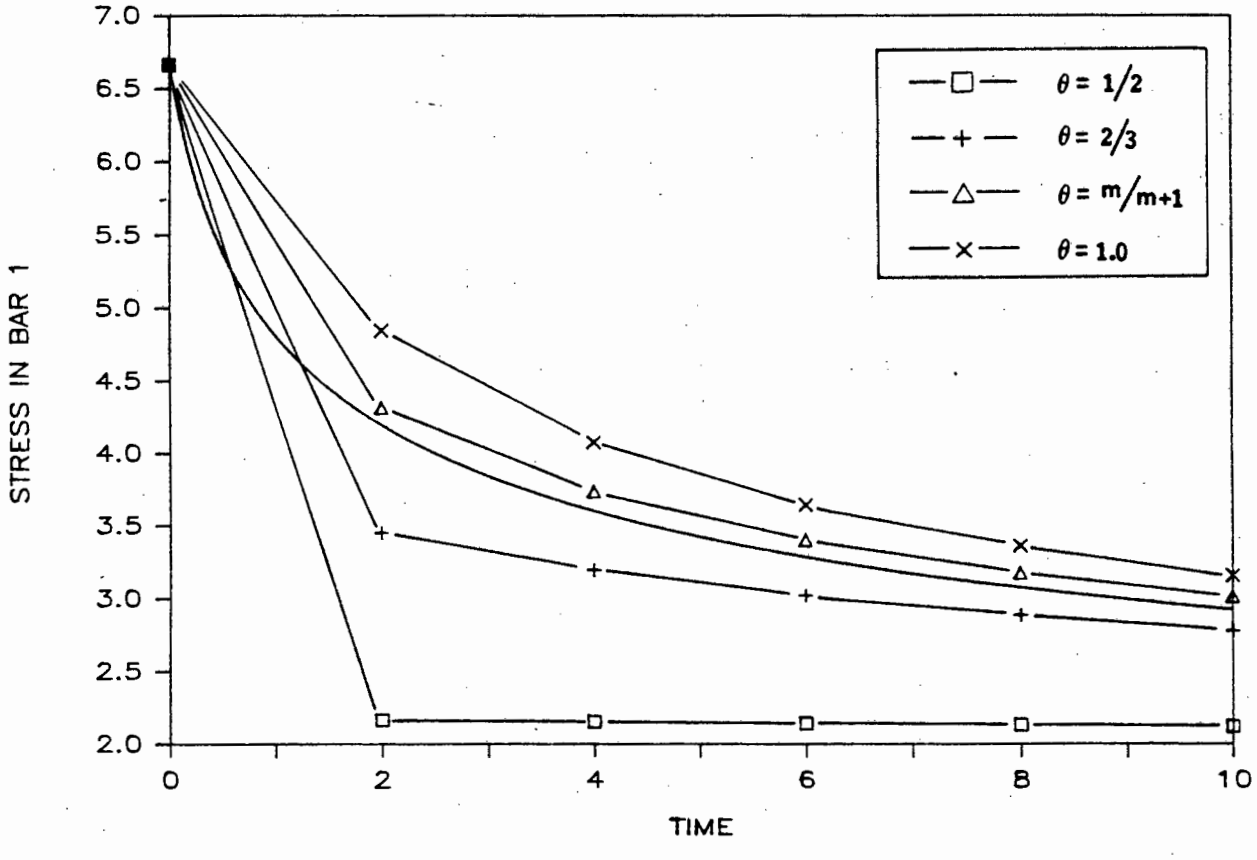

Figure 3.2(a) : Stress predictions for the two-bar truss under a constant load

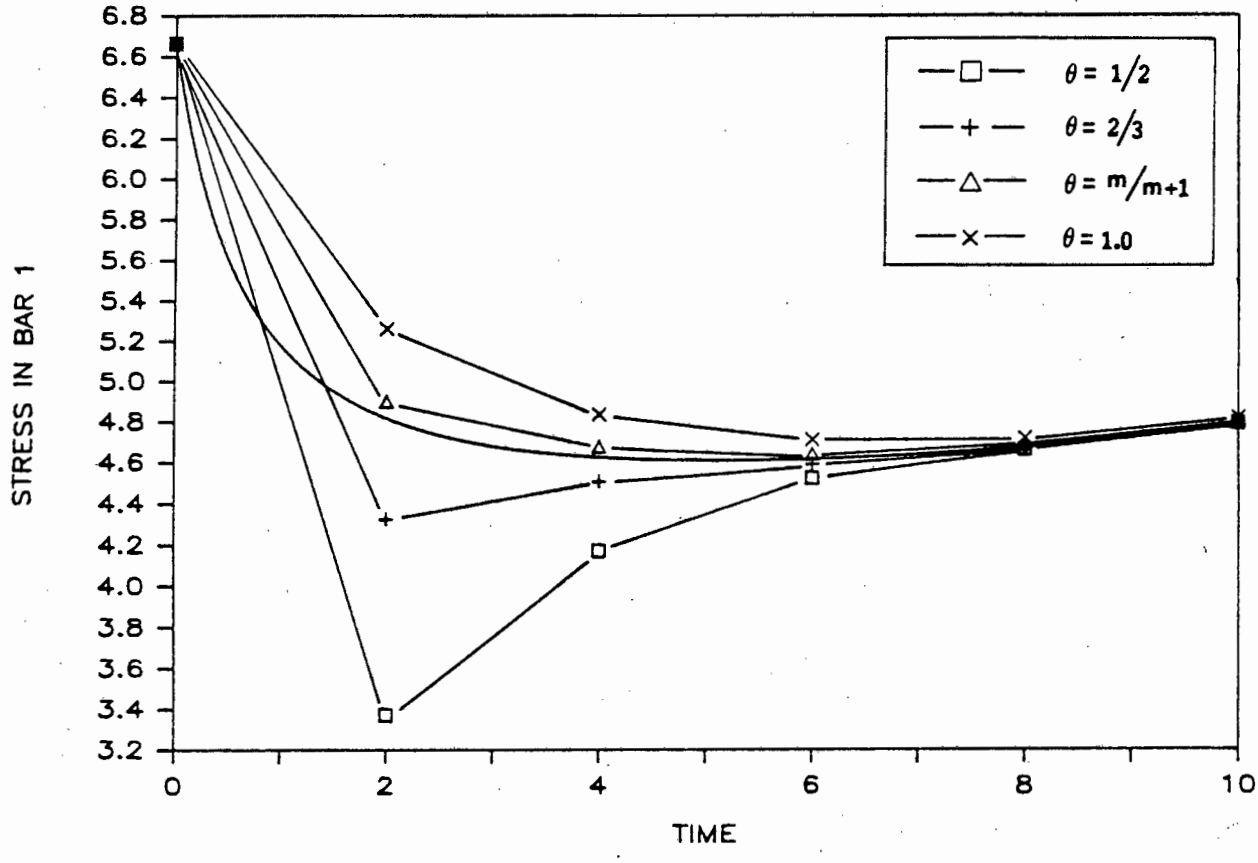

Figure 3.2(b) : Stress predictions for the two-bar truss under an increasing load

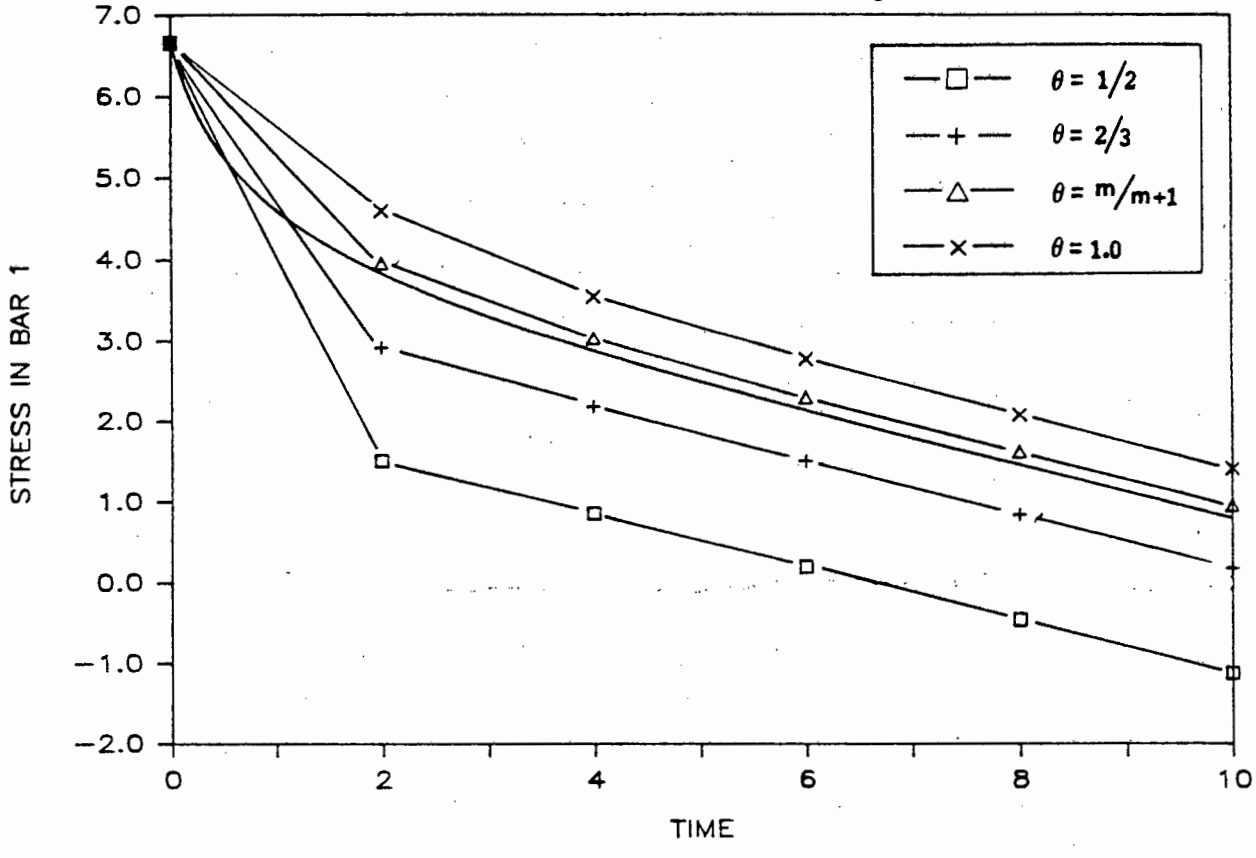

Figure 3.2(c) : Stress predictions for the two-bar truss under a decreasing load

While counter examples may be found, the above results appear typical of many numerical studies on multi-element structures under a range of loading and material parameters. The choice $\theta = m/m+1$, where m is the power law index in the constitutive relations, appears to be near optimal by showing faster convergence and greater accuracy than others. This would suggest a link between the time integration algorithm and the material properties. For $m = 1$ we have a linear creep law and mid-point rule ($\theta = 1/2$) [29], while as $m \to \infty$ we recover an elastic-perfectly plastic material and a backward difference algorithm ($\theta = 1$) [30].

The numerical characteristics of the solution algorithm are in agreement with the response of trapezoidal schemes discussed in Chapter 1. For any power index the ratio $m/m+1 \geq 1/2$ so that $\theta \geq 1/2$. This coincides with the restrictions placed on θ to make a trapezoidal scheme unconditionally stable [2]. The time-marching scheme will therefore be numerically stable for any time step length, although in practice some restriction on the length is necessary to maintain accuracy.

3.5 NUMERICAL EXAMPLES

The stability and accuracy of the proposed solution procedure is demonstrated in two examples illustrating characteristic creep behaviour. In each example the value $\theta = m/m+1$ is adopted for the integration of the constitutive equations and analyses with increasing time step lengths are performed.

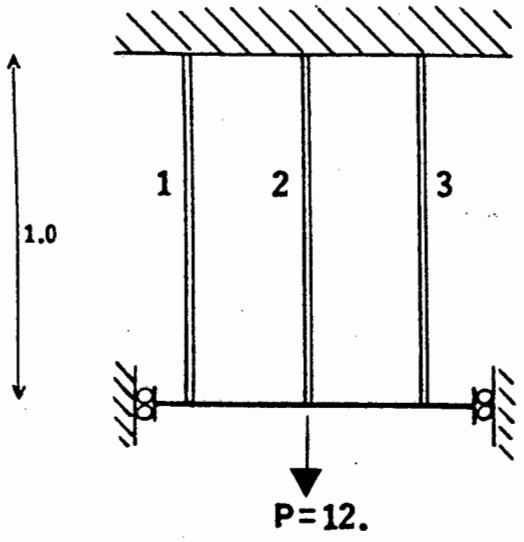

Member	E	k	m
1	300	256×10^{-5}	1
2	100	1×10^{-5}	3
3	200	16×10^{-5}	5

All cross-sectional areas = 1.0

Figure 3.3 : Geometric and material parameters for the three-bar truss example

3.5.1 Three-bar Truss

The three-bar truss depicted in Figure 3.3 exhibits highly nonlinear stress distribution from the elastic to the steady state solution. The redistribution of the stresses and the displacement history of the free end are plotted in Figures 3.4(a) and 3.4(b) respectively.

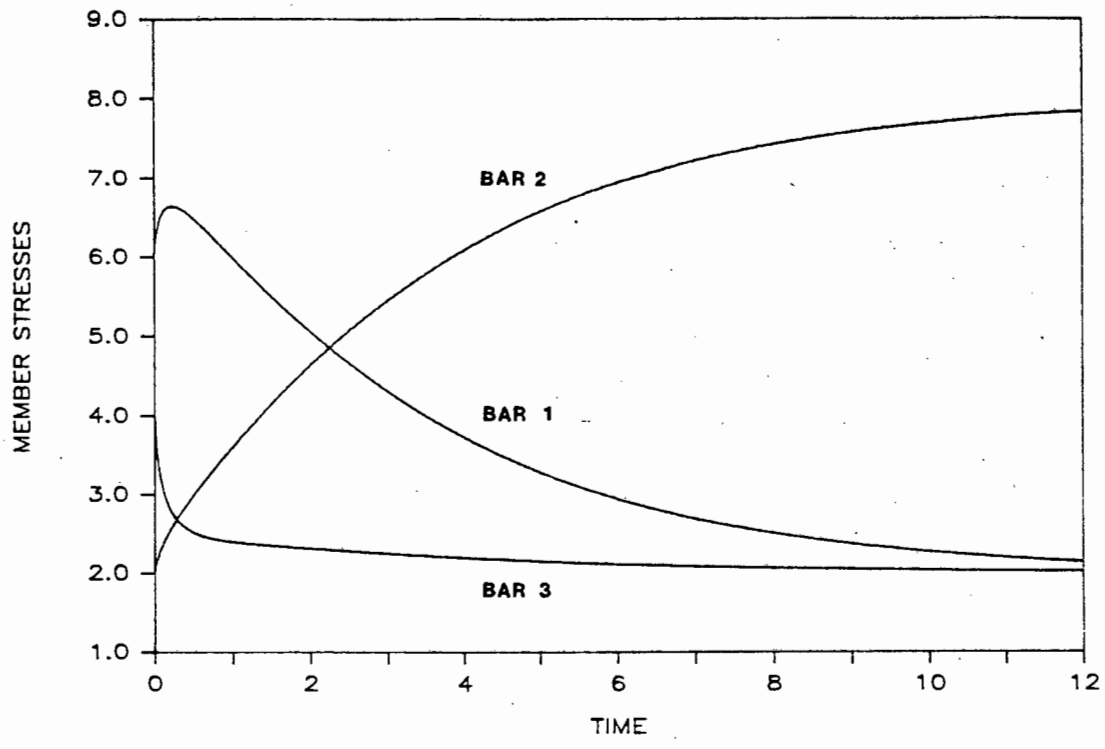

Figure 3.4(a) : Redistribution of stresses in the three-bar truss problem ($\Delta t = 0.001$)

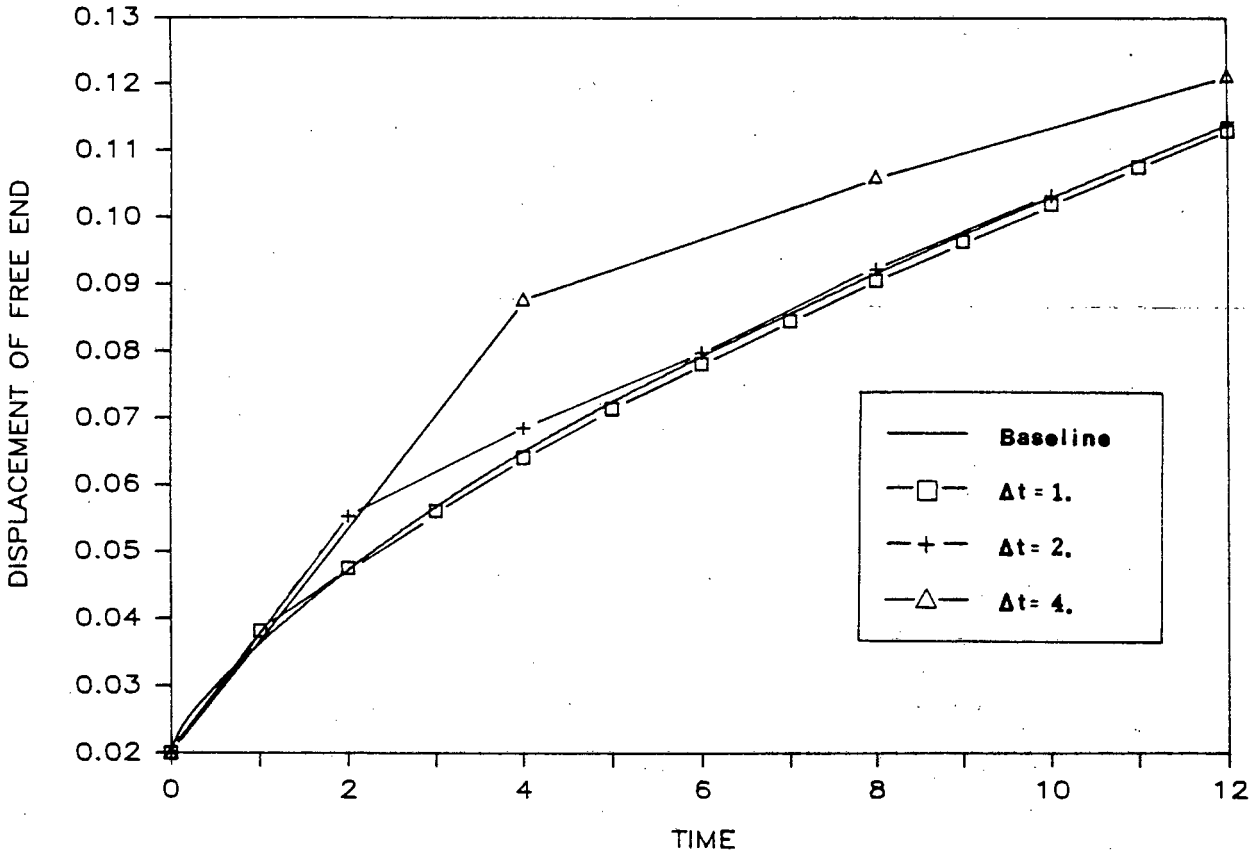

Figure 3.4(b) : Predictions of end displacements for different step lengths in the three bar problem. (Baseline solution obtained with $\Delta t = 0.001$).

The critical time step length for an explicit analysis is 0.0464 (Cormeau [19]). For the purposes of demonstrating the stability and accuracy of the solution algorithm, the structure is analysed using much larger time step lengths. The results are illustrated in Figure 3.4(b) and Table 3.2. The baseline solution is obtained with Δt = 0.001 and the results for ABAQUS [31] using Δt = 0.05 and NOSTRUM using Δt = 0.05, 1.0, 2.0 and 4.0 are tabulated. ABAQUS initially uses an explicit procedure, but switches to an implicit (backward difference) scheme if the time step restrictions are too severe. Analyses using initial steps larger than 0.05 were prevented by ABAQUS for stability reasons.

Table 3.2 : Prediction of displacements and member stresses using different time step lengths.

TIME ELAPSED	STEP-LENGTH	DISPLACE-MENT(U)	MEMBER STRESSES BAR 1	BAR 2	BAR 3
0.0	0.0	0.2000	4.000	6.000	2.000
4.0	NOSTRUM .001	0.0651	3.723	6.086	2.191
	NOSTRUM .050	0.0650	3.731	6.077	2.192
	ABAQUS .050	0.0652	3.709	6.102	2.190
	NOSTRUM 1.0	0.0642	3.767	5.940	2.189
	NOSTRUM 2.0	0.0686	2.910	6.181	1.798
	NOSTRUM 4.0	0.0878	6.757	7.507	-1.866
8.0	NOSTRUM .001	0.0917	2.505	7.433	2.063
	NOSTRUM .050	0.0917	2.510	7.426	2.063
	ABAQUS .050	0.0919	2.496	7.443	2.062
	NOSTRUM 1.0	0.0906	2.600	7.296	2.072
	NOSTRUM 2.0	0.0923	2.412	7.230	2.079
	NOSTRUM 4.0	0.1062	0.442	7.512	1.496
12.0	NOSTRUM .001	0.1139	2.141	7.840	2.018
	NOSTRUM .050	0.1139	2.144	7.838	2.019
	ABAQUS .050	0.1140	2.137	7.845	2.018
	NOSTRUM 1.0	0.1130	2.196	7.769	2.024
	NOSTRUM 2.0	0.1144	2.179	7.705	2.031
	NOSTRUM 4.0	0.1215	4.259	7.398	1.880

Note that the power law is different in each member. The integration scheme would therefore compute a different value of θ from θ = m/m+1 in each member. This differs from the traditional methods employing a single constant value of θ for all integration points.

The tabulated results show that analyses using time steps much larger than the usual stability limits were stable and accurate. The accuracy progressively deteriorates as the time step lengths increase, but the asymptotic solution for large times is given accurately.

3.5.2 Cantilever Beam

The creep bending of a cantilever beam under a constant bending-moment at the tip is investigated. This structure, illustrated in Figure 3.5(a), was also analysed by Bathe [7]. For comparison, dimensions and material data are in imperial units. The cantilever is modelled by considering only the part above the neutral axis and applying the correct displacement boundary conditions. The finite element model, using eight 8-noded elements with 3x3 Gaussian quadrature and plane stress assumptions, is shown in Figure 3.5(b).

The transient creep behaviour is analysed using a time step length of 25 hours. The displaced shape, after 400 hours of creep, is shown in Figure 3.5(c) while the redistribution of the stress σ_{xx} through the depth of the beam, at point A in Figure 3.5(b), is illustrated in Figure 3.6(a).

The analytical steady state stress σ_{xx} at stress point A is 5688 psi. The stress-history depicted in Figure 3.6(b) shows a redistribution from the initial elastic value of 7085 psi to 5704 psi after 400 hours. The structure was also analysed using different time step lengths. The stress-history curve converged to the continuous solution for time steps of 1.0 and smaller. The stresses obtained with larger steps of 10.0 and 25.0 are also shown in Figure 3.6(b). This demonstrates that the solution algorithm is convergent and accurate, even for relatively large time steps.

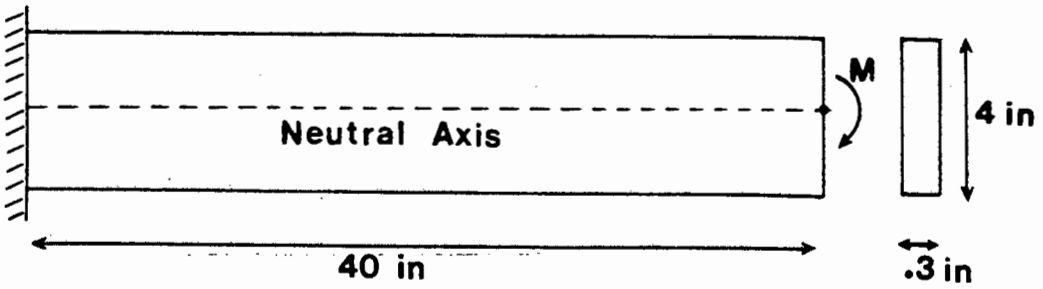

Moment : $M = 6000$ in-lb

Creep law : $\dot{\epsilon}^c = k\,\sigma_e^m \quad (\sigma_e^2 = \frac{1}{2}\, s_{ij}\, s_{ij})$

Material data: $E = 30 \times 10^6$ psi $\quad \nu = 0.3$

$k = 6.4 \times 10^{-18} \quad m = 3.15$

Figure 3.5(a) : Geometric and material description of the cantilever problem

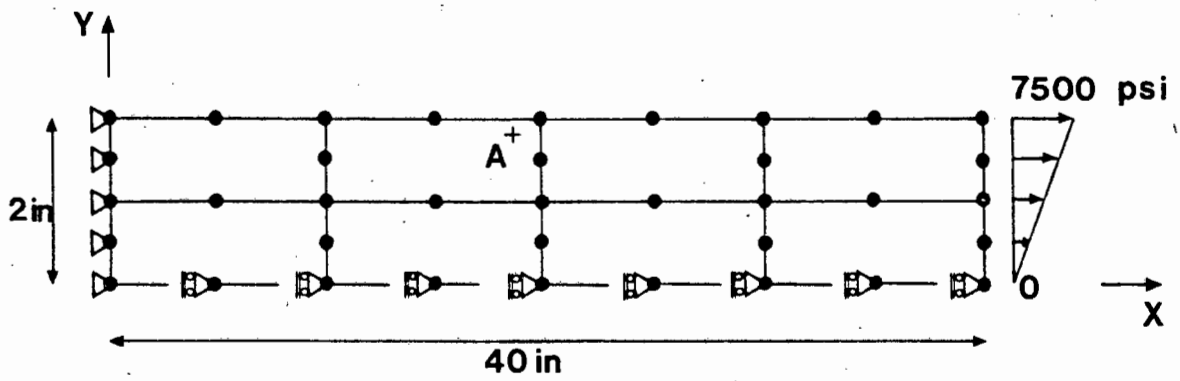

Coordinates of A = (18.873, 1.887)

Eight 8-noded plane stress elements

3x3 Gauss integration

Figure 3.5(b) : Finite element model of the cantilever problem

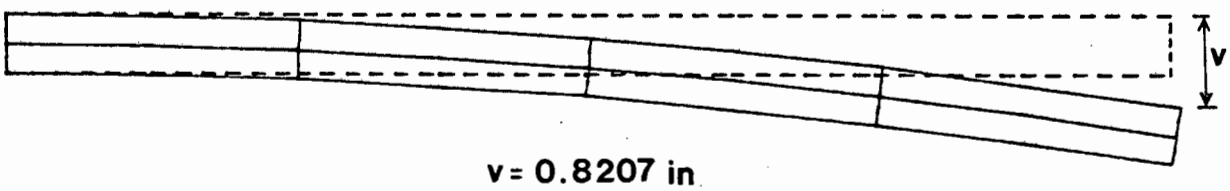

Figure 3.5(c) : Displaced shape of the cantilever after 400 hours of creep

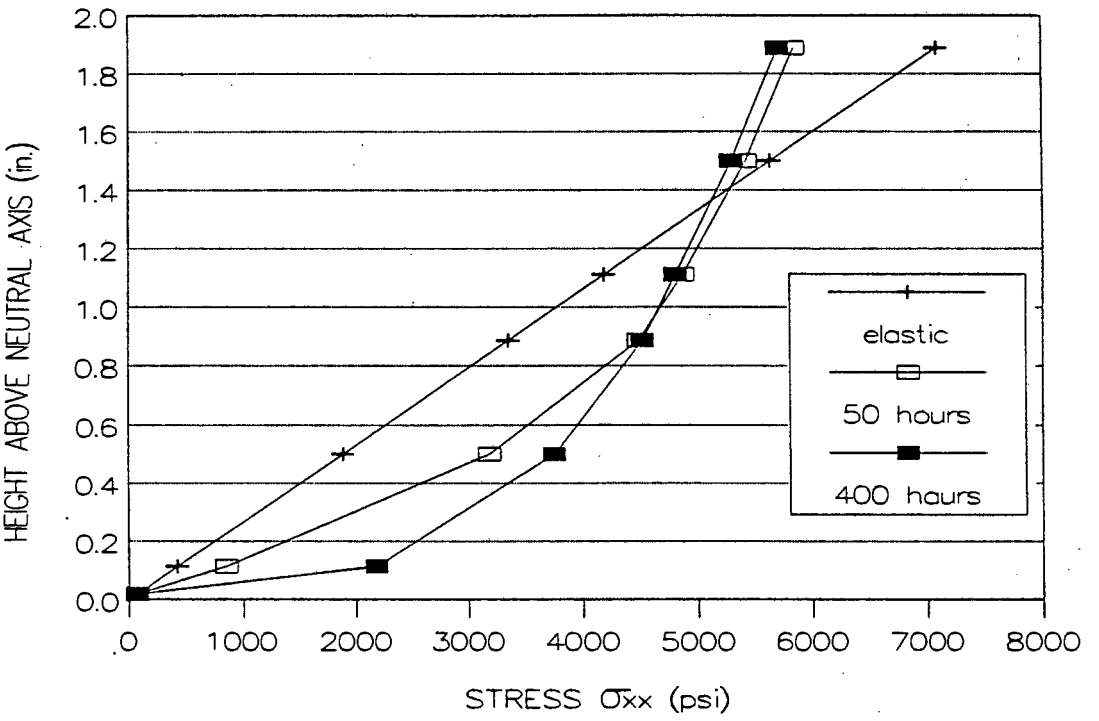

Figure 3.6(a) : Redistribution of the stress through the depth of the beam at a section through A

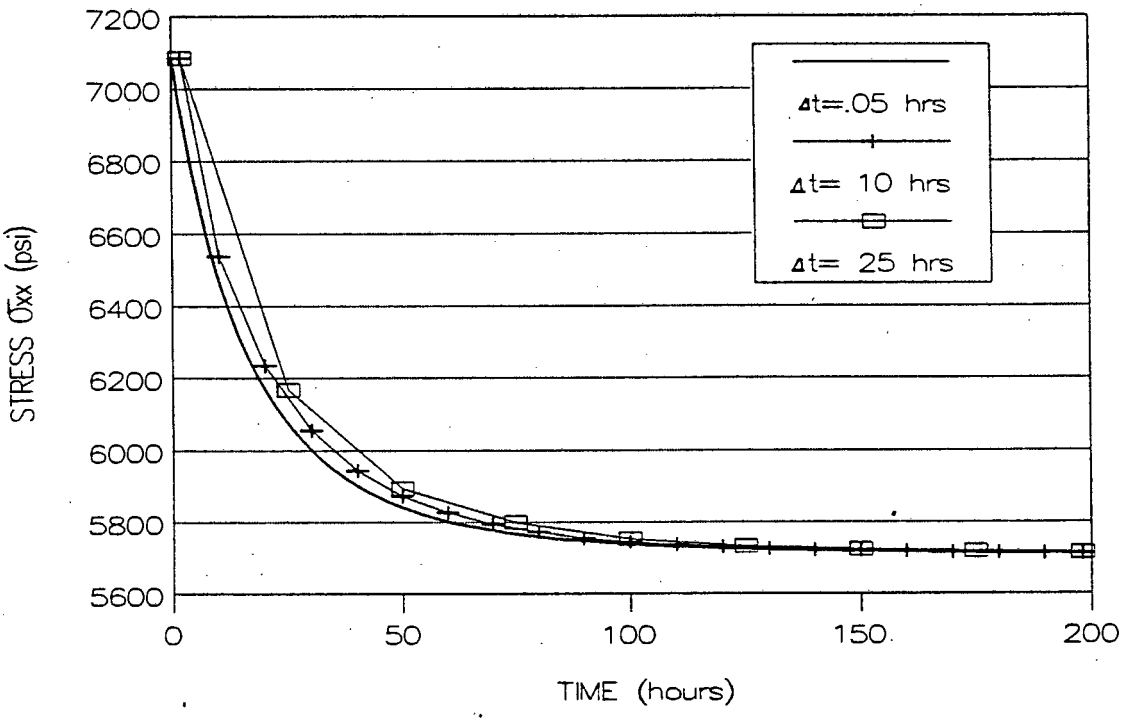

Figure 3.6(b) : Redistribution history of σ_{xx} at A

3.6 CONCLUSIONS

The numerical solution algorithm for the creep problem is equivalent to that of an iterative solution of a nonlinear mathematical programming problem. The minimum principle corresponding to the solution of the incremental problem is solved by means of a two-step strategy. We have shown that consistent predictors and a corrector step can be formulated for any creep problem provided that the constitutive law and time integration scheme lead to a potential function of $W_n(\Delta\underset{\sim}{\varepsilon}^c)$. Other than this assumption the solution algorithm was formulated in a completely general framework to solve creep problems under constant or variable loads.

As suggested by the results in Chapter 2, we selected a general trapezoidal rule to approximate the creep strains over a time step. This choice, when used with simple power laws governing uniaxial and multi-axial creep, provided a reliable solution procedure. The numerical stability and accuracy of the algorithm was demonstrated in typical creep redistribution problems. It should be noted that we are concerned only with the effectiveness of the solution algorithm and the accuracy of the results. We have made no attempt to enhance the efficiency of the algorithm, which can be achieved by selective reformation of the stiffness matrix and implementing dynamic time stepping.

Of greater concern is the requirement that the response over any given time step would be stable, convergent and accurate. This is clearly linked to the choice of θ in the trapezoidal rule. A specific form of

the trapezoidal rule appeared to be optimal. This established a link between the material and the appropriate integration parameters. In particular, the extreme case approaching plasticity as $m \to \infty$ which would result in the backward difference integration scheme, suggests that the results for plasticity could be extended to time-dependent material behaviour. The choice of integration scheme, or the approximation of stresses and strains over a time step, may therefore be governed by the mechanics of the problem. We investigate this possibility in the next chapter.

CHAPTER 4

INTEGRATION PATHS FOR CREEP

4.1 INTRODUCTION

In Chapters 2 and 3 we have presented an internal variable formulation of the creep problem, leading to a convex nonlinear programming problem for each time interval. An iterative Newton-Raphson procedure was developed for the programming problem, based on a quadratic approximation of the potential function relating the creep strain increment and the stress at the end of the interval.

The formulation was predicated on the adoption of the trapezoidal rule to provide an approximate relation between the creep strain increment $\Delta\underset{\sim}{\epsilon}^{c}_{n}$ and the creep strain rates at the beginning and end of the interval, $\dot{\underset{\sim}{\epsilon}}^{c}_{n-1}$, $\dot{\underset{\sim}{\epsilon}}^{c}_{n}$. This choice was developed by an appreciation of the fact that the differential equations for the problem, formulated in the internal variable framework, contain creep strain rates as the only derivatives. It was noted in Section 2.4, however, that in the conventional finite element formulation, the trapezoidal rule is applied to stresses, leading to different difference equations. The two difference equations can be shown to be identical only in the case of explicit integration schemes. We shall therefore consider only implicit forms of the trapezoidal rules, so that $\alpha > 0$ in equation (2.17b) and $\theta > 0$ in equation (2.40).

It is appropriate to ask whether the relationship between these two sets of difference equations can be understood, and we set out to achieve this in this chapter. The link is based on the identification of a set of difference equations with an assumed stress-history $\underset{\sim}{\sigma}(t)$ in the interval $[t_{n-1}, t_n]$. The paths associated with the two sets of difference equations are readily found, and are distinct.

This leads to the further question of whether the choice of approximating path can be made on the basis of the mechanics of the problem, rather than on heuristic grounds. This can be achieved in plasticity, where the choice of a path of minimum work, or maximum complementary work, leads to the backward difference algorithm ([4,30,32-34]). Further evidence that such a result may be obtainable in the case of creep is seen in the numerical results given in Chapter 3, where the optimum choice of the parameter θ appears to depend on the index m in the Norton creep law, with the optimal θ given approximately by m/m+1. This leads to $\theta = 1/2$ for a linear material, where it is known that this choice is associated with quadratic convergence, and $\theta = 1$ for large m, which is the case of an elastic, perfectly plastic material.

We shall identify the minimum net work path, or maximum net complementary work path. This path may be adopted within the framework presented in Chapters 2 and 3, and we shall present some numerical results for the two and three bar truss structures considered earlier. The discussion in this chapter will be carried out in terms of uniaxial stress-strain relations; we have seen that we can generalise from the case of the truss structure to multiaxial relations in a straightforward way.

4.2 APPROXIMATING STRESS PATHS

The concept which we will use to unify the two sets of difference equations discussed in Chapter 2 is that of an assumed stress path (or

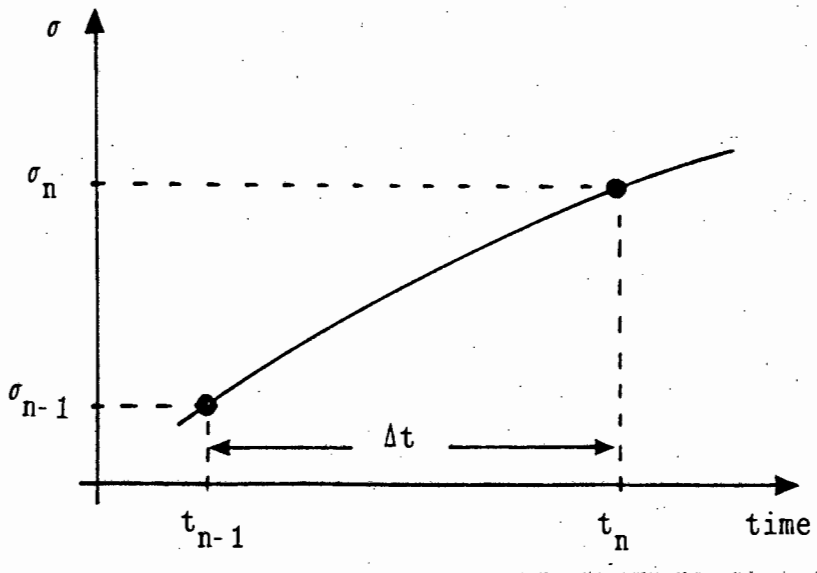

Figure 4.1 : A typical stress curve of a time step

equivalently strain path) over each time interval at each sample point. For the case of the truss, we consider only one component of stress and strain. The assumed stress path is shown diagrammatically in Figure 4.1; with $\sigma(t_{n-1}) = \sigma_{n-1}$, $\sigma(t_n) = \sigma_n$, we adopt an assumed path $\sigma(t)$ over the interval $[t_{n-1}\ ,\ t_n]$. The constitutive equations,

$$\dot{\epsilon} = \frac{\dot{\sigma}}{E} + k\ \sigma^m \quad , \tag{4.1}$$

are then integrated along this path to obtain a relationship between σ_n , σ_{n-1} , $\Delta\epsilon_n^c$ and Δt . The application of the trapezoidal rule to the creep strain (equation (2.40)) gives

$$\Delta\epsilon_n^c = \epsilon_n^c - \epsilon_{n-1}^c = (1 - \theta)\ \Delta t\dot{\epsilon}_{n-1}^c + \theta\Delta t\dot{\epsilon}_n^c \quad . \tag{4.2}$$

This implies that it is assumed that the creep strain rate remains constant at the value $\dot{\epsilon}^c_{n-1}$ for the interval $[t_{n-1}\ ,\ t_*]$, and constant at the value $\dot{\epsilon}^c_n$ for the interval $[t_*\ ,\ t_n]$, where

$$t_* = t_{n-1} + (1 - \theta)\,\Delta t \quad , \quad 0 \le \theta \le 1 \quad . \tag{4.3}$$

From this we infer that the stress path is that shown in Figure 4.2(a). The stress remains constant at its initial value σ_{n-1} for the interval $[t_{n-1}\ ,\ t_*]$, jumps to σ_n at time t_* , and remains constant over the interval $[t_*\ ,\ t_n]$. The corresponding strain path is shown in Figure 4.2(b). Integration of the constitutive equation (4.1) along with the stress path of Figure 4.2(a) gives

$$\Delta\epsilon^c_n = (1 - \theta)\,k\Delta t\sigma^m_{n-1} + \theta k\Delta t\sigma^m_n \tag{4.4a}$$

$$\Delta\epsilon^e_n = \frac{1}{E}\,(\sigma_n - \sigma_{n-1}) \tag{4.4b}$$

$$\Delta\epsilon_n = \frac{1}{E}\,(\sigma_n - \sigma_{n-1}) + (1 - \theta)\,k\Delta t\sigma^m_{n-1} + \theta k\Delta t\sigma^m_n \quad . \tag{4.4c}$$

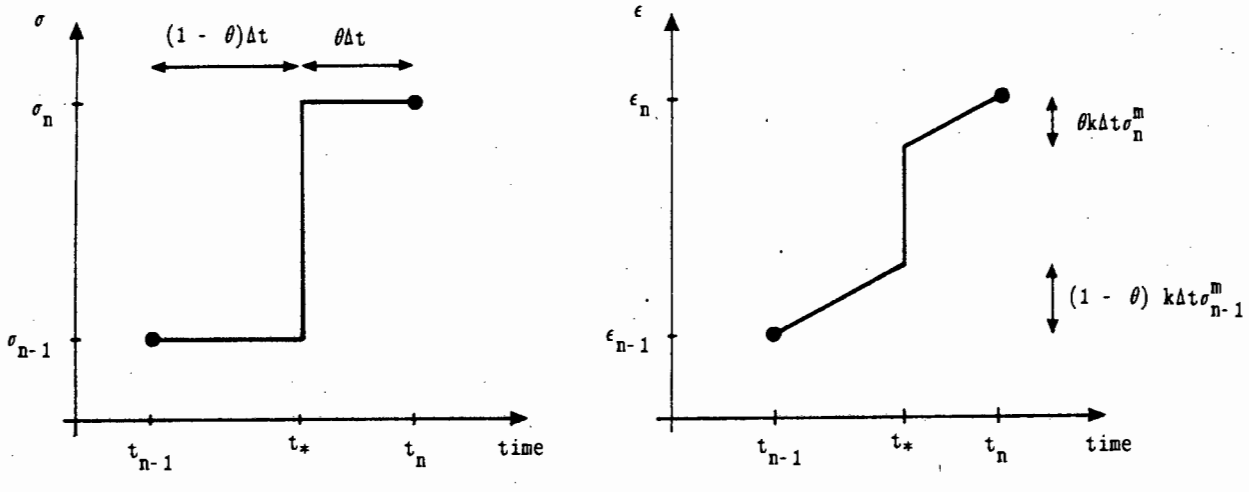

(a) Stress path (b) Strain path

Figure 4.2 : Stress and strain paths implied by the trapezoidal approximation of the creep strains (t_* path)

In the internal variable formulation we write equation (4.4a) as

$$\sigma_n = \left[\frac{1}{\theta k \Delta t}\,\Delta\epsilon_n^c - \left[\frac{1-\theta}{\theta}\right]\sigma_{n-1}^m\right]^{1/m} \quad , \tag{4.5}$$

and introduce the potential function

$$W(\Delta\epsilon^c) = \frac{m}{m+1}\,\theta k\Delta t\left[\frac{1}{\theta k\Delta t}\,\Delta\epsilon^c - \left[\frac{1-\theta}{\theta}\right]\sigma_{n-1}^m\right]^{\frac{m+1}{m}} \quad . \tag{4.6}$$

Then

$$\sigma_n = \left.\frac{\partial W}{\partial \Delta\epsilon^c}\right|_{\Delta\epsilon_n^c} \quad . \tag{4.7}$$

These relationships are shown diagrammatically in Figure 4.3. For convenience, we will refer to this path as the t_* path.

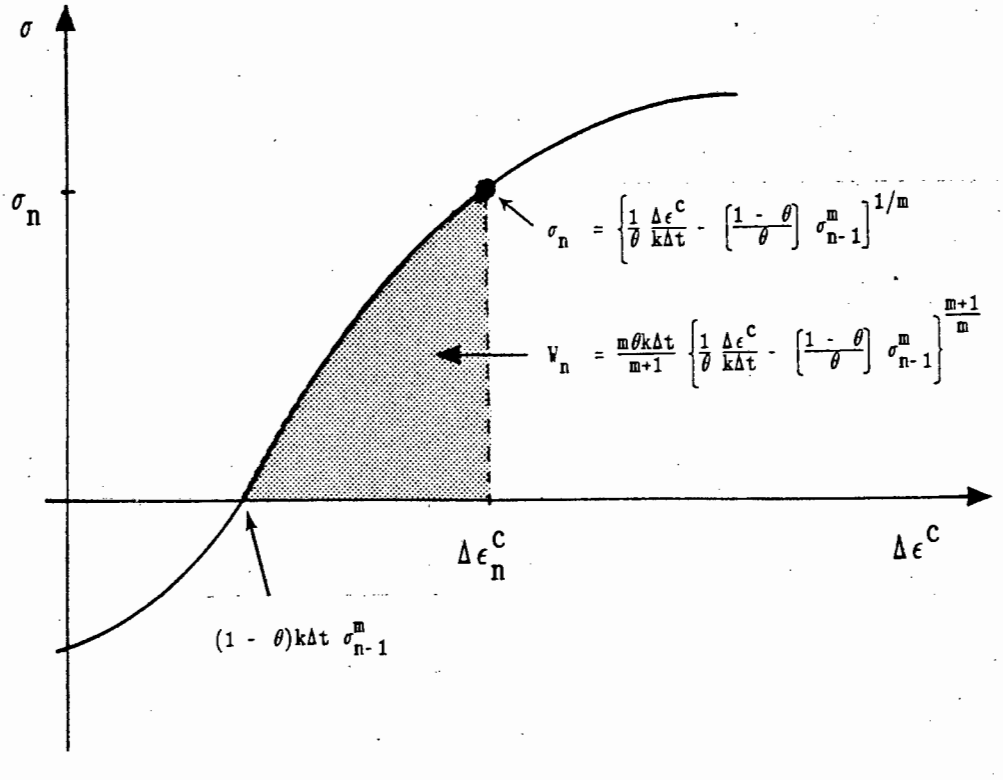

Figure 4.3 : Potential forms of the t_* path

The potential function W appears in the nonlinear programming problem (equation (2.57)), and is the only contribution to the formulation which is affected by the choice of the stress or strain path, or equivalently the difference expression of equation (4.2). Thus, if we adopt a different stress or strain path, we need only formulate the appropriate potential function $W(\Delta\epsilon^c)$ in order to incorporate it into the formulation of the problem.

The alternative difference expression, used conventionally in finite element analysis, assumes that the creep strain increment can be computed on the basis of an "average" stress

$$\sigma_* = (1 - \alpha)\sigma_{n-1} + \alpha\,\sigma_n$$

$$= \sigma_{n-1} + \alpha(\sigma_n - \sigma_{n-1}) \quad , \quad 0 \le \alpha \le 1 \quad . \tag{4.8}$$

From this, we infer a stress path of the form shown in Figure 4.4(a). The stress jumps at time t_{n-1} to the value σ_* , remains constant at this value until time t_n , and then jumps to σ_n . The associated strain path is shown in Figure 4.4(b). Integration of the constitutive equations along the path leads to

$$\Delta\epsilon_n^c = k\Delta t\,[(1 - \alpha)\sigma_{n-1} + \alpha\,\sigma_n]^m \tag{4.9a}$$

$$\Delta\epsilon_n^e = \frac{1}{E}\,(\sigma_n - \sigma_{n-1}) \tag{4.9b}$$

$$\Delta\epsilon_n = \frac{1}{E}\,(\sigma_n - \sigma_{n-1}) + k\Delta t\,[(1 - \alpha)\sigma_{n-1} + \alpha\,\sigma_n]^m \quad . \tag{4.9c}$$

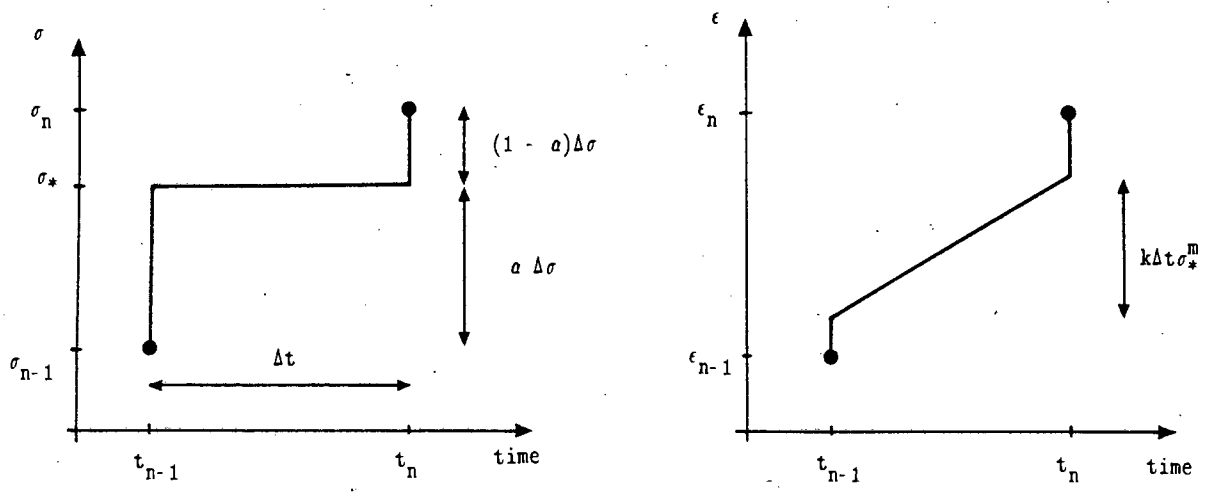

(a) Stress path (b) Strain path

Figure 4.4 : Stress and strain paths implied by a trapezoidal approximation of the stress path (σ_* path)

For $a > 0$, equation (4.9a) can be rewritten as

$$\sigma_n = \frac{1}{a}\left[\frac{\Delta\epsilon_n^c}{k\Delta t}\right]^{1/m} - \left[\frac{1 - a}{a}\right]\sigma_{n-1} \quad . \tag{4.10}$$

This relation is shown diagrammatically in Figure 4.5. The potential function is

$$W(\Delta\epsilon^c) = \frac{m}{m+1}\,\frac{k\Delta t}{a}\left[\frac{\Delta\epsilon^c}{k\Delta t}\right]^{\frac{m+1}{m}} - \left[\frac{1 - a}{a}\right]\sigma_{n-1}\,\Delta\epsilon^c \quad , \tag{4.11a}$$

and

$$\sigma_n = \left.\frac{\partial W}{\partial \Delta\epsilon^c}\right|_{\Delta\epsilon_n^c} \quad . \tag{4.11b}$$

For convenience, we will refer to this path as the σ_* path. The potential function W is convex, and can be used in the nonlinear programming problem given in equation (2.57) in place of that for the t_* path without further modification.

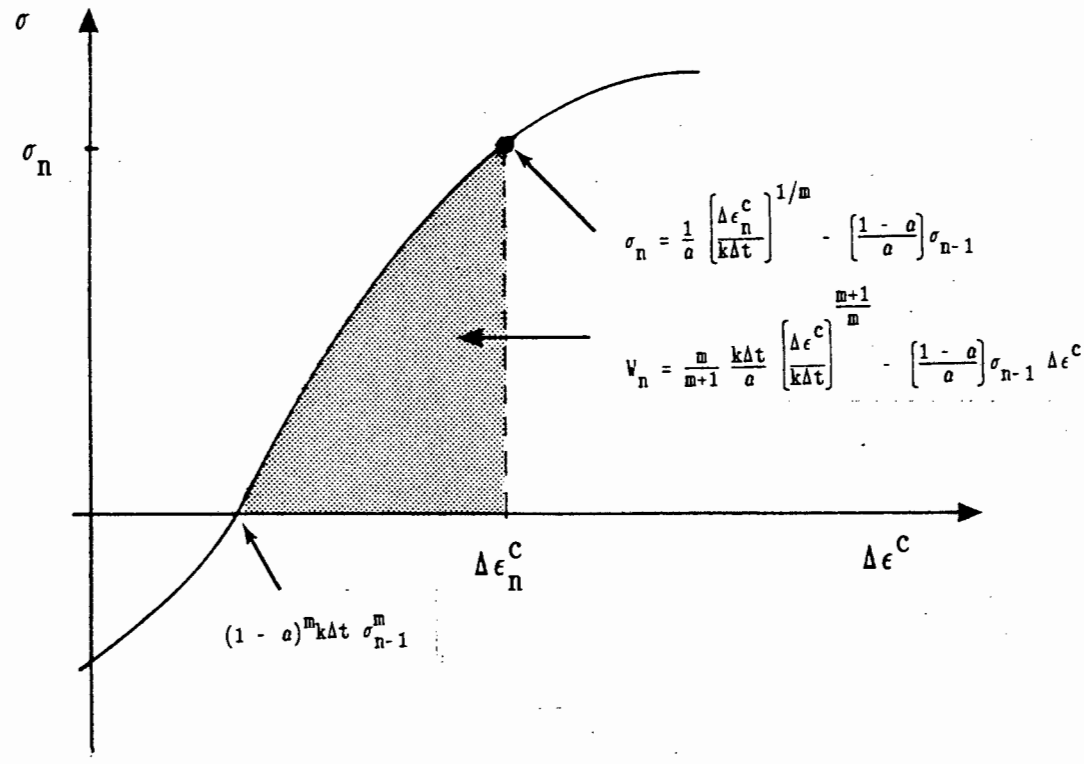

Figure 4.5 : Potential form of the σ_* path

The identification of the t_* and the σ_* paths leave us in the position of making a heuristic choice of which is the more effective. In addition, each has a parameter (θ or a) which must be chosen, and we have no firm *a priori* basis on which to make this choice.

We may note that for $\theta = 1$, $a = 1$, the two stress paths are identical. In addition, for the linear case m=1 , the t_* path with $\theta = 1/2$ and the σ_* path with $a = 1/2$ give identical results at time t_n .

In the next section we shall explore the possibility of deriving an appropriate stress path on the basis of work principles.

4.3 EXTREMAL PATHS

The concept of minimum work and maximum complementary work paths were introduced for time independent materials by Martin [35] and for time-dependent materials by Ponter [36]. Further, it was shown that the work or complementary work along the extremal paths provides a potential function relating the terminal stress and strain [36-38].

In the case of incremental plasticity, application of this concept to choose an approximating path over a time interval leads to a backward difference algorithm, i.e. the choice of either $\theta = 1$ in the t_* path or $a = 1$ in the σ_* path. This choice accords with computational experience in that the backward difference scheme is widely regarded as the most effective choice in the application of the generalised trapezoidal rule in incremental plasticity.

In our present context, it is simplest to find the maximum complementary work path. We confine ourselves to uniaxial behaviour; generalisations to multi-axial behaviour are straightforward.

Ponter [36,37] considered the case of a Maxwell creep model governed by the relation

$$\dot{\epsilon} = \frac{\dot{\sigma}}{E} + k\,\sigma^m \quad . \tag{4.12}$$

He showed that the complementary work

$$\Omega = \int_0^{t_n} \epsilon\,\dot{\sigma}\,dt \tag{4.13}$$

for a stress-history in which $\sigma(0) = 0$, $\epsilon(0) = 0$ and $\sigma(t_n) = \sigma_n$ is maximised by a path in which the stress jumps to a value $m\sigma_n/m+1$, remains fixed at this value until time t_n , and then jumps again to σ_n at time t_n . The path is shown diagrammatically in Figure 4.6, together with the associated strain history. The maximum complementary work is given by

$$\Omega^c(\sigma_n) = \int_0^{t_n} \epsilon\, \dot{\sigma}\, dt = \int_0^{t_n} \epsilon^e \dot{\sigma}\, dt + \int_0^{t_n} \epsilon^c \dot{\sigma}\, dt$$

$$= \frac{\sigma_n^2}{2E} + kt_n \left[\frac{m}{m+1}\,\sigma_n\right]^m \left[\sigma_n - \frac{m}{m+1}\,\sigma_n\right]$$

$$= \frac{\sigma_n^2}{2E} + \frac{kt_n}{m}\left[\frac{m}{m+1}\,\sigma_n\right]^{m+1} \quad . \qquad (4.14)$$

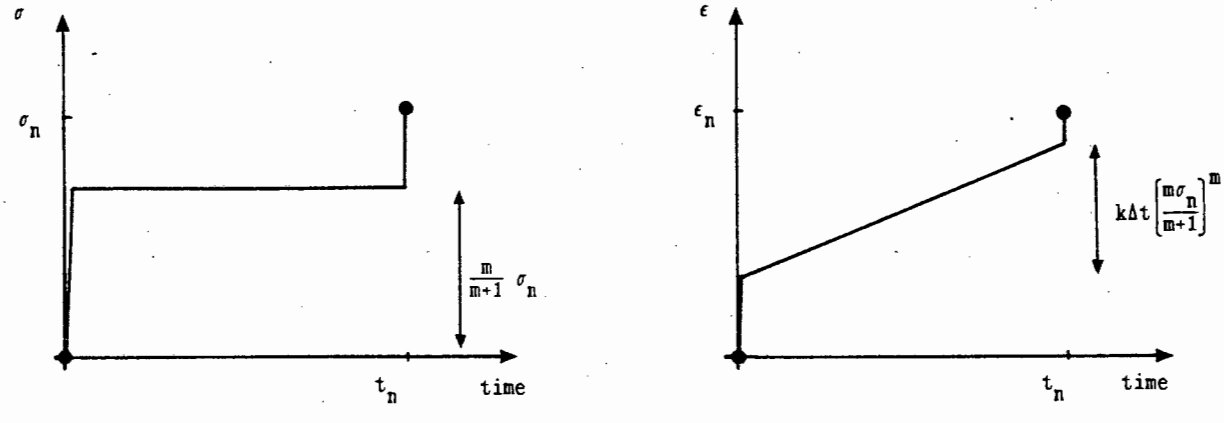

(a) Stress path (b) Strain path

Figure 4.6 : Stress and strain paths maximising complementary work over a time-step

We may confirm the potential nature of Ω^o ;

$$\epsilon_n = \left.\frac{\partial \Omega^o(\sigma)}{\partial \sigma}\right|_{\sigma_n}$$

$$= \frac{\sigma_n}{E} + kt_n\left[\frac{m}{m+1}\,\sigma_n\right]^m \quad . \tag{4.15}$$

The extremal stress path for this case would appear to be similar to the σ_* path discussed in the previous section, and we shall thus refer to extremal paths as generalised σ_* paths for convenience.

Ponter's extremal path does not cover the case of interest in incremental analysis, however, except for the first time step. We wish to consider the more general problem of a stress-history over time $[t_{n-1}\ ,\ t_n]$, with $\sigma(t_{n-1}) = \sigma_{n-1}$, $\epsilon(t_{n-1}) = \epsilon_{n-1}$ and $\sigma(t_n) = \sigma_n$. We shall assume that the extremal path in this case has the same essential characteristic as Ponter's case: as shown in Figure 4.4; the stress jumps to a value of σ_* at time t_{n-1} , remains fixed, and then jumps again at time t_n to a value of σ_n . However, since we are concerned with the change in strain $\Delta\epsilon_n = \epsilon_n - \epsilon_{n-1}$, we write the complementary work as

$$\Omega = \int_{t_{n-1}}^{t_n} (\epsilon - \epsilon_{n-1})\ \dot{\sigma}\ dt$$

$$= \int_{t_{n-1}}^{t_n} (\epsilon^e - \epsilon^e_{n-1})\ \dot{\sigma}\ dt + \int_{t_{n-1}}^{t_n} (\epsilon^c - \epsilon^c_{n-1})\ \dot{\sigma}\ dt$$

$$= \left[\frac{\sigma_n - \sigma_{n-1}}{2E}\right]^2 + k\Delta t\ \sigma_*^m(\sigma_n - \sigma_*) \quad . \tag{4.16}$$

The maximum value is given by $\partial\Omega/\partial\sigma_* = 0$, and thus

$$\sigma_* = \frac{m}{m+1}\,\sigma_n \quad . \tag{4.17}$$

This is precisely the same result as that of Ponter, and indicates that σ_* does not depend on σ_{n-1} . The maximum complementary work is

$$\Omega(\sigma_n) = \left[\frac{\sigma_n - \sigma_{n-1}}{2E}\right]^2 + \frac{k\Delta t}{m}\left[\frac{m}{m+1}\,\sigma_n\right]^{m+1} \quad . \tag{4.18}$$

We see further that

$$\Delta\epsilon_n = \left.\frac{\partial\Omega(\sigma)}{\partial\sigma}\right|_{\sigma_n}$$

$$= \left[\frac{\sigma_n - \sigma_{n-1}}{E}\right] + k\Delta t\left[\frac{m}{m+1}\,\sigma_n\right]^m \quad . \tag{4.19}$$

On consideration, however, this path could not be an appropriate choice for the incremental problem. If, for example, $\sigma_n = \sigma_{n-1}$, it seems intuitively clear that the best path is $\sigma = \sigma_{n-1}$ in $[t_{n-1}\ ,\ t_n]$, whereas the maximum complementary work path drops σ to a lower value. The only exception to this objection occurs when $m \to \infty$, when we recover the backward difference path used in incremental plasticity. At the other extreme, when m=1 , the path will clearly not give good results.

This suggests that we must look more carefully at the concept of net complementary work. Following ideas put forward by Drucker [39] in discussing the stability of time-dependent materials, and focussing on our difficulty when σ remains constant over the interval, we note that

an important feature of a time-dependent material is that the creep strain continues to change when the stress remains constant. Thus we propose that we should define the net complementary work on the basis of the difference between two stress and strain histories. The first is the actual history $\sigma(t)$, with $\sigma(t_{n-1}) = \sigma_{n-1}$, $\sigma(t_n) = \sigma_n$. The second is $\sigma_1(t)$ which is constant and equal to σ_{n-1} . For both strain histories, $\epsilon(t)$, $\epsilon_1(t)$, we have the same values at t_{n-1} . Thus

$$\epsilon(t_{n-1}) = \epsilon_1(t_{n-1}) = \frac{\sigma_{n-1}}{E} + \epsilon^c_{n-1} \quad . \tag{4.20}$$

It is clear then that

$$\epsilon_1(t) = \frac{\sigma_{n-1}}{E} + \epsilon^c_{n-1} + k(t - t_{n-1})\sigma^m_{n-1} \quad . \tag{4.21}$$

We shall assume that the history $\sigma(t)$ has the same form as Figure 4.4, and seek to maximise

$$\Omega^N(\sigma_n) = \int_{t_{n-1}}^{t_n} (\epsilon - \epsilon_1) \frac{d}{dt} (\sigma - \sigma_1)\, dt$$

$$= \int_{t_{n-1}}^{t_n} (\epsilon^e - \epsilon^e_1) \frac{d}{dt} (\sigma - \sigma_1)\, dt + \int_{t_{n-1}}^{t_n} (\epsilon^c - \epsilon^c_1) \frac{d}{dt} (\sigma - \sigma_1)\, dt$$

$$= \left[\frac{\sigma_n - \sigma_{n-1}}{2E}\right]^2 + k\Delta t(\sigma^m_* - \sigma^m_{n-1})(\sigma_n - \sigma_*) \quad . \tag{4.22}$$

Putting $\partial\Omega^N/\partial\sigma_* = 0$, the value of σ_* which maximises Ω^N is given by the equation

$$(m+1)\sigma^m_* = m\,\sigma_n\,\sigma^{m-1}_* + \sigma^m_{n-1} \quad . \tag{4.23}$$

This is a complex equation for $m \neq 1$, but we can draw some general conclusions. First, for $\sigma_{n-1} = 0$, we recover Ponter's result of equation (4.17). Second, for the linear case, m=1 , we find

$$\sigma_* = \frac{\sigma_{n-1} - \sigma_n}{2} = \sigma_{n-1} + \frac{1}{2}(\sigma_n - \sigma_{n-1}) \quad , \tag{4.24}$$

which corresponds to the choice $\alpha = 1/2$ in the σ_* path and $\theta = 1/2$ in the t_* path . Third, for $\sigma_n = \sigma_{n-1}$, we find

$$\sigma_* = \sigma_{n-1} \quad . \tag{4.25}$$

In the general case, however, we cannot find an explicit solution for σ_* . Nevertheless, if we adopt this path we can determine the relationship between σ_n and $\Delta\epsilon_n^c$, and the associated potential function W which we use in the internal variable formulation of the incremental creep problem given in Chapters 2 and 3. For the generalised σ_* path, shown in Figure 4.4, the creep strain increment is

$$\Delta\epsilon_n^c = k\Delta t \ \sigma_*^m \quad . \tag{4.26}$$

Substituting this into equation (4.23), we have

$$(m+1)\left[\frac{\Delta\epsilon_n^c}{k\Delta t}\right] = m\sigma_n\left[\frac{\Delta\epsilon_n^c}{k\Delta t}\right]^{\frac{m-1}{m}} + \sigma_{n-1}^m \quad . \tag{4.27a}$$

Solving for σ_n , this gives

$$\sigma_n = \left[\frac{m+1}{m}\right]\left[\frac{\Delta\epsilon_n^c}{k\Delta t}\right]^{1/m} - \frac{1}{m}\left[\frac{k\Delta t}{\Delta\epsilon_n^c}\right]^{\frac{m-1}{m}} \sigma_{n-1}^m \quad . \tag{4.27b}$$

It is convenient to define

$$\Delta\epsilon_1^c = k\Delta t\ \sigma_{n-1}^m \quad , \tag{4.28}$$

which is the creep increment associated with the $\sigma_1(t)$ path.

Equation (4.27b) can then be rewritten as

$$\sigma_n = \left[1 + \frac{\Delta\epsilon_n^c - \Delta\epsilon_1^c}{m\ \Delta\epsilon_n^c}\right]\left[\frac{\Delta\epsilon_n^c}{k\Delta t}\right]^{1/m} \quad . \tag{4.29}$$

This relationship is shown diagrammatically in Figure 4.7. Note that $\sigma_n = \sigma_{n-1}$ if $\Delta\epsilon_n^c = \Delta\epsilon_1^c$, that $\sigma_n = 0$ if $\Delta\epsilon_n^c = \Delta\epsilon_1^c/m+1$, and that $\Delta\epsilon_n^c$ is always of the same sign as $\Delta\epsilon_1^c$. This implies that if $\Delta\epsilon_n$ is of the opposite sign to $\Delta\epsilon_1^c$ it is accommodated primarily by an elastic change. The potential function $W(\Delta\epsilon^c)$ is defined only for creep strain increments of the same sign as $\Delta\epsilon_1^c$, but it is convex. It is given by

$$W(\Delta\epsilon^c) = k\Delta t\ \left[\frac{\Delta\epsilon_n^c}{k\Delta t}\right]^{\frac{m+1}{m}} - \Delta\epsilon_1^c\left[\frac{\Delta\epsilon_n^c}{k\Delta t}\right]^{1/m} \quad . \tag{4.30}$$

This function can be used directly in the structural problem, and no further parameters need be chosen. In the following section we shall consider its implications in simple numerical examples.

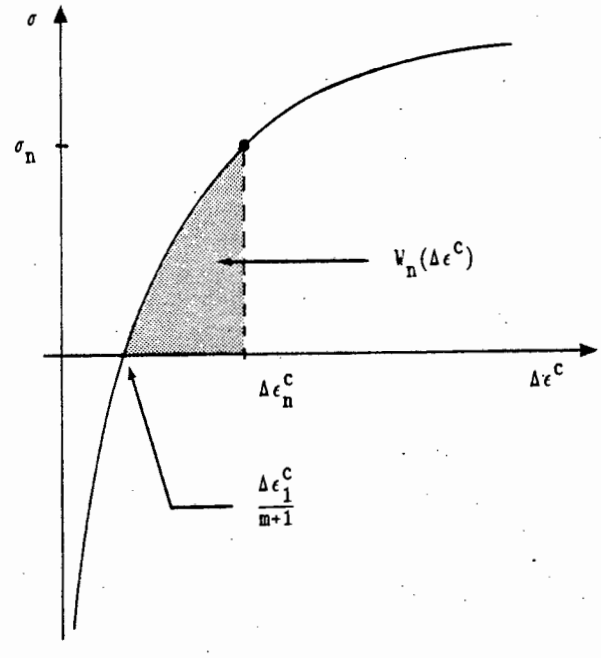

Figure 4.7 : Potential form of the generalised σ_* path (maximum net complementary work path)

4.4 NUMERICAL COMPARISON OF STRESS PATHS

The different paths were discussed in a form which is readily identifiable with the internal variable formulation. The numerical solution algorithm developed in Chapter 3 is therefore an appropriate procedure in which the numerical performance of the different stress paths can be compared. The framework is sufficiently general that a detailed discussion of the implementation of each path need not be repeated. We have shown that the different applications of the trapezoidal rule lead to different forms of the potential function in

the incremental minimum principal in equation (3.3a). This, in turn, results in different forms of a consistent predictor and corrector step. These will be summarised for each path.

In order to gain insight into the numerical performance of the different formulations, we will conduct simple numerical studies on each path individually before comparing the optimal form of each path with each other.

4.4.1 The t_* path

The t_* path is defined by the selection of the integration parameter θ in the trapezoidal rule contained in equation (4.2). The solution algorithm and its numerical performance has already been discussed in Chapter 3. Detailed discussion of numerical studies on the parameter θ and its generalised form (i.e. based on θ = m/m+1) is contained in Section 3.4. For completeness, we summarise the essential formulations of the t_* path and its generalised form in Table 4.1.

4.4.2 The σ_* path

The essential steps in the formulation of the solution procedure based on the σ_* path (and its generalised form) are shown in Table 4.2. The formulations in Tables 4.1 and 4.2 illustrate the different approaches resulting from application of the trapezoidal rule to the creep strains and the stresses respectively.

Table 4.1 : Essential steps in the t_* path

Path	t_* path
Trapezoidal rule	$\Delta\epsilon_n^c = k\Delta t\left\{(1 - \theta)\ \sigma_{n-1}^m + \theta\sigma_n^m\right\}$
Constitutive relation	$\sigma_n = \left\{\frac{1}{\theta}\frac{\Delta\epsilon_n^c}{k\Delta t} - \left[\frac{1 - \theta}{\theta}\right]\sigma_{n-1}^m\right\}^{1/m}$
Potential function	$W_n = \frac{m\theta k\Delta t}{m+1}\left\{\frac{1}{\theta}\frac{\Delta\epsilon_n^c}{k\Delta t} - \left[\frac{1 - \theta}{\theta}\right]\sigma_{n-1}^m\right\}^{\frac{m+1}{m}}$
Consistent predictor	$A_n = \frac{1}{m\theta k\Delta t}\left\{\frac{1}{\theta}\frac{\Delta\epsilon_n^c}{k\Delta t} - \left[\frac{1 - \theta}{\theta}\right]\sigma_{n-1}^m\right\}^{\frac{1-m}{m}}$
Corrector step	$\sigma_n + Ek\Delta t\theta\ \sigma_n^m = E(\Delta\epsilon_n - k\Delta t(1 - \theta)\sigma_{n-1}^m) + \sigma_{n-1}$
Path	**Generalised t_* path**
Trapezoidal rule	$\Delta\epsilon_n^c = k\Delta t\left\{\frac{\sigma_{n-1}^m}{m+1} + \frac{m\sigma_n^m}{m+1}\right\}$
Constitutive relation	$\sigma_n = \left\{\frac{(m+1)\ \Delta\epsilon_n^c}{mk\Delta t} - \frac{\sigma_{n-1}^m}{m}\right\}^{1/m}$
Potential function	$W_n = \left[\frac{m}{m+1}\right]^2 k\Delta t\left\{\frac{(m+1)\ \Delta\epsilon_n^c}{mk\Delta t} - \frac{\sigma_{n-1}^m}{m}\right\}^{\frac{m+1}{m}}$
Consistent predictor	$A_n = \frac{m+1}{m^2 k\Delta t}\left\{\frac{(m+1)\ \Delta\epsilon_n^c}{mk\Delta t} - \frac{\sigma_{n-1}^m}{m}\right\}^{\frac{1-m}{m}}$
Corrector step	$\sigma_n + \frac{mEk\Delta t}{m+1}\ \sigma_n^m = E\left[\Delta\epsilon_n - \frac{k\Delta t}{m+1}\ \sigma_{n-1}^m\right] + \sigma_{n-1}$

Table 4.2 : Essential steps in the formulation of the solution algorithm for the σ_* path

Path	σ_* path
Trapezoidal rule	$\Delta\epsilon_n^c = k\Delta t \left\{(1 - \alpha)\sigma_{n-1} + \alpha\, \sigma_n\right\}^m$
Constitutive relation	$\sigma_n = \frac{1}{\alpha}\left[\frac{\Delta\epsilon_n^c}{k\Delta t}\right]^{1/m} - \left[\frac{1 - \alpha}{\alpha}\right]\sigma_{n-1}$
Potential function	$W_n = \frac{m}{m+1}\frac{k\Delta t}{\alpha}\left[\frac{\Delta\epsilon_n^c}{k\Delta t}\right]^{\frac{m+1}{m}} - \left[\frac{1 - \alpha}{\alpha}\right]\sigma_{n-1}\,\Delta\epsilon_n^c$
Consistent predictor	$A_n = \frac{1}{\alpha}\frac{1}{mk\Delta t}\left[\frac{\Delta\epsilon_n^c}{k\Delta t}\right]^{\frac{1-m}{m}}$
Corrector step	$\sigma_n + Ek\Delta t\left\{(1 - \alpha)\sigma_{n-1} + \alpha\sigma_n\right\}^m = E\Delta\epsilon_n + \sigma_{n-1}$
Path	**Generalised σ_* path**
Trapezoidal rule	$\Delta\epsilon_n^c = k\Delta t\ \sigma_*^m\ ;\ (m+1)\sigma_*^m = m\sigma_n\ \sigma_*^{m-1} + \sigma_{n-1}^m$
Constitutive relation	$\sigma_n = \left[\frac{m+1}{m}\right]\left[\frac{\Delta\epsilon_n^c}{k\Delta t}\right]^{1/m} - \frac{1}{m}\left[\frac{k\Delta t}{\Delta\epsilon_n^c}\right]^{\frac{m-1}{m}}\sigma_{n-1}^m$
Potential function	$W_n = k\Delta t\left[\frac{\Delta\epsilon_n^c}{k\Delta t}\right]^{\frac{m+1}{m}} - k\Delta t\ \sigma_{n-1}^m\left[\frac{\Delta\epsilon_n^c}{k\Delta t}\right]^{1/m}$
Consistent predictor	$A_n = (m+1)\left[\frac{\Delta\epsilon_n^c}{k\Delta t}\right]^{\frac{1-m}{m}} - \left[\frac{1-m}{m^2}\right]\left[\frac{\Delta\epsilon_n^c}{k\Delta t}\right]^{\frac{1-2m}{m}} k\Delta t\ \sigma_{n-1}^m$
Corrector step	$\left[\frac{m+1}{m}\right]\sigma_* - \left[\frac{\sigma_1^m}{m}\right]\sigma_*^{1-m} + Ek\Delta t\ \sigma_*^m = E\Delta\epsilon_n + \sigma_{n-1}$

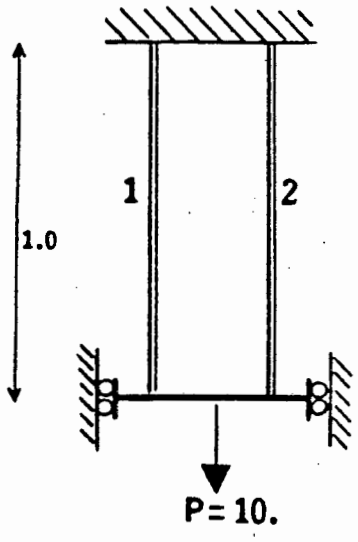

Case	Member	E	k	m
(a)	1	100	0.010	1
	2	50	0.025	1
(b)	1	100	$.32 \times 10^{-5}$	3
	2	50	0.5×10^{-5}	3
(c)	1	100	1024×10^{-8}	5
	2	50	1×10^{-8}	5

All cross-sectional areas = 1.0

Figure 4.8 : Geometric and material properties of 2-bar problem

The implementation of the σ_* path in the numerical solution algorithm leads to a stable and convergent procedure. As expected, the choice of integration parameter α has a marked effect on the accuracy of the solution. The simple two-bar problem depicted in Figure 4.8 again allows us to demonstrate this effect over a range of nonlinear creep laws. The redistribution problem is analysed for a single time step with α ranging from 0.1 to 1.0 in order to study the accuracy for creep laws using m = 1, 3 and 5 . We monitor the prediction of stresses and creep strains in the first member. The percentage errors, computed from

$$e\% = 100 \times \left[\frac{x - \bar{x}}{\bar{x}}\right] \qquad (4.31)$$

where $\bar{x}$ is the baseline solution and x the numerical prediction, are tabled in Table 4.3. The baseline solution was obtained from analyses

using very small time steps ($\Delta t = 0.001$). Further reductions in time step lengths do not result in different solutions.

Table 4.3 : Percentage errors in the predictions of stresses and creep strains in member 1 of the 2-bar redistribution problem

CASE	ALPHA	ERROR PERCENTAGES: e% Stress	Creep Strain
(a) m = 1 (Δt=2.)	0.100	-23.613994	22.094362
	0.200	-17.248493	16.138398
	0.300	-11.731776	10.977014
	0.400	-6.904462	6.461166
	0.500	-2.645155	2.474716
	0.600	1.140731	-1.067505
	0.700	4.528415	-4.236729
	0.800	7.576984	-7.089281
	0.900	10.335343	-9.670167
	1.000	12.842964	-12.016356
	Ω^N path	-2.645155	2.474716
(b) m = 3 (Δt=2.)	0.100	-58.304867	45.344302
	0.200	-38.691995	22.564723
	0.300	-25.279535	7.016695
	0.400	-15.382362	-4.435809
	0.500	-7.707069	-13.300460
	0.600	-1.544641	-20.407839
	0.700	3.536886	-26.258118
	0.750	5.762241	-28.817130
	0.800	7.812578	-31.173288
	0.900	11.469867	-35.371014
	1.000	14.640577	-39.004694
	Ω^N path	-12.053762	-7.942899
(c) m = 5 (Δt=2.)	0.100	-76.836341	66.490201
	0.200	-44.131009	28.247762
	0.300	-25.289465	6.219211
	0.400	-12.726781	-8.466586
	0.500	-3.629485	-19.100411
	0.600	3.321897	-27.225550
	0.700	8.838863	-33.671812
	0.800	13.342701	-38.934333
	0.833	14.668133	-40.482845
	0.900	17.101030	-43.325333
	1.000	20.292841	-47.053859
	Ω^N path	-13.966813	-6.956787

The results in Table 4.3 show that no one value of α gives the most accurate result, and in fact the accuracy of stress and creep strains are noticeably different for nonlinear creep laws. Most accurate stresses are obtained using α in the range 0.5-0.6, while for most accurate creep strain predictions we need α in the range 0.3-0.4. Table 4.3 also contains the percentage errors for the solution based on the maximum net complementary work path in each case. While these predictions are clearly not the most accurate, they provide a choice of path which is consistently reasonably accurate if both stress and strain predictions are considered.

Counter examples may exist, but the above results are representative of numerical studies on different structures under a range of material and loading parameters. The accuracy of the solution algorithm appears to be sensitive to the choice of α , and no one value gives good predictions of both stress and creep strain solutions. The generalised σ_* path clearly does not provide optimal predictions for stresses or creep strains, but allows a reasonably accurate basis for selecting the appropriate form of the σ_* path.

4.4.3 Comparisons of the t_* path and the σ_* path

The generalised forms of the t_* path (θ = m/m+1) and the σ_* path (maximum net complementary work path) appeared to be the most suitable forms of their implied stress paths. The simple uniaxial redistribution problems are sufficient to demonstrate the differences in solutions obtained by the two approaches.

In the first comparison, the two-bar problem in Figure 4.8 is again considered. The structure was analysed under several load conditions, material constants and time step lengths for both paths. Figures 4.9(a) and (b) show a typical trend for the predictions of stress and creep strain histories. The structure was analysed for a constant load P = 10, using m = 5 and Δt = 2 for both algorithms. More accurate results are obtained by the t_* path. Both paths display similar convergence characteristics, but the σ_* path required marginally less iterations per step in the early steps when most redistribution occurs.

The three-bar structure in Figure 4.10 consists of members with different creep power indices. The structure was analysed using 6 time steps of length 1.5 units each. Results obtained with analyses using the two generalised paths are summarised in Table 4.4. Again the procedure based on the trapezoidal path produces more accurate results, but requires an additional iteration in the first step.

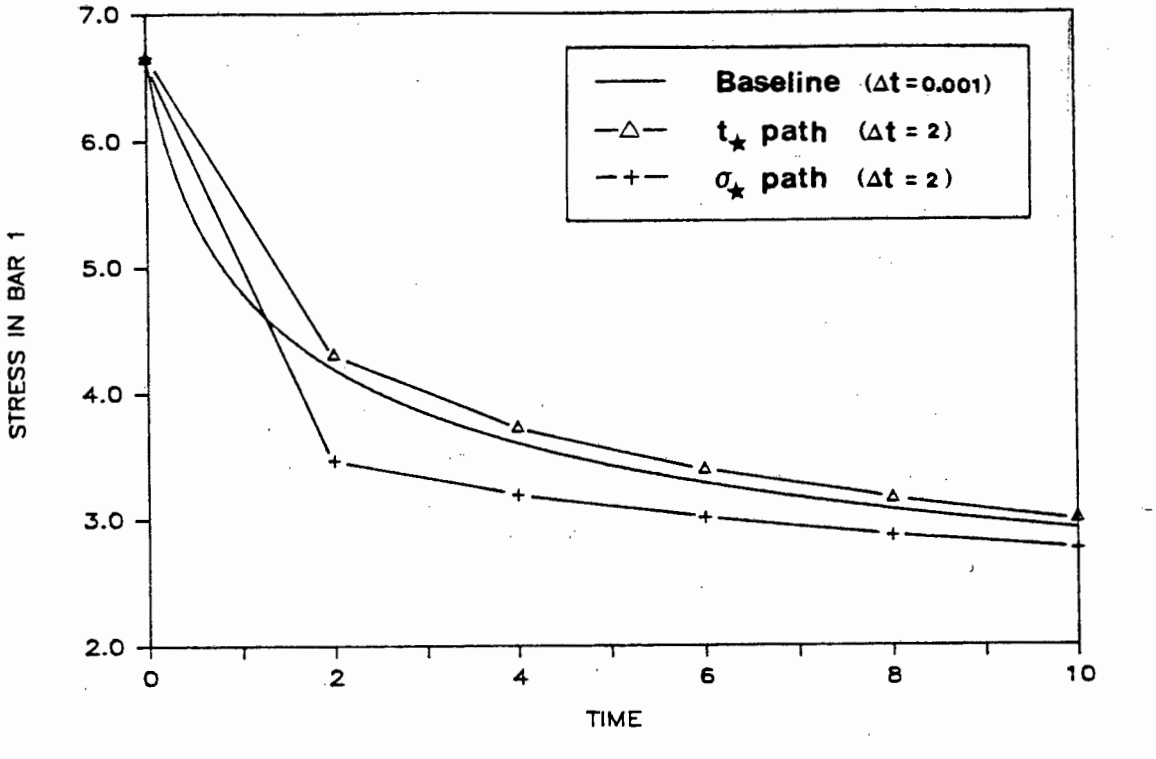

Figure 4.9(a) : Stress predictions in bar 1 of the 2-bar problem

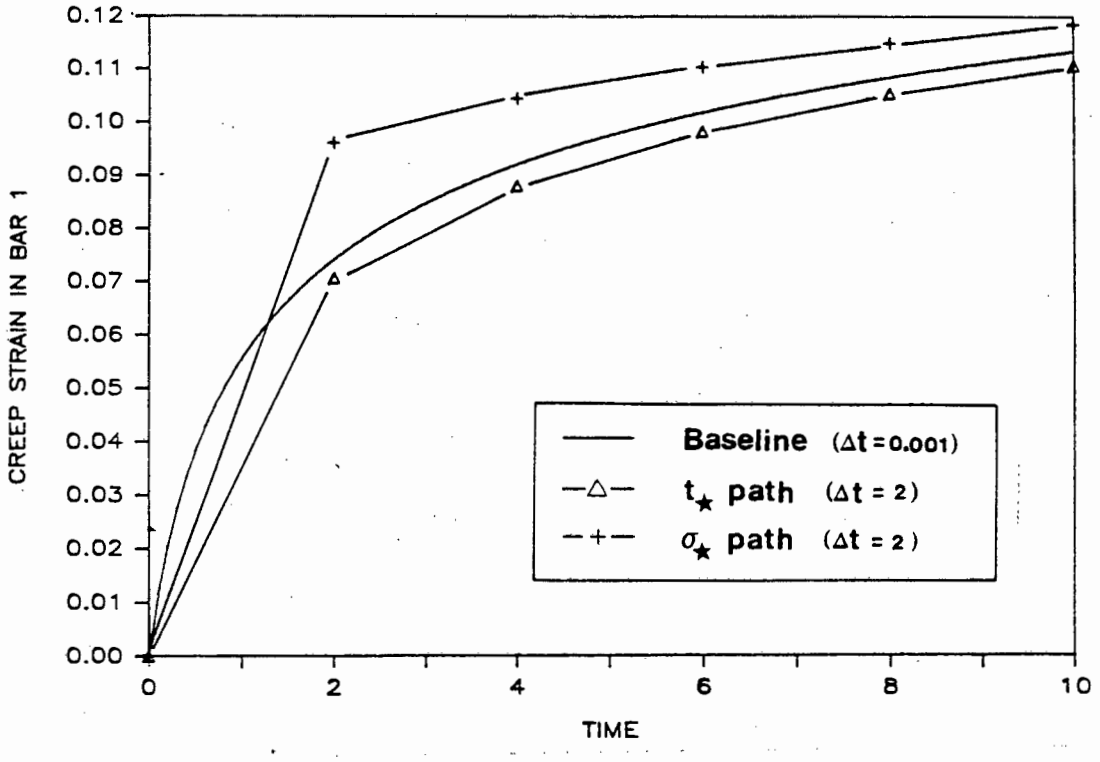

Figure 4.9(b) : Comparison of creep strain predictions in bar 1 of the 2-bar problem using the generalised t_* and σ_* paths

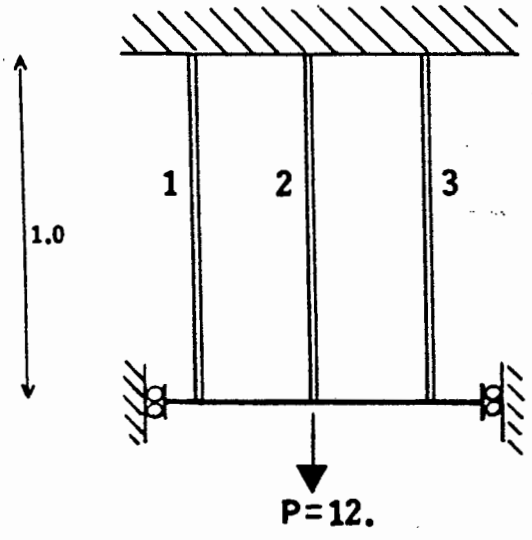

Member	E	k	m
1	300	256×10^{-5}	1
2	100	1×10^{-5}	3
3	200	16×10^{-5}	5

All cross-sectional areas = 1.0

Figure 4.10 : Geometric and material properties for the 3-bar problem

Table 4.4 : Comparison of results for the 3-bar structure.

ANALYSIS	TIME	ITERATIONS	DISPLACEMENT	BAR STRESSES A	B	C
Analytical solution	0.00		0.020000	6.00000	2.00000	4.00000
	1.50		0.042079	5.50334	4.15103	2.34510
	3.00		0.056789	4.30651	5.44892	2.24429
	4.50		0.068909	3.48543	6.34657	2.16776
	6.00		0.079363	2.94176	6.94630	2.11176
	7.50		0.088765	2.59077	7.33639	2.07270
	9.00		0.097511	2.36807	7.58537	2.04646
t_* stress	0.00	0	0.020000	6.00000	2.00000	4.00000
path	1.50	4	0.045931	6.55030	4.48837	0.96133
	3.00	3	0.059363	4.31911	5.60008	2.08081
	4.50	2	0.071159	3.40735	6.41657	2.17608
	6.00	2	0.081563	2.89729	6.97605	2.12666
	7.50	2	0.090974	2.57088	7.34418	2.08494
	9.00	2	0.099747	2.36171	7.58252	2.05576
σ_* stress	0.00	0	0.020000	6.00000	2.00000	4.00000
path	1.50	3	0.047849	6.91537	4.71010	0.37452
	3.00	3	0.060129	4.19816	5.72208	2.07976
	4.50	2	0.071485	3.29108	6.51207	2.19685
	6.00	2	0.081774	2.84399	7.06997	2.08603
	7.50	2	0.090962	2.51401	7.41801	2.06798
	9.00	2	0.099594	2.31953	7.64074	2.03974

4.5 CONCLUSION

We have identified two distinct forms of the stress and strain paths followed over a time interval. The different paths result from the application of the trapezoidal rule to the creep strain history (t_* path) or alternatively to the stress-history (σ_* path). In both cases the actual path followed is, however, still prescribed by the choice of integration parameters θ or α . We have seen that, for two special cases, the paths may become identical. For m = 1 , and setting $\alpha = \theta = 1/2$ the paths both predict the same stress and strain

increments. This is also achieved if we set $\alpha = \theta = 1$ and let $m \to \infty$. We expect most creep problems to fall within these two bounds.

In an attempt to choose the approximating paths on the basis of the mechanics of the problem, we identified a maximum net complementary work path. This resulted in a generalised form of the σ_* path which prescribed a specific path over the step, thus eliminating the heuristic choice of α. The generalised σ_* path showed good performance, more consistent than that of an arbitrary choice of α, in the numerical studies on a wide range of creep problems. The generalised t_* path, based on a $\theta = m/m+1$ assumption also exhibits improved results in numerical studies which compared arbitrary choices of θ. This assumption, however, still remains a heuristic one.

When the generalised forms of both paths were compared, the t_* path showed greater numerical accuracy and stability. This result was expected. In Chapter 2 we showed that the creep problem is a first order ordinary nonlinear differential equation in the creep strains only. Solution algorithms employing trapezoidal approximations of the creep strain history (as in the t_* path) are expected to yield better numerical performance.

The identification of the stress and strain paths implied by the two different approaches, and their generalised forms, have provided insight into suitable choices of the integration parameters. The heuristic choice $\theta = m/m+1$ and the maximum net complementary work path are suitable bases for such choices. Other bases may be appropriate. This will be demonstrated in the next chapter.

CHAPTER 5

LINEAR AND BILINEAR APPROXIMATIONS OF THE STRESS PATHS

5.1 INTRODUCTION

In previous chapters we have considered approximate stress paths for each time interval based on the application of trapezoidal rule. It is clear that the choice of the parameter θ or α affects the accuracy of the solution and thus the issue of an appropriate choice is an important one. The ratio of θ = m/m+1 in the t_* path appears, heuristically, to be a good choice, and the generalised σ_* path enforces specific forms of the σ_* path which behaves well. This suggests that we should explore other bases for the choice of θ and α , as we shall do in this chapter.

Since stress histories in creep problems often tend to be relatively smooth, a piecewise linear approximation of the stress path is likely to be a good one. We shall consider the problem of choosing θ and α in such a way that the t_* and σ_* paths exactly reproduce a linear stress path over each time interval. This leads to analytical expressions for the suitable choice of the integration parameters θ and α at each integration point. We demonstrate the implementation of this modified integration algorithm in an improved solution procedure. The concept can be further extended to a consideration of higher order approximation of the actual stress path. In particular, a bilinear approximation is shown to lead to improved numerical results.

In each case numerical examples are presented for the truss problem. We confine ourselves to uniaxial creep governed by a Norton power law.

5.2 A LINEAR APPROXIMATION OF THE STRESS PATH

In this section the integration parameters θ and α in the t_* and σ_* paths respectively, are selected to exactly reproduce a straight path in the actual stress-time space over each successive time interval. Analytical expressions are derived so that the parameters can be adjusted to compute exact approximations of the creep strain increment for a given linear path between the initial and final stress.

For an accurate solution, the numerical approximation $\Delta\epsilon^c$ of the actual creep strain increment $\Delta\bar{\epsilon}^c$, must be such that

$$\Delta\epsilon^c = \Delta\bar{\epsilon}^c \tag{5.1}$$

is satisfied. We look at a stress change from an initial stress σ_{n-1} at time t_{n-1} to a final stress σ_n at time t_n over the time interval $\Delta t = t_n - t_{n-1}$. The stress change for a linear path in stress-time space and the creep strain rate curve for a Norton creep law is depicted in Figure 5.1. The actual creep strain increment for the step is represented by the shaded area under the curve. This can be determined analytically for known σ_{n-1} , σ_n and Δt .

For convenience, the final stress σ_n is expressed as $\sigma_n = \beta\ \sigma_{n-1}$ with $\beta \neq 1$ to exclude the trivial case of $\sigma_{n-1} = \sigma_n$. The initial stress σ_{n-1} is assumed to be non-zero and may be either positive or negative.

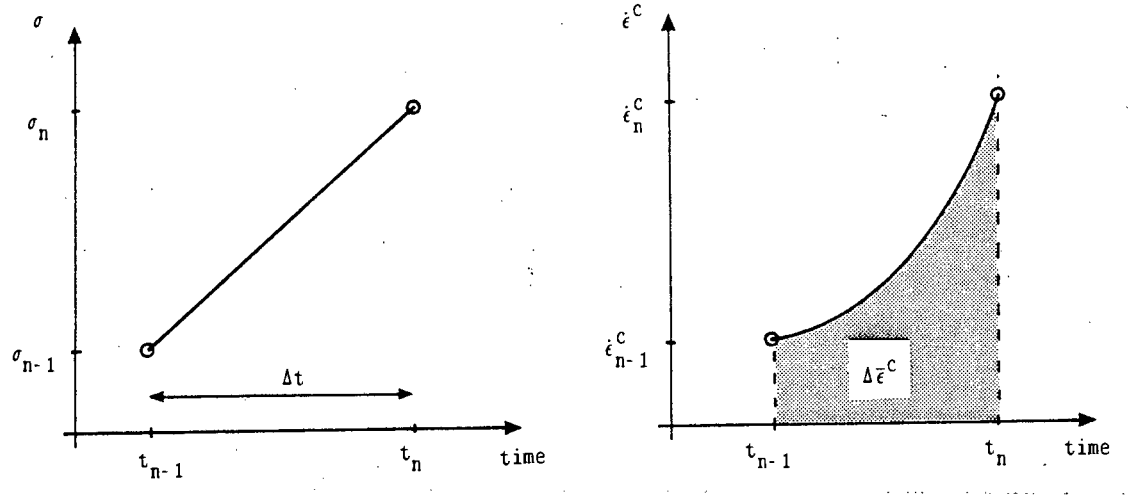

Figure 5.1 : A linear variation of stresses in the stress-time space

The analytical creep strain increment $\Delta\bar{\epsilon}^c$ is given by

$$\Delta\bar{\epsilon}^c = \int_{t_{n-1}}^{t_n} k[\sigma(t)]^m \, dt = kJ$$

where $$J = \int_{t_{n-1}}^{t_n} [\sigma(t)]^m \, dt \quad . \tag{5.2}$$

For changes of stress along a linear path in the stress-time space the analytical evaluation of J is as follows:

$$J = \int_0^1 [\sigma_{n-1} + \xi(\beta - 1)\, \sigma_{n-1}]^m \, \Delta t \, d\xi =$$

$$= \frac{\Delta t}{(\beta - 1)(m+1)\, \sigma_{n-1}} \left[(\beta^{m+1} - 1)\, \sigma_{n-1}^{m+1}\right] \quad . \tag{5.3}$$

Alternatively, the above expression can be formulated in terms of the final stress σ_n . By assuming σ_n non-zero and setting $\sigma_{n-1} = \eta\, \sigma_n$, it

can be shown that

$$J = \frac{\Delta t}{(1 - \eta)(m+1)\ \sigma_n} \left[(1 - \eta^{m+1})\ \sigma_n^{m+1}\right] \quad . \tag{5.4}$$

This yields the exact analytical creep strain increment for the assumed linear stress variations. The numerical approximation of this increment depends on the values of θ and α in the two time integration schemes and their assumed paths.

5.2.1 The t_* Path

The t_* path is based on a trapezoidal approximation of the creep strain history. The numerical approximation of the creep strain increment for a given straight line in stress space is shown in Figure 5.2.

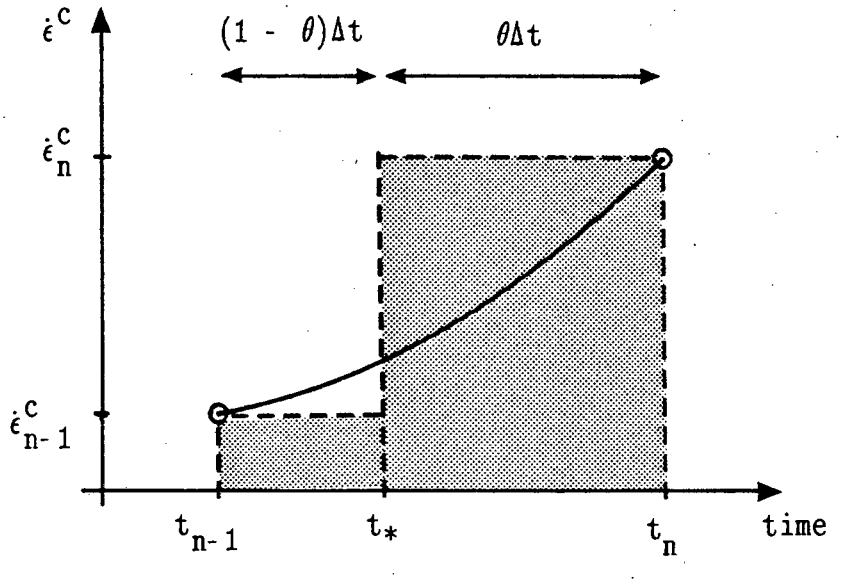

Figure 5.2 : Numerical approximation of the creep strain increment for the t_* path

The creep strain increment predicted by the t_* path is given by equation (3.13), so that we write

$$\Delta\epsilon_t^c = (1 - \theta)\ k\Delta t\ \sigma_{n-1}^m + \theta\ k\Delta t\ \sigma_n^m \quad . \tag{5.5}$$

The value of θ to equate the analytical and the numerically approximated creep strain increments is found by substituting equation (5.5) into equation (5.1). We find

$$\theta = \frac{(\beta^{m+1} - 1) - (\beta - 1)(m+1)}{(\beta^{m} - 1)(\beta - 1)(m+1)} \quad , \qquad (5.6)$$

where $\beta = \sigma_n/\sigma_{n-1}$.

The relationship between θ and the stress ratio β is shown in Figure 5.3 for several finite values of the power index m . It is clear that $\theta \rightarrow m/m+1$ when $\beta = 0$ (i.e. $\sigma_n = 0$) , while θ asymptotically tends to $1/m+1$ when $\beta \rightarrow \pm \infty$. These results may also be derived analytically from equation (5.6), firstly by setting $\beta = 0$ and secondly by finding the limits as $\beta \rightarrow \pm \infty$.

By adopting the ratio $\eta = \sigma_{n-1}/\sigma_n$, the value of θ satisfying equation (5.1) can be expressed as

$$\theta = \left[\frac{1 - \eta^{m+1}}{(1 - \eta)(m+1)} - \eta^{m}\right] \quad . \qquad (5.7)$$

This function $\theta = \theta(\eta)$ is depicted graphically in Figure 5.4 for a range of values of m . As expected, $\theta = 1/m+1$ for the case $\eta = 0$ and $\theta = m/m+1$ when $\eta \rightarrow \pm \infty$.

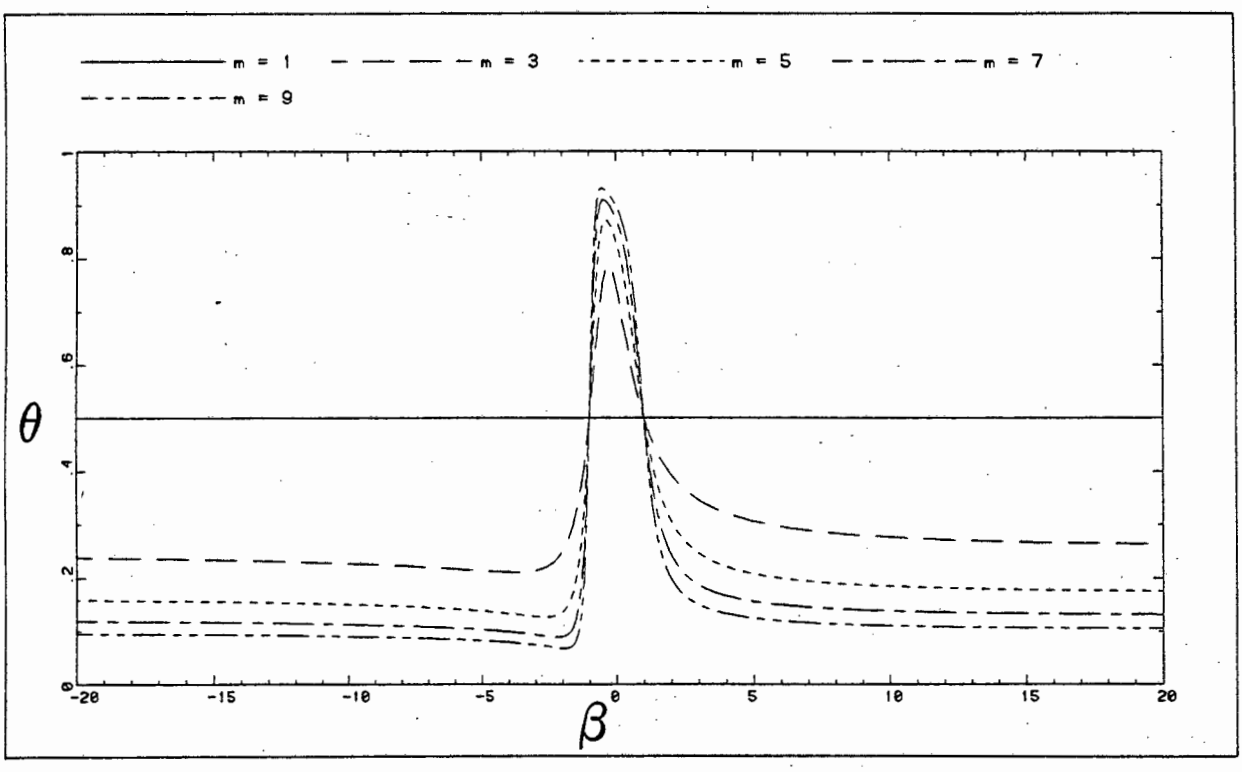

Figure 5.3 : Optimal values of θ in the t_* path for linear stress-time histories (stress ratio $\beta = \sigma_n/\sigma_{n-1}$)

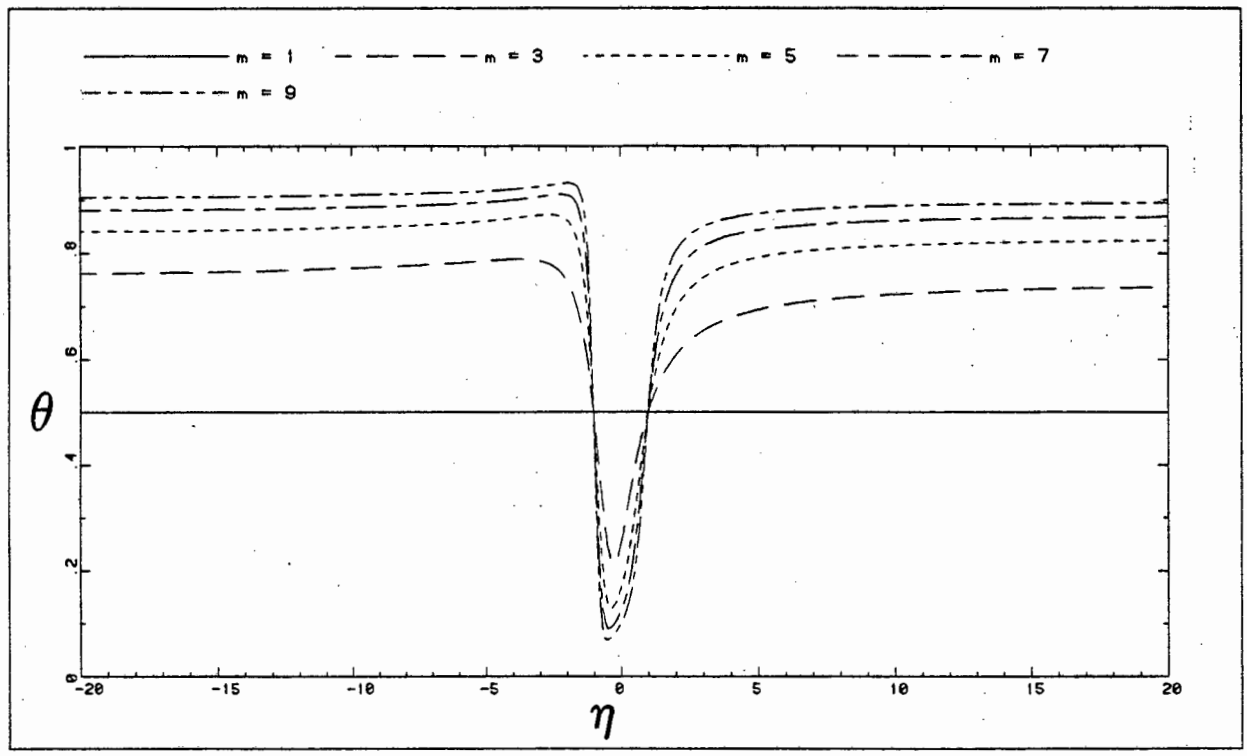

Figure 5.4 : Optimal values of θ in the t_* path for linear stress-time histories (stress ratio $\eta = \sigma_{n-1}/\sigma_n$)

The choice of θ = m/m+1 provided good results in the numerical studies in earlier chapters. The same ratio has now been demonstrated to be near optimal to find exact approximations of linear stress variations under certain conditions. For instances where the final stress is smaller than the initial stress (i.e. $|\sigma_n|<|\sigma_{n-1}|$) this value of θ is optimal. Accurate integration is therefore achieved in problems exhibiting nearly linear decreasing stresses over a given step. The value of θ = 1/m+1 , required for cases where $|\sigma_n|>|\sigma_{n-1}|$, is however outside the permissible range for unconditional numerical stability. The solution algorithm may become unstable for this choice of θ if large time steps are used in the analysis.

It is evident from Figures 5.3 and 5.4 that the choice of θ is largely bounded by two extreme cases. For a linear creep problem (m=1) the mid-point rule (θ = 1/2) consistently reproduces an exact creep strain approximation, while as m $\rightarrow \infty$ and plasticity is approached a backward difference integration scheme (θ = 1) is required.

5.2.2 The σ_* Path

The remarks of the preceeding section are easily extended to the case of the σ_* path which results from a trapezoidal approximation of the stresses over a time increment. The numerical approximation of the creep strain increment $\Delta\epsilon_\sigma^c$ and the analytical solution $\Delta\bar{\epsilon}^c$ must be equated so that

$$\Delta\epsilon_\sigma^c = \Delta\bar{\epsilon}^c \quad . \tag{5.8}$$

The creep strain increment predicted by assuming a σ_* path is shown in Figure 5.5. From equation (4.9a) we find

$$\Delta\epsilon^c_\sigma = k\ \sigma_*^m\ \Delta t = k\left[\sigma_{n-1} + \alpha(\sigma_n - \sigma_{n-1})\right]^m \Delta t \quad . \qquad (5.9)$$

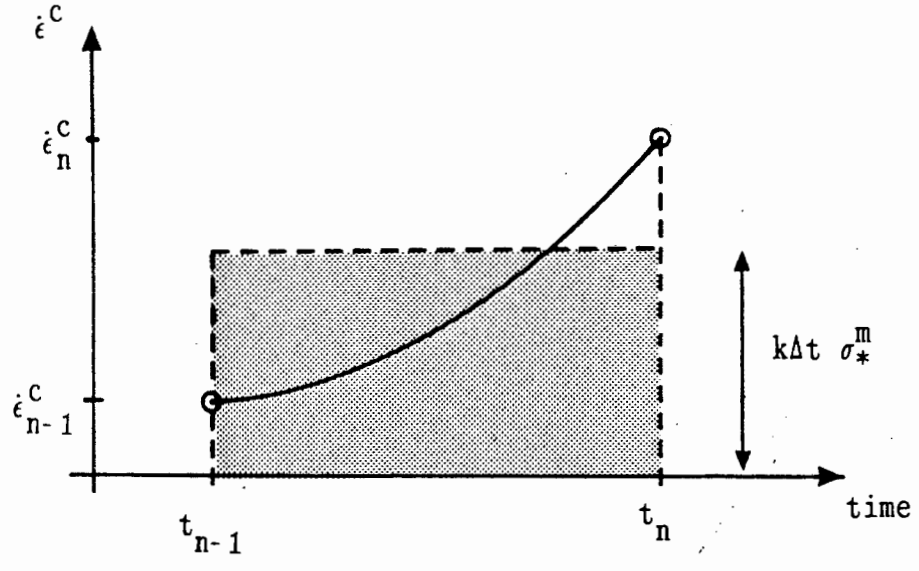

Figure 5.5 : Numerical approximation of the creep strain increment for the σ_* path

By writing the final stress as $\sigma_n = \beta\ \sigma_{n-1}$, so that

$$\sigma_* = \sigma_{n-1} + \alpha(\beta - 1)\ \sigma_{n-1} \quad , \qquad (5.10)$$

the value of α for exact approximation of the actual creep strain increment is determined by substituting equations (5.9) and (5.10) into equation (5.8). This leads to a nonlinear expression in which α must satisfy

$$[1 - \alpha(\beta - 1)]^m = \frac{\beta^{m+1} - 1}{(\beta - 1)(m+1)} \quad . \qquad (5.11)$$

Alternatively by selecting the stress ratio $\sigma_{n-1} = \eta\ \sigma_n$, hence

$$\sigma_* = \eta\ \sigma_n + \alpha(1 - \eta)\ \sigma_n \quad , \tag{5.12}$$

we can show that equation (5.8) is satisfied when

$$[\eta + \alpha(1 - \eta)]^m = \frac{1 - \eta^{m+1}}{(1 - \eta)(m+1)} \quad . \tag{5.13}$$

The relationships $\alpha = \alpha(\beta)$ and $\alpha = \alpha(\eta)$ are shown in Figures 5.6 and 5.7 respectively. Note that the singularities at $\beta = 1$ and $\eta = 1$ are not indicated on the figures. These are the trivial cases of constant stress $\sigma_n = \sigma_{n-1}$ when any value of α (or θ in the t_* path) would yield exact estimates of the creep strain increment. Figures 5.6 and 5.7 similarly show typical trends and asymptotic values for the integration parameter α . Equations (5.11) and (5.13) imply that

$$\alpha = 1 - \frac{1}{(m+1)^{1/m}} \tag{5.14}$$

when $\beta = 0$ and $\eta = 0$ respectively. Asymptotic values of α may also be obtained from these equations for both $\beta \to \pm \infty$ and $\eta \to \pm \infty$. It can be shown that

$$\lim_{\beta \to \pm \infty} \alpha = \lim_{\eta \to \pm \infty} \alpha = \frac{1}{(m+1)^{1/m}} \quad . \tag{5.15}$$

The trends for values of α to exactly reproduce a staight line stress change are again in agreement with our intuitive results. The mid-point rule gives an exact approximation for linear creep laws, while backward difference integration is required as $m \to \infty$.

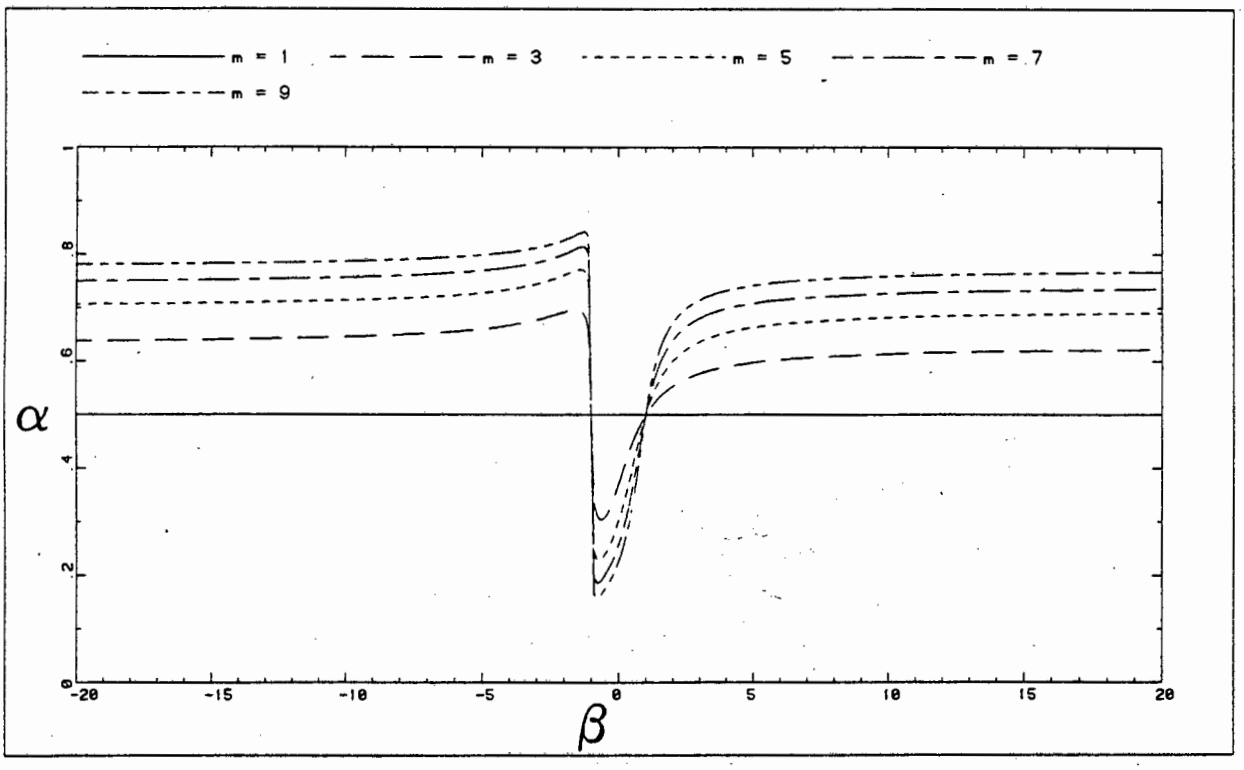

Figure 5.6 : Optimal values of α in the σ_* path for linear stress-time histories (stress ratio $\beta = \sigma_n/\sigma_{n-1}$)

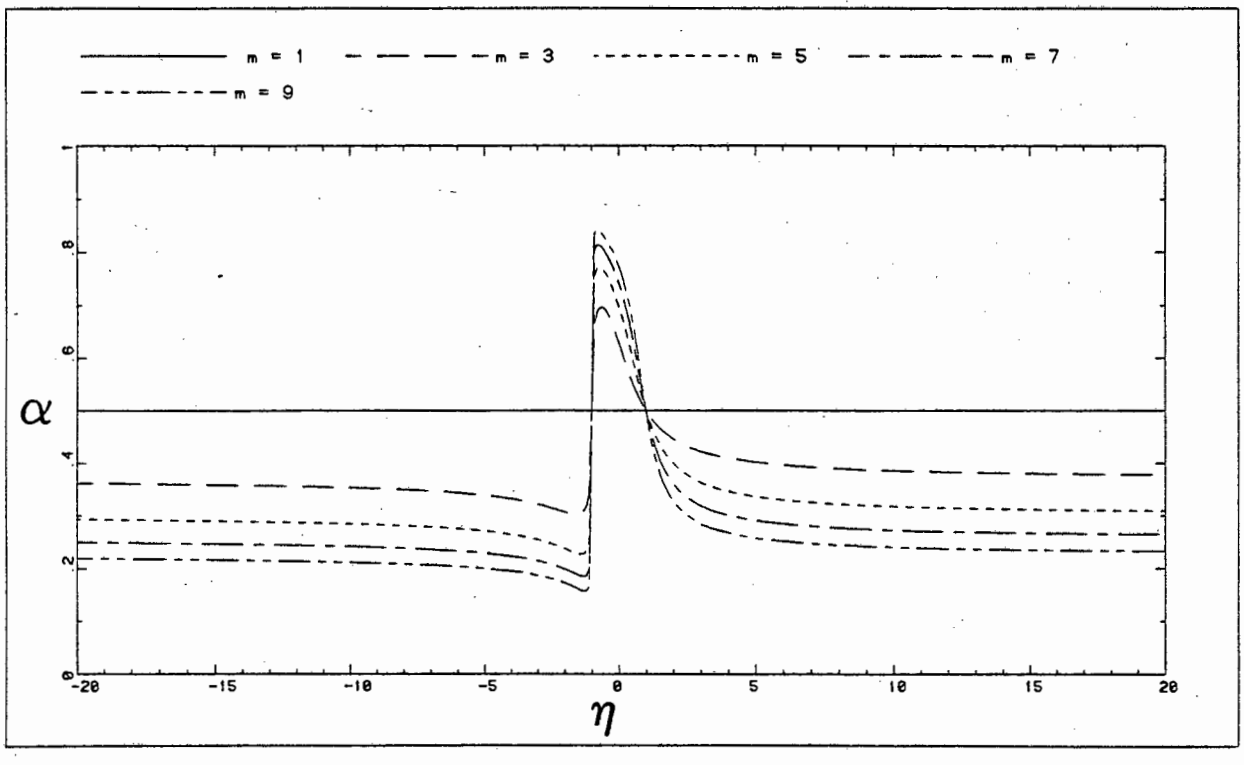

Figure 5.7 : Optimal values of α in the σ_* path for linear stress-time histories (stress ratio $\eta = \sigma_{n-1}/\sigma_n$)

5.3 AN IMPROVED SOLUTION PROCEDURE

The iterative solution procedure developed in Chapters 3 has been applied to solve problems for both t_* and σ_* stress paths. These used either arbitrarily selected integration parameters, or the generalised forms of the paths to perform the integration at each sample point. The iterative scheme within each step is terminated when the procedure converges to the correct stress state at the end of the step. The integration path, initial and final stresses are then used to determine the creep strain increment at each sample point. It has however been demonstrated that any constant value of θ (or α) does not always provide the most accurate predictions. This value depends on the actual path in stress-time space; determined by the ratio of initial and final stresses for a straight line path. This can be exploited by adopting a second iterative loop upon convergence of the iterative procedure within a step. The objective of this loop is to recalculate the value of θ (or α) in each case so that the path between the initial and the predicted final stress over the step can be more accurately or possibly even exactly integrated. This procedure is repeated until the successive recalculation of θ (or α) converges to a constant value at each sample point.

The "double loop" integration scheme will ensure that the stress-history is suitably approximated and the creep strains are updated consistently. Once a stress function $\sigma(t)$ is selected to approximate the stress-time curve, the improved numerical solution algorithm for either of the t_* or σ_* path is summarised in the following steps:

1. Perform an elastic analysis to compute the initial displacement and stress fields $\underset{\sim}{u}_0$ and $\underset{\sim}{\sigma}_0$.
2. Define initial values ${}^{j}\theta$ if a t_* path (or ${}^{j}a$ if a σ_* path) is assumed for each element at the beginning of the n-th time interval.
3. Predict the vectors ${}^{i}\underset{\sim}{\dot{\varepsilon}}^{c}_{n}$ and ${}^{i}\underset{\sim}{\varepsilon}^{c}_{n}$ (with i=1) for end of step values, assuming steady state conditions for the first iteration.
4. Compute the modified stiffness matrix $\underset{\sim}{K}^{*}$ and residual force vector ${}^{i}\underset{\sim}{R}_{n}$ to find the displacement increment $\Delta\underset{\sim}{\hat{u}}$, and the predicted strain increment ${}^{i+1}\Delta\underset{\sim}{\varepsilon}_{n}$ for the current time step.
5. Update the final stresses ${}^{i+1}\underset{\sim}{\sigma}_{n}$ and creep strains ${}^{i+1}\underset{\sim}{\dot{\varepsilon}}^{c}_{n}$, ${}^{i+1}\underset{\sim}{\varepsilon}^{c}_{n}$ for the predicted strain increment.
6. Return to Step 4 if the specified tolerance is exceeded for the convergent criterion. We choose $\left\{{}^{i+1}\underset{\sim}{\dot{\varepsilon}}^{c}_{n} - {}^{i}\underset{\sim}{\dot{\varepsilon}}^{c}_{n}\right\} \leq$ tolerance % at each sample point for convergence.
7. Compute the value of ${}^{j+1}\theta$ or ${}^{j+1}a$ according to the initial and final stresses and the assumed stress path. Return to step 3 if different values of the parameter is required for an exact approximation of the creep strain increment at any sample point.
8. Upon convergence to unchanged successive updates of the integration parameters, that is $\left\{{}^{j+1}\theta - {}^{j}\theta\right\} \leq$ tolerance % for the t_* path or $\left\{{}^{j+1}a - {}^{j}a\right\} \leq$ tolerance % for the σ_* path, the solutions are updated.
9. The next time step is started at step 2 using the last updated values of the integration parameters. This time stepping is continued until the desired solution history has been determined.

Note that the "double loop" can be circumvented by updating sample point values of θ (or α) within each iteration of the Newton-Raphson procedure, rather than performing the second loop. Numerical experience demonstrates that this saves computing time without sacrificing stability, convergence or accuracy of the above solution procedure.

5.4 NUMERICAL TESTS ON LINEAR STRESS PATHS

We assumed that the stress-history is reasonably well approximated by successive linearisation of the path between discrete instants. Any stress-history $\sigma(t)$ would be closely approximated by this assumption upon increasing number of steps as $\Delta t \rightarrow 0$. In this section the improved numerical solution procedure is tested on the simple 2- and 3-bar structures used earlier. A convergence tolerance of 0.01% is used throughout. We shall demonstrate only the results achieved by updating θ in a t_* path assumption. The studies are equally applicable to a procedure based on a σ_* path in which α is iteratively updated.

5.4.1 The Two-bar Truss Problem

The two-bar truss represents a problem with typical creep redistribution characteristics. For comparative purposes, a constant applied load and typical power index m = 3 is assumed. The structure and its mechanical properties are depicted in Figure 5.8. In Chapter 3 it was shown that selecting a constant value of θ = m/m+1 at each sample point provides reliable results for a wide range of stresses and loading conditions. The improved solution procedure is thus compared with results given by the constant θ = m/m+1 choice. The percentage

error e% is again defined as

$$e_i\% = 100 \times \frac{x_i - \bar{x}_i}{\bar{x}_i} \qquad (5.16)$$

where x_i is the computed result and $\bar{x}_i$ is considered the converged continuous result in the i-th member. The values for $\bar{x}_i$ are obtained from numerical analyses in which successive reduction of the time step length does not change the solution.

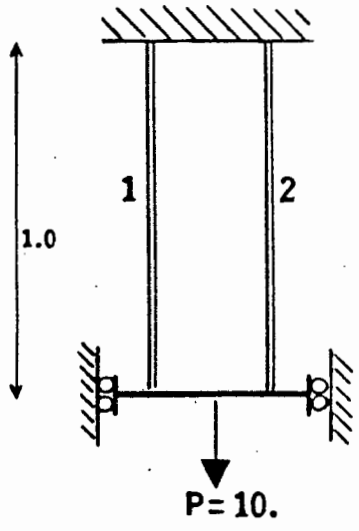

Member	E	k	m
1	100	64×10^{-5}	3
2	50	1×10^{-5}	3

All cross-sectional areas = 1.0

Figure 5.8 : Geometric and material properties for the 2-bar truss problem

The member stresses predicted by both strategies after 2 time units, using increasing number of steps, are shown in Table 5.1. For relatively large steps the new procedure fails to give accurate results while the original method (based on θ = m/m+1) yields more accurate but still rather crude results. This phenomenon can be attributed to the nonlinear curve followed by the member stresses over the initial redistribution time. Linear approximations of these curves over large steps are clearly inaccurate. On the other hand, fairly small increments in the number of steps soon provide more accurate solutions: the

Table 5.1 : Comparison of results for different step-sizes after two units of time (2-bar truss)

STEPS	BAR 1				BAR 2			
	UPDATED θ		θ = m/m+1		UPDATED θ		θ = m/m+1	
	σ	e%	σ	e%	σ	e%	σ	e%
1	2.13140	-31.848	2.90576	-7.088	7.86860	14.493	7.09424	3.226
2	2.92846	-6.362	3.25170	3.974	7.07154	2.895	6.74830	-1.808
4	3.08518	-1.351	3.23971	3.591	6.91482	0.615	6.76029	-1.633
5	3.10089	0.848	3.22537	3.132	6.89911	0.386	6.77463	-1.425
10	3.12099	-0.206	3.18483	1.836	6.87901	0.094	6.81517	-0.835
20	3.12580	-0.052	3.15837	0.990	6.87420	0.024	6.84163	-0.450
50	3.12716	-0.008	3.14036	0.414	6.87284	0.004	6.85964	-0.188
100	3.12735	-0.002	3.13399	0.210	6.87265	0.001	6.86601	-0.095
200	3.12740	-0.001	3.13073	0.106	6.87260	0.001	6.86927	-0.048
500	3.12742	0.000	3.12875	0.043	6.87258	0.000	6.87125	-0.019
1000	3.12742	0.000	3.12808	0.021	6.87258	0.000	6.87192	-0.009
2000	3.12742	0.000	3.12775	0.011	6.87258	0.000	6.87225	-0.004
5000	-	-	3.12755	0.004	-	-	6.87245	-0.001
10000	-	-	3.12748	0.002	-	-	6.87252	-0.000
20000	-	-	3.12745	0.001	-	-	6.87255	0.000

new method yields errors less than 1% when 5 steps are used to subdivide the interval between t = 0 and t = 2.0. The progressive improvement in the solutions by both methods are illustrated in Figure 5.9. The improved solution procedure exhibits a quasi-exponential improvement.

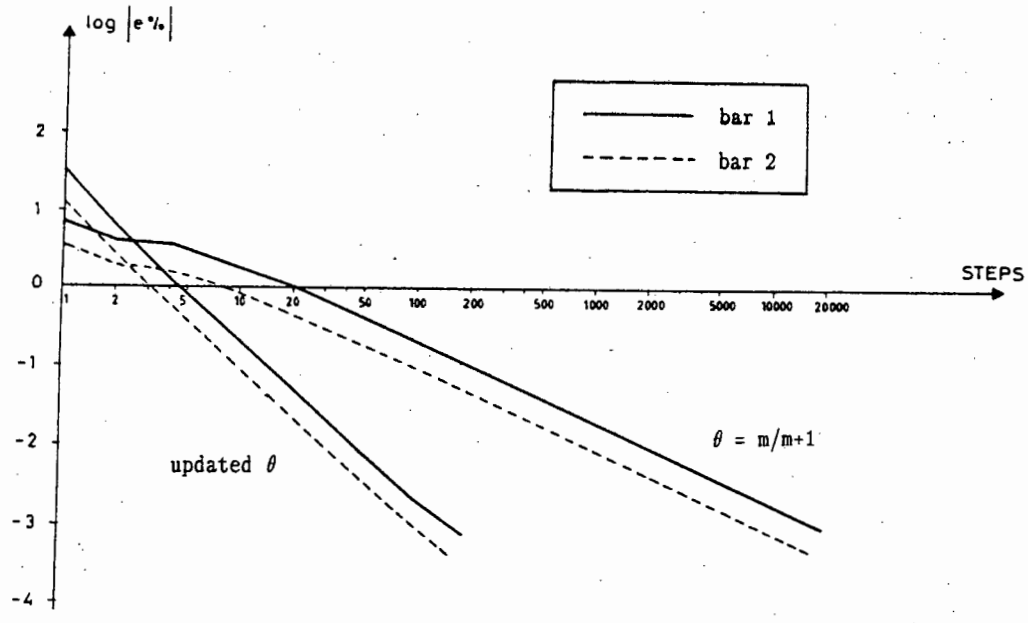

Figure 5.9 : Percentage errors in the procedures based on the updated θ and the θ = m/m+1 approaches

The stresses and percentage errors obtained up to 10 time units after loading are presented in Tables 5.2, 5.3 and 5.4 for analyses conducted with time step lengths of 2, 1 and 0.5 time units respectively. Converged results used for computing percentage errors were obtained using $\Delta t = 0.004$. Table 5.2 demonstrates that $\theta = m/m+1$ provides more accurate results throughout the interval for large time steps, while for smaller steps in Table 5.4 the new procedure performs better because the linear stress approximation is now more applicable.

Table 5.2 : Stresses and percentage errors with step length equal to 2.0 (2-bar structure)

TIME	BAR 1				BAR 2			
	UPDATED θ		$\theta = m/m+1$		UPDATED θ		$\theta = m/m+1$	
	σ	e%	σ	e%	σ	e%	σ	e%
2.0	2.13140	-31.848	2.90576	-7.088	7.86860	14.493	7.09424	3.226
4.0	2.12104	-14.614	2.44889	-1.416	7.87896	4.830	7.55111	0.468
6.0	2.06076	-7.750	2.23871	0.216	7.93924	2.229	7.76129	-0.062
8.0	2.03091	-4.124	2.13094	0.598	7.96909	1.108	7.86906	-0.161
10.0	2.01582	-2.195	2.07295	0.577	7.98418	0.570	7.92705	-0.150

Table 5.3 : Stresses and percentage errors with step length equal to 1.0 (2-bar structure)

TIME	BAR 1				BAR 2			
	UPDATED θ		$\theta = m/m+1$		UPDATED θ		$\theta = m/m+1$	
	σ	e%	σ	e%	σ	e%	σ	e%
1.0	3.58886	-9.082	4.06612	3.009	6.41114	5.923	5.93388	-1.962
2.0	2.92846	-6.362	3.25170	3.974	7.07154	2.895	6.74830	-1.808
3.0	2.60325	-4.340	2.82539	3.823	7.39675	1.623	7.17461	-1.429
4.0	2.40775	-3.072	2.56766	3.365	7.59225	1.015	7.43234	-1.112
5.0	2.28208	-2.212	2.40012	2.846	7.71792	0.673	7.59988	-0.866
6.0	2.19799	-1.607	2.28644	2.352	7.80201	0.462	7.71356	-0.677
7.0	2.14030	-1.173	2.20720	1.916	7.85970	0.324	7.79280	-0.530
8.0	2.10006	-0.860	2.15095	1.543	7.89994	0.231	7.84905	-0.415
9.0	2.07167	-0.631	2.11053	1.233	7.92883	0.173	7.88947	-0.325
10.0	2.05150	0.464	2.08122	0.978	7.94850	0.120	7.91878	-0.254

Table 5.4 : Stresses and percentage errors with step length equal to 0.5 (2-bar structure)

TIME	BAR 1				BAR 2			
	UPDATED θ		θ = m/m+1		UPDATED θ		θ = m/m+1	
	σ	e%	σ	e%	σ	e%	σ	e%
0.5	4.69609	-2.324	4.93363	3.055	5.32319	2.121	5.06637	-2.806
1.0	3.86647	-2.049	4.09514	3.744	6.13353	1.336	5.90486	-2.442
1.5	3.39757	-1.648	3.58499	3.777	6.60243	0.870	6.41501	-1.994
2.0	3.08518	-1.351	3.23971	3.591	6.91482	0.615	6.76029	-1.634
2.5	2.86220	-1.120	2.99091	3.327	7.13780	0.456	7.00909	-1.355
3.0	2.69585	-0.937	2.80410	3.041	7.30415	0.350	7.19590	-1.137
3.5	2.56795	-0.790	2.65974	2.757	7.43205	0.276	7.34026	-0.963
4.0	2.46747	-0.668	2.54582	2.486	7.53253	0.221	7.45418	-0.822
4.5	2.38725	-0.568	2.45448	2.233	7.61275	0.179	7.54552	-0.705
5.0	2.32242	-0.483	2.38035	1.999	7.67758	0.147	7.61965	-0.609
5.5	2.26951	-0.412	2.31960	1.786	7.73049	0.122	7.68040	-0.527
6.0	2.22601	-0.353	2.26944	1.591	7.77399	0.101	7.73056	-0.458
6.5	2.19003	-0.302	2.22776	1.416	7.80997	0.085	7.77224	-0.399
7.0	2.16011	-0.259	2.19295	1.258	7.83989	0.071	7.80705	-0.348
7.5	2.13515	-0.222	2.16376	1.115	7.86485	0.060	7.83624	-0.304
8.0	2.11424	-0.190	2.13920	0.988	7.88576	0.051	7.86080	-0.266
8.5	2.09669	-0.163	2.11847	0.874	7.90331	0.043	7.88153	-0.232
9.0	2.08191	-0.140	2.10094	0.773	7.91809	0.037	7.89906	-0.204
9.5	2.06945	-0.121	2.08608	0.682	7.93055	0.032	7.91392	-0.178
10.0	2.05893	-0.103	2.07346	0.602	7.94107	0.027	7.92654	-0.156

An interesting result is obtained in Table 5.3: the constant value of θ initially provides more accurate results, but final results achieved by updating θ are more accurate in spite of a rather poor performance at the beginning of the analysis. In each case, both methods clearly exhibit more accurate solutions as the time or number of successive steps increases. This appears to be related to the properties of solutions concerned with inelastic strains. Following the same reasoning of Martin [40] for the elastic-plastic problem, it can be shown that differences in the numerical and actual solutions are not likely to increase in time [41]. This means that discrepancies in the numerical solution during the initial highly nonlinear redistribution phase will probably decrease after the strong nonlinearities are over.

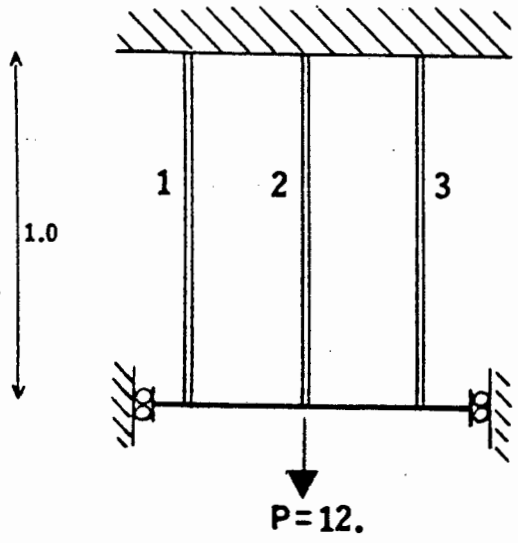

Member	E	k	m
1	300	256×10^{-5}	1
2	100	1×10^{-5}	3
3	200	16×10^{-5}	5

All cross-sectional areas = 1.0

Figure 5.10 : Geometric and material parameters for the 3-bar structure

5.4.2 The Three-bar Structure

The structure in Figure 5.10 is subjected to a constant load. Results obtained after 10 units of time, using different time step lengths are shown in Table 5.5. The updated θ approach again does not provide accurate results when a crude time discretisation is adopted. The accuracy increases rapidly upon reduction of the time step size and results are accurate to 0.2% for a step length of 0.5 time units. The updated approach shows more accurate performance for this highly nonlinear problem in which the standard θ = m/m+1 scheme already allows different integration parameters in each member.

Table 5.5 : Comparison of results for different step sizes after ten units of time (3-bar structure)

METHOD	TIME STEP LENGTH	BAR 1		BAR 2		BAR 3	
		STRESS	e%	STRESS	e%	STRESS	e%
UPDATED θ	1.00	2.23905	-1.257	7.73024	0.416	2.03072	-0.172
UPDATED θ	0.50	2.26332	-0.187	7.70297	0.062	2.03371	-0.025
UPDATED θ	0.25	2.26647	-0.048	7.69944	0.016	2.03409	-0.006
θ = m/m+1	1.00	2.27900	0.505	7.68020	-0.234	2.04080	0.323
θ = m/m+1	0.50	2.27717	0.424	7.68494	-0.173	2.03789	0.180
θ = m/m+1	0.25	2.27321	0.249	7.69067	-0.098	2.03612	0.093

Numerical studies have shown that the double loop integration scheme leads to accurate results, unless a crude time discretisation is used. In this case, however, traditional methods based on constant values of θ also tend to provide inaccurate results (although sometimes closer to the correct solution). In addition, accuracy tends to improve consistently as step sizes are reduced. While counter examples can be found, these trends appear to be fairly typical.

It should be borne in mind that this satisfactory performance is achieved at the cost of additional iterations within each step. However, when fairly small time steps are used, rapid convergence occurs. The actual computational burden is therefore definitely limited. For instance, a typical 20 step analysis of the two-bar structure on a microcomputer has taken 16s with the double loop integration scheme and 11s with the θ = m/m+1 method. In addition some computing time can be saved by updating θ in each iteration of the Newton-Raphson scheme rather than performing updates in a second iterative loop.

5.5 APPROXIMATING A BILINEAR STRESS PATH

In the previous sections a linear approximation of the stress path between initial and final stresses in each time interval was assumed. However, when initial and final stresses are given, the initial and final values of its derivatives $\dot{\sigma}(t)$ are also known. In Chapter 3 we used the internal variable formulation to show that

$$\begin{aligned} \underset{\sim}{\sigma}(t) &= \underset{\sim}{\sigma}^{e}(t) - \underset{\sim}{Z}\ \underset{\sim}{\varepsilon}^{c}(t) \cdot , \\ &= \underset{\sim}{N}^{T}\ \underset{\sim}{P}(t) - \underset{\sim}{Z}\ \underset{\sim}{\varepsilon}^{c}(t) \quad , \end{aligned} \tag{5.17}$$

where $\underset{\sim}{Z}$ and $\underset{\sim}{N}$ are structural matrices defined in equation (2.38b) and (2.37c). It follows that

$$\dot{\underset{\sim}{\sigma}}(t) = \underset{\sim}{N}^T \dot{\underset{\sim}{P}} - \underset{\sim}{Z}\, \dot{\underset{\sim}{\varepsilon}}^c$$
$$= \underset{\sim}{N}^T \dot{\underset{\sim}{P}} - \underset{\sim}{Z}\, \underset{\sim}{k}\, \underset{\sim}{\sigma}^m \quad . \tag{5.18}$$

Equation (5.18) allows us to determine the derivatives of the stresses at any discrete solution instant. In creep problems the external forces $\underset{\sim}{P}$ and therefore their derivatives are prescribed. In fact, we often find that $\underset{\sim}{P}$ is a constant and hence $\dot{\underset{\sim}{P}} = 0$. The actual stress-time curve at any sample point can thus be approximated by a function $\sigma(t)$ whose values and derivatives are known at the beginning and at the end of the time step.

This yields four boundary conditions for the stress-time path over the time step, and these can be used to fit a selected function to the actual path. The selection of the function is however not straightforward. A cubic function, for example, may lead to undesirable changes in curvature in the step. Exponential functions on the other hand yield curves whose second derivatives never change sign, and also necessitate the solution of nonlinear equations to determine the constants defining the curve. A good compromise is provided by a simple bilinear approximation of the actual stress-time curve. This is illustrated in Figure 5.11.

The bilinear curve is modelled with two lines:

$$\sigma(t) = a + b\,t \quad \text{for} \quad 0 \le t \le \hat{t} \tag{5.19a}$$

and $$\sigma(t) = c + d\,t \quad \text{for} \quad \hat{t} \le t \le \Delta t \quad , \tag{5.19b}$$

where $t_{n-1} = 0$ and $t_n = \Delta t$ is chosen for simplicity. The point of inter-section of these lines $\hat{t}$ is determined geometrically, so that

$$\hat{t} = (a - c)/(d - b) \quad . \tag{5.20}$$

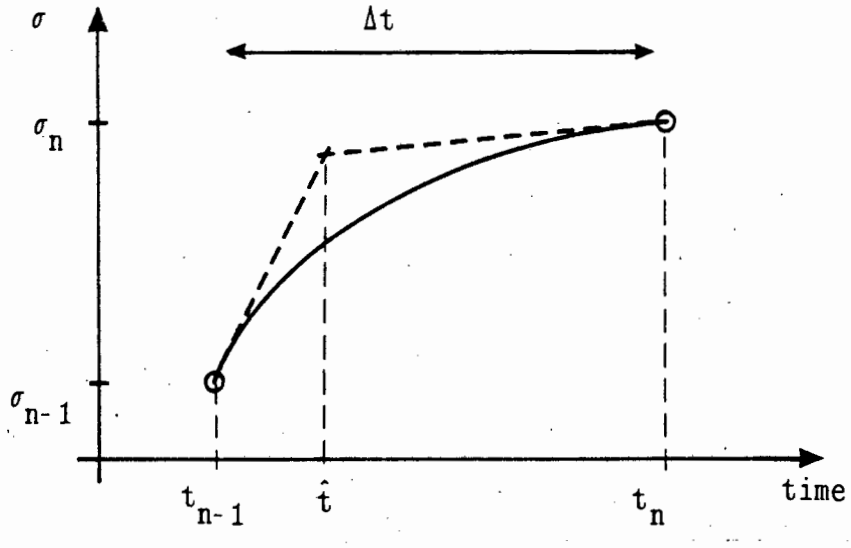

Figure 5.11 : A bilinear approximation of the stress-time history over a single step

The four constants in the bilinear path are determined by applying the boundary conditions: $a = \sigma(t_{n-1})$, $b = \dot{\underset{\sim}{\varepsilon}}(t_{n-1})$, $c = \sigma(t_n) - \dot{\underset{\sim}{\varepsilon}}(t_n)\Delta t$, $d = \dot{\underset{\sim}{\varepsilon}}(t_n)$. Given the above stress path, the exact creep strain increment can be expressed analytically in the form given in equation (5.2) by setting

$$J = \frac{(a + b\,\hat{t})^{m+1} - a^{m+1}}{b(m+1)} + \frac{(c + d\,\Delta t)^{m+1} - (c + d\,\hat{t})^{m+1}}{d(m+1)} \quad . \tag{5.21}$$

The value of θ in the t_* path to reproduce this creep strain increment is given by

$$\theta = \frac{J - \sigma_{n-1}^m\,\Delta t}{\Delta t(\sigma_n^m - \sigma_{n-1}^m)} \quad . \tag{5.22}$$

From equation (5.9) we can show that, for the σ_* path the exact integration of the bilinear stress approximation is achieved when

$$a = \frac{(J/\Delta t)^{1/m} - \sigma_{n-1}}{\sigma_n - \sigma_{n-1}} \quad . \tag{5.23}$$

Note that θ and a are functions of the stresses, their derivatives, the creep law constants and the time step length. The derivatives are computed from structural matrices $\underset{\sim}{N}$ and $\underset{\sim}{Z}$ which depend only on the geometric and mechanical properties of the problem.

The computation and updating of the integration parameters to model bilinear stress paths over time steps is easily implemented in the framework of the implicit creep solution algorithm described earlier. Additional computational effort is required to compute the entries of the $\underset{\sim}{N}$ and $\underset{\sim}{Z}$ matrices needed for evaluating the stress derivatives according to equation (5.18). These, however, need only be performed once, because they remain constant for small displacement analyses.

It may also be noted that the bilinear curve and consequently the individual values of θ or a may not automatically fall in the physically reasonable domain. In particular, equation (5.22) and (5.23) must be applied with caution to cases when the bilinear approximation based on the four stress values becomes unreliable and θ or a fall outside the range $0 < \theta, a \leq 1$. This may occur in multi-element structures when large redistribution takes place within the selected time step. In these cases the stress predictions for the initial iterations are crude and hence their derivatives are also inaccurate. When any one choice of the integration parameter falls

outside the permitted range, the algorithm should revert to adopting less sophisticated schemes such as the linear stress path for the particular stress point.

5.6 NUMERICAL STUDIES ON THE BILINEAR APPROXIMATION

The numerical accuracy of predicting structural response with a bilinear stress-time approximation is best illustrated in the two simple examples. We again demonstrate the use of this assumption in the t_* path only. The algorithm presented in Section 5.3 is used and θ is updated according to equation (5.22). In particular the accurate modelling of the redistributing stresses in the structures are of interest. Results obtained with relatively large steps are compared to the converged solution to demonstrate the accuracy of the choice of θ based on a bilinear stress path. Note that, for comparison, the results are presented in the same format as those obtained with the linear path in Section 5.4.

5.6.1 The Two-bar Problem

The results from numerical studies on the 2-bar structure (Figure 5.8) are shown in Tables 5.6 to 5.9. Stress predictions are progressively improved as step lengths are reduced. In Table 5.6 the computed stresses and error percentages in both bars are given at a time 2 units after loading.

A rapid improvement in the computed stresses occurs upon reduction of time step lengths. However, even at relatively large step lengths, the updating of θ based on integrating a bilinear stress path exhibits good

numerical accuracy. The corresponding results for θ based on m/m+1 and a linear stress path appeared in Table 5.1.

Table 5.6 : Stresses in the 2-bar problem after 2 time units for a bilinear stress path

STEPS	BAR 1 STRESS	e%	BAR 2 STRESS	e%
1	3.33223	6.54885	6.66777	-2.98010
2	3.19357	2.11516	6.80643	-0.96252
4	3.14625	0.60209	6.85375	-0.27399
5	3.13976	0.39457	6.86024	-0.17955
10	3.13061	0.10200	6.86939	-0.04642
20	3.12823	0.02590	6.87177	-0.01179
50	3.12755	0.00416	6.87245	-0.00189
100	3.12745	0.00096	6.87255	-0.00044
200	3.12743	0.00032	6.87257	-0.00015
500	3.12742	0.00000	6.87258	0.00000
1000	3.12742	0.00000	6.87258	0.00000

These trends are repeated in Tables 5.7-5.9 in which the stress-history of the redistributions of stresses in the 2-bar structure are presented. Analyses are performed from the application of the load until 10 time units later, using time step lengths of $\Delta t = 2.0$, 1.0 and 0.5 , respectively. Reduction of time step lengths consistently yields improved numerical accuracy. The larger step lengths are computationally more efficient and reasonably accurate. The bilinear stress path procedure also shows a consistent reduction in the error percentage in consecutive steps throughout the analysis history.

Table 5.7 : Stresses in the 2-bar problem after 5 steps of $\Delta t = 2.0$ each for a bilinear stress path

TIME	BAR 1 STRESS	e%	BAR 2 STRESS	e%
2.00	3.33223	6.54885	6.66777	-2.98010
4.00	2.57286	3.57438	7.42714	-1.18136
6.00	2.27784	1.96742	7.72216	-0.56592
8.00	2.14143	1.09335	7.85857	-0.29384
10.00	2.07363	0.60988	7.92637	-0.15833

Table 5.8 : Stresses in the 2-bar problem after 10 steps of $\Delta t = 1.0$ each, based on bilinear stress functions

TIME	BAR 1 STRESS	BAR 1 e%	BAR 2 STRESS	BAR 2 e%
1.00	4.06216	2.90827	5.93784	-1.89669
2.00	3.19357	2.11516	6.80643	-0.96252
3.00	2.76243	1.50954	7.23757	-0.56439
4.00	2.51119	1.09176	7.48881	-0.36083
5.00	2.35231	0.79745	7.64769	-0.24275
6.00	2.24699	0.58642	7.75301	-0.16868
7.00	2.17509	0.43265	7.82491	-0.11960
8.00	2.12506	0.32054	7.87494	-0.08615
9.00	2.08978	0.23743	7.91022	-0.06254
10.00	2.06469	0.17612	7.93531	-0.04572

Table 5.9 : Stresses in the 2-bar problem after 20 steps of $\Delta t = 0.5$ each using a bilinear stress path

TIME	BAR 1 STRESS	BAR 1 e%	BAR 2 STRESS	BAR 2 e%
0.50	4.83213	0.93517	5.16787	-0.85887
1.00	3.98131	0.86007	6.01869	-0.56091
1.50	3.47946	0.72254	6.52054	-0.38133
2.00	3.14625	0.60209	6.85375	-0.27399
2.50	2.90920	0.50369	7.09080	-0.20520
3.00	2.73289	0.42405	7.26711	-0.15855
3.50	2.59766	0.35814	7.40234	-0.12507
4.00	2.49162	0.30394	7.50838	-0.10045
4.50	2.40709	0.25866	7.59291	-0.08172
5.00	2.33885	0.22068	7.66115	-0.06718
5.50	2.28322	0.18913	7.71678	-0.05582
6.00	2.23750	0.16160	7.76250	-0.04648
6.50	2.19970	0.13839	7.80030	-0.03896
7.00	2.16829	0.11867	7.83171	-0.03280
7.50	2.14208	0.10234	7.85792	-0.02786
8.00	2.12013	0.08781	7.87987	-0.02360
8.50	2.10170	0.07571	7.89830	-0.02013
9.00	2.08618	0.06475	7.91382	-0.01706
9.50	2.07310	0.05550	7.92690	-0.01451
10.00	2.06205	0.04803	7.93795	-0.01247

5.6.2 The Three-bar Problem

The problems foreseen earlier in computing some values of θ is evident in studies of the 3-bar structure (Figure 5.10). The algorithm was not able to predict the initial redistribution of stresses in the bars with large time step lengths. A bilinear approximation of the highly nonlinear stress redistribution immediately after loading cannot be accomplished with time step lengths exceeding 0.25 units. The results from numerical analyses using different time step lengths are given in Table 5.10. Note that, for the case Δt = 0.5 time units, the updating of θ was based on a linear stress path for θ in bar 1 for steps 1 and 3. No convergence was achieved for time step lengths of 1.0 or greater. Comparing results in Table 5.10 with those for θ based on a linear path or m/m+1 value, the bilinear function again shows superior accuracy.

Table 5.10 : Stresses in the 3-bar problem after 10 time units with different step lengths based on a bilinear approximation

STEP LENGTHS	BAR 1		BAR 2		BAR 3	
	Stress	e%	Stress	e%	Stress	e%
* 0.500	2.26532	-0.09967	7.70073	0.03299	2.03394	-0.01426
0.250	2.26787	0.01279	7.69787	-0.00416	2.03426	0.00147
0.125	2.26766	0.00353	7.69811	-0.00104	2.03424	0.00049

For given time step lengths the bilinear updating algorithm consistently achieves superior accuracy to the previous methods. This scheme thus presents an accurate and reasonably efficient algorithm for implicit creep solution procedures. This is on the condition that caution is used to prevent individual entries of θ falling outside the range $0 \leq \theta \leq 1$. In these cases the choice of θ may be based on other considerations. In

addition, the scheme may be more robust if we enforce the condition $\theta \geq 0.5$ to ensure unconditional numerical stability of the implicit solution procedure.

5.7 CONCLUSION

Time integration schemes can be selected and fine-tuned to follow actual stress-histories at integration points. This approximation of actual stress paths forms a reasonable criterion for adopting specific forms of integration schemes. Simple piecewise approximations of the stress path over successive steps provide accurate solution strategies for the problems considered.

We have shown that the value of θ in the t_* path and a in the σ_* path can be determined analytically on the basis of achieving exact integration of simple stress curves. Linear and bilinear approximations were presented. Both lead to consistent bases for the choice of integration parameters. These criteria are also easily included in the implicit solution algorithm developed earlier. A second iterative loop for updating the appropriate values of the integration parameters is required. Numerical results demonstrate that improved solutions are achieved, at a small extra computational cost, for both piecewise linear and bilinear approximations of the actual stress-history. Higher order approximations of the stress path are in theory possible, but are not suitable in the finite element context because additional variables will have to be stored to determine the necessary curve parameters.

The linear approximation of the stress-history over any one time step produced interesting results. Firstly, it forms a simple choice for the

integration parameters which leads to accurate and stable solutions. As our discretisation of the time domain becomes increasingly refined, the more appropriate the linear approximation becomes. The solution strategies therefore rapidly converge to the continuous solution as the time step lengths are reduced. The analytical expressions for the parameters required for the linear stress curve are also of interest. Similarities between these values and our earlier results emerged. In particular, the value of θ in the t_* path was again bounded by extreme cases. We found that the appropriate choice of θ ranged from $\theta = 1/2$ for linear creep to $\theta = 1$ for the extreme case as plasticity is approached. Our heuristic choice of $\theta = m/m+1$ appears to have been fortuitous in that it lies in the unconditionally stable range, and is optimal for exact integration of almost linearly decreasing stresses.

CHAPTER 6

CONCLUSION

The formulations of the incremental problem for creep have provided valuable insight into understanding the mechanics of the physical problem. In particular, we have shown how the minimum principle for the incremental creep problem can be formulated in terms of potential functions that govern the creep response. This led to the development of numerical solution algorithms which are based on an appreciation of appropriate forms of the trapezoidal time integration scheme. The traditional approach of applying the trapezoidal rule to the stress and, as an alternative, a trapezoidal approximation of the creep strain history have been presented. The latter approach is justified by the fact that we have shown that the creep problem is contained in a first order nonlinear ordinary differential equation in creep strains only.

We looked at the mechanics of the creep problem to provide guidance for the choice of the appropriate integration schemes, and their specific forms. While the choice is clear for the case of plasticity, it is not so for creep analyses. The two different applications of the trapezoidal schemes led to different approximations of the stress and strain paths over successive steps. The paths are identical for the extreme case of plastic behaviour, but different and distinct for the general creep problem. This resulted in the question as to appropriate choices for α in the σ_* path and θ in the t_* path in order to achieve the best performance in the numerical solution of creep problems.

Theoretical and numerical investigations were conducted to determine optimal choices for the integration parameters at each integration point. Two bounds emerged for this choice. Firstly, for linear creep laws (m = 1 in Norton's power law), $\theta = 1/2$ and $\alpha = 1/2$ are optimal in the sense of providing the most accurate solutions. For this case both paths predict the same stress and strain increments. Secondly, as the creep law becomes highly nonlinear and approaches plastic behaviour ($m \to \infty$), we found that $\theta = 1$ and $\alpha = 1$ are, in general, optimal choices for the integration parameters in both paths. This corresponds to results achieved in plasticity, and the two paths become identical as a fully backward difference integration is required. By considering the mechanics of the creep problem, appropriate choices of θ and α were found to be in the range of 0.5 to 1.0. This range is also required to achieve unconditional numerical stability for a solution algorithm which uses a trapezoidal scheme for first order differential equations.

In the numerical studies on the t_* path, the heuristic choice of $\theta = m/m+1$ appeared to be optimal. This result is intuitively attractive since it provides a logical choice of integration parameter which is consistent with the bounds provided by the mechanics of the problem and the conditions for numerical stability.

Other criteria were also considered. We have shown that a work or energy approach also dictates a particular set of stress and strain paths in the same way as it does in plasticity. A generalised form of the σ_* path is the one associated with the maximum net complementary work done over a time step. This approach led to a procedure where the choice of α in the σ_* path was made so as to enforce an extremal work path. The resulting numerical solution procedure however, could not

consistently predict accurate stress and strain solutions in simple uniaxial examples. The energy approach, therefore, provides a basis for the choice of integration paths for creep problems, but is clearly not the best one.

Linear and bilinear approximations of the actual stress history over each time step also provides criteria for selecting suitable forms of the trapezoidal schemes. Integration parameters were chosen, (and iteratively updated), to perform accurate integration of simple approximations of the actual stress history. This resulted in accurate solutions from an improved numerical solution procedure. The trends that emerged from the study of linear approximations of the stress path again confirmed earlier results. We found that for a large range of almost linearly decreasing stresses the most accurate integration is achieved if we choose $\theta = \alpha = 1/2$ for linear laws, $\theta = m/m+1$ for the general case and let $\theta = \alpha = 1$ as the power index in the creep laws become large.

This thesis has considered only simple creep constitutive relations and focussed mainly on uniaxial creep. The general results obtained can be extended conceptually to more complex laws and continuum problems. We have demonstrated that time integration schemes using the trapezoidal rule should not be based on an arbitrary choice of the integration parameter. An appreciation of the mechanics of the problem as well as an understanding of physical implications of the application and selection of specific forms of the scheme is required to determine accurate and reliable numerical solution procedures for the creep problem. Accurate integration schemes will require careful selection of parameters at each integration point, rather than the current

practice of arbitrarily selecting a parameter for all integration points throughout the analysis.

The author wishes to point out that research contained in this thesis has been published in references [27] and [41-43].

REFERENCES

1. Zienkiewicz, O C, 'Finite elements in the time domain', State-of-the-art Surveys on Finite Element Technology, eds. A K Noor and W D Pilkey, ASME, USA, 405-450, 1983.

2. Belytschko, T and Hughes, T J R, Computational Methods for Transient Analysis, North-Holland Publishing Company, 1983.

3. Irons, B M, 'Applications of a theorem on eigenvalues to finite element problems', CR/132/70, Department of Civil Engineering, University of Wales, Swansea, 1970.

4. Perego, U, 'Backward difference operators and consistent predictors for linear hardening elastic-plastic constitutive laws', AMRU Technical Report No. 91, University of Cape Town, South Africa, 1987.

5. Zienkiewicz, O C, The Finite Element Method, 3rd edition, McGraw-Hill, 1977.

6. Owen, D R J and Hinton, E, Finite Elements in Plasticity: Theory and Practice, Pineridge Press, 1980.

7. Bathe, K-J, Finite Element Procedures in Engineering Analysis, Prentice-Hall, New Jersey, USA, 1982.

8. Levy, A and Pifko, A B, 'On computational strategies for problems involving plasticity and creep', Int. J. Num. Meth. Engng., 17, 747-771, 1981.

9. Snyder, M D and Bathe, K-J, 'A solution procedure for thermo-elasticplastic and creep problems', Nuclear Engineering & Design, 64, 49-80, 1981.

10. Zienkiewicz, O C and Cormeau, I, 'Visco-plasticity - plasticity and creep in elastic solids - a unified numerical approach', Int. J. Num. Meth. Engng., 8, 821-845, 1974.

11. Hibbitt, Karlsson and Sorensen, Inc., ABAQUS Theory Manual, Version 4.6, Providence, Rhode Island, 1988.

12. Kojic, M and Bathe, K-J, 'The effective-stress-function algorithms for thermo-elastic-plasticity and creep', Int. J. Num. Meth. Engng., 24, 1509-1532, 1987.

13. Bushnell, D, 'A strategy for the solution of problems involving large deflections, plasticity and creep', Int. J. Num. Meth. Engng., 11, 693-700, 1977.

14. Levy, A, 'High temperature inelastic analysis', Computers & Structures, 13, 249-256, 1981.

15. Ottosen, N S and Gunneskov, O, 'Nonlinear sub-incremental method for determination of elastic-plastic-creep behaviour', Int. J. Num. Meth. Engng., 21, 2237-2256, 1985.

16. Marques, J M M C and Owen, D R J, 'Implicit-explicit time integration in quasi-static elastoviscoplasticity using finite and infinite elements', Computer Methods in Applied Mechanics and Engineering, 41, 167-182, 1984.

17. Mendelson, A, Hirschberg, M H and Manson, S S, 'A general approach to the practical solution of creep problems', Journal of Basic Engineering, 585-598, 1959.

18. Greenbaum, G A and Rubinstein, M F, 'Creep analysis of axisymmetric bodies using finite elements', Nuclear Engineering & Design, 7, 379-397, 1968.

19. Cormeau, I, 'Numerical stability in quasi-static elasto-viscoplasticity', Int. J. Num. Meth. Engng., 9, 109-127, 1975.

20. Hughes, T J R and Taylor, R L, 'Unconditionally stable algorithms for quasi-static elasto/visco-plastic finite element analysis', Computers and Structures, 8, 169-173, 1978.

21. Park, K C, 'Practical aspects of numerical time integration', Computers & Structures, 7, 343-353, 1977.

22. Owen, D R J and Damjanic, F, 'Viscoplastic analysis of solids: stability considerations', Recent Advances in Non-linear Computational Mechanics, eds. E Hinton, D R J Owen and C Taylor, Pineridge Press Ltd, Swansea, UK, 1982.

23. Patterson, C and Oldale, M C, 'A stability criterion restricting the choice of time stepping increment in initial strain creep analyses', Numerical Methods for Nonlinear Problems, eds. C Taylor, E Hinton, D R J Owen, Swansea, Pineridge Press, 505-511, 1980.

24. Rodic, T, Owen D R J and Damjanic, F, 'An approach to correct elastoviscoplastic stress predictors', Proc. Int. Conf. Numerical Methods in Engineering : Theory and Applications, NUMETA '87, eds. G N Pande and J Middleton, Swansea, D55/1-9, 1987.

25. Hayhurst, D S R and Krzeczkowski, A J, 'Numerical solution of creep problems', Computer Methods in Applied Mechanics and Engineering, 20, 151-171, 1979.

26. Martin, J B, 'An internal variable approach to the formulation of finite element problems in plasticity', Physical Nonlinearities in Structural Analysis (eds. J Holt and J LeMaitre), SpringerVerlag, 165-176, 1981.

27. Marais, N J and Martin, J B, 'A solution algorithm for the finite element analysis of creep problems', Engineering Computations, 4, 223-228, 1987.

28. Duffett, G A, Griffin, T B, Martin, J B, Mercer C D, Reddy, B D and Resende, L, 'NOSTRUM - A Finite Element Program for Nonlinear Structural Mechanics', AMRU Technical Report No 18b, University of Cape Town, November 1983.

29. Gerald, C F and Wheatley, P O, Applied Numerical Analysis, Addison-Wesley Publishing Co., USA, 465-467, 1984.

30. Martin, J B, Reddy, B D, Griffin, T B and Bird, W W, 'Applications of mathematical programming concepts to incremental elastic-plastic analysis', AMRU Technical Report No. 52, University of Cape Town, South Africa, 1984.

31. Hibbitt, Karlsson and Sorensen, Inc., ABAQUS User's Manual, Version 4.6, Providence, Rhode Island, 1988.

32. Martin, J B and Bird, W W, 'Integration along the path of loading in elastic-plastic problems', Engineering Computations, 5, 217-223, 1988.

33. Ortiz, M and Simo, J C, 'An analysis of a new class of integration algorithms for elastoplastic constitutive relations', Int. J. Num. Meth. Engng., 23, 353-366, 1986.

34. Ortiz, M and Popov, E, 'Accuracy and stability analysis of integration algorithms for elastoplastic constitutive relations', Int. J. Num. Meth. Engng., 21, 1561-1576, 1986.

35. Martin, J B, International Journal of Solids and Structures, 2, 9, 1966.

36. Ponter, A R S, 'An energy theorem for time dependent materials', Journal of the Mechanics and Physics of Solids, 19, 63-71, 1969.

37. Ponter, A R S, 'The derivation of energy theorems for creep constitutive relationships', IUTAM Conference Proceedings, Sweden, 123-136, 1970.

38. Ponter, A R S, 'Convexity conditions and energy theorems for time-independent materials', Journal of Mechanics and Physics of Solids, 16, 283, 1968.

39. Drucker, D C, 'A more fundamental approach to plastic stress-strain relations', Proc. 1st US Nat. Congr. Appl. Mech., ASME, 487, 1951.

40. Martin, J B, 'Plasticity: Fundamentals and General Results', MIT Press, 1975.

41. Marais, N J and Nappi, A, 'A numerical approach to uniaxial creep problems', AMRU Technical Report No. 117, University of Cape Town, South Africa, 1988.

42. Marias, N J and Nappi, A, 'Approximate solutions of creep problems', AMRU Technical Report No. 118, University of Cape Town, South Africa, 1988.

43. Marais, N J and Martin, J B, 'Energy principles for time integration schemes in creep and viscoplastic analyses', Proc. Finite Element Methods in South Africa, FEMSA '88, Pretoria, South Africa, 1988.